To the Graduate Council:

I am submitting herewith a dissertation written by Chii-Jong Hwang entitled "A Theoretical Study of Compressible Two Phase Internal Flow." I have examined the final copy of this dissertation for form and content and recommend that it be accepted in partial fulfillment of the requirements for the degree of Doctor of Philosophy, with a major in Mechanical Engineering.

Robert L. Young, Major Professor

We have read this dissertation
and recommend its acceptance:

Accepted for the Council:

The Graduate School

A THEORETICAL STUDY OF COMPRESSIBLE TWO PHASE INTERNAL FLOW

A Dissertation

Presented for the

Doctor of Philosophy

Degree

The University of Tennessee, Knoxville

Chii-Jong Hwang

August 1984

ACKNOWLEDGMENTS

The work reported herein was supported by The University of Tennessee Space Institute Energy Conversion Research and Development Programs under Contract No. DE-AC02-79ET10815.

The author wishes to express his sincere appreciation to his major advisor, Dr. Robert L. Young, for his academic assistance. Most special thanks are due to his working advisor, Dr. Roy J. Schulz, for defining the topic and valuable guidance throughout this work. Without the advice of Drs. Young and Schulz this work would not have been possible.

Grateful appreciation is extended to Dr. Jain-Ming Wu, Dr. Carrol E. Peters, Dr. Lloyd W. Crawford and Dr. Mancil W. Milligan, for their serving as members of the committee.

The assistance of the personnel of the UTSI Computer Center, Tullahoma, and the UTCC, Knoxville, is acknowledged. Also, a special thanks to Ms. Madge Gibson for typing the dissertation.

Finally, the author wishes to express his most sincere gratitude to his wife, parents, sister and brothers for their encouragement and support by dedicating the present work to them.

ABSTRACT

A numerical solution procedure has been developed for solving one phase, gas-only flow or fully coupled, gas-particle two phase flow in axisymmetric or two-dimensional geometries. The numerical basis of the present research is a time-dependent, unsplit, explicit, second-order accurate MacCormack finite difference scheme. Some special numerical techniques are developed to ensure numerical stability. The finite difference scheme has been used to solve the Navier-Stokes equations for the interior of the flow domain and an integral method is incorporated into this program to treat the turbulent boundary layer regimes. In order to evaluate the program, the results are compared to physical phenomena and evaluated on the basis of basic physical principles.

The purpose of the present work is to serve as a method for predicting both one and two phase flow in nozzles, especially those of solid fueled rocket motors. However, it is the primary objective of the present study to investigate the behavior of one and two phase flow passing through the combustor outlet, nozzle, and channel inlet of the Coal Fired Flow Facility, which is an MHD power generation system being developed at The University of Tennessee Space Institute for the United States Department of Energy. The results of the study indicate the level of gas-particle coupling in flow acceleration devices such as nozzles, and the differences that can be expected between two phase and single phase gas flows.

TABLE OF CONTENTS

CHAPTER		PAGE
I.	INTRODUCTION	1
	Two Phase Solid Rocket Nozzle Flow	1
	Two Phase Flow in CFFF	2
	Review of Previous Related Work	4
	Objective of the Present Work	6
II.	MATHEMATICAL MODEL	8
	Inviscid Gas-Particle Flow	8
	Basic assumptions	8
	Governing equations	10
	Drag coefficient and Nusselt number	11
	Viscous Gas-Particle Flow	13
	Simple effective turbulent viscosity approach	14
	Viscous-inviscid interaction technique	15
III.	NUMERICAL METHOD	17
	Inviscid Gas-Particle Approach	17
	Coordinate transformation	17
	Finite difference approximation	20
	Boundary conditions	22
	Inlet grid points	23
	Exit grid points	25
	Wall grid points	26
	Initial conditions, stability and convergence criteria	28

CHAPTER PAGE

Viscous Gas-Particle Approach. 33

Simple effective turbulent viscosity model 33

Viscous-inviscid interaction model 34

IV. NUMERICAL RESULTS AND DISCUSSIONS. 38

Two Phase Flow in Conical Rocket Nozzle. 38

Discussion of the results 40

Two Phase Flow in CFFF 56

Discussion of results for the inviscid gas-particle flow 59

Discussion of results for the effective turbulent viscosity model 86

Discussion of results for the viscous-inviscid interaction model 94

V. CONCLUSIONS AND RECOMMENDATIONS. 106

Conclusions. 106

Recommendations. 107

LIST OF REFERENCES 114

APPENDICES 119

APPENDIX A. DERIVATION OF COMPRESSIBLE, TWO PHASE, GAS-PARTICLE FLOW EQUATIONS 120

APPENDIX B. TURBULENT BOUNDARY LAYER RELATIONS 127

APPENDIX C. DERIVATION OF CHARACTERISTIC EQUATIONS OF TWO PHASE FLOW FOR WALL BOUNDARY CONDITION 130

CHAPTER PAGE

APPENDIX D. DERIVATION OF CHARACTERISTIC EQUATIONS OF TWO PHASE FLOW FOR INLET AND EXIT BOUNDARY CONDITIONS. 136

APPENDIX E. DESCRIPTION OF COMPUTER PROGRAM 139

VITA 150

LIST OF TABLES

TABLE PAGE

1. Data Analysis for Two Phase Flow with Different Wall Conditions[a] 29
2. Error Analysis of Mass Flow Rate between Inlet and Throat Planes[a] 79
3. Error Analysis for One Phase Flow (CFFF) 80
4. Error Analysis for Two Phase Flow (CFFF, 1.43%). 81
5. Computational Time[a]. 108
6. The Ratio of Mean Free Path of Particle-to-Particle Collision to the Interparticle Spacing[a] 110
7. The Ratio of Radiative Heat Transfer to Convective Heat Transfer[a] 112

LIST OF FIGURES

FIGURE		PAGE
1.	Schematic of the Low Mass Flow (LMF) Train in the Coal Fired Flow Facility (CFFF)	3
2.	Physical Plane and Computational Plane	19
3.	Iteration Procedure for Viscous-Inviscid Interaction Technique.	36
4.	Grid for Conical Rocket Nozzle	39
5.	Gas Density Contour for One Phase Flow	41
6.	Gas Concentration Contour for Two Phase Flow	42
7.	Particle Concentration Contour for Two Phase Flow.	43
8.	Temperature Distribution at the Nozzle Exit Plane.	44
9.	Temperature Distribution at the Nozzle Wall.	45
10.	Mach Number Contour for One Phase Flow	46
11.	Mach Number Contour for Two Phase Flow	47
12.	Mach Number Distribution at the Nozzle Centerline.	48
13.	Mach Number Distribution at the Nozzle Wall.	49
14.	Mach Number Distribution at the Nozzle Exit Plane.	50
15.	Mach Number Distribution for One Phase Flow.	51
16.	Mach Number Distribution for Two Phase Flow.	52
17.	Particle Concentration Distribution at the Nozzle Wall.	53
18.	Grid for CFFF.	57
19.	Limiting Particle Streamline for Two Phase Flows with ϕ = 1.43%	60

FIGURE PAGE

20. Particle Concentration Contour for Two Phase Flow with r_j = 15μ and ϕ = 1.43% 61

21. Particle Concentration Distribution at the Wall for Two Phase Flows with ϕ = 1.43%. 62

22. Particle Concentration Distribution at the Exit Plane for Two Phase Flows with ϕ = 1.43%. 63

23. Temperature Distribution at the Wall for One Phase Flow and Two Phase Flow with r_j = 1μ and ϕ = 1.43% 64

24. Temperature Distribution at the Wall for One Phase Flow and Two Phase Flow with r_j = 15μ and ϕ = 1.43%. . . . 65

25. Gas Velocity Vector for One Phase Flow and Two Phase Flow with r_j = 15μ and ϕ = 1.43% 66

26. Gas Velocity Vector for Two Phase Flows with ϕ = 1.43%. 67

27. Gas Velocity Vector for Two Phase Flows with r_j = 1μ. 68

28. Velocity Vector for Two Phase Flow with r_j = 15μ and ϕ = 1.43% 69

29. Mach Number Distribution at the Wall for One Phase Flow and Two Phase Flows with ϕ = 1.43%. 70

30. Mach Number Distribution at the Exit Plane for One Phase Flow and Two Phase Flows with ϕ = 1.43%. 71

FIGURE PAGE

31. Mach Number Contour for One Phase Flow and Two Phase Flow with r_j = 15μ and ϕ = 1.43% 72

32. Mach Number Contour for Two Phase Flows with ϕ = 1.43%. 73

33. Mach Number Contour for Two Phase Flows with r_j = 1μ. 74

34. Particle Concentration Distribution at the Wall for Two Phase Flow with r_j = 1μ and ϕ = 1.43%. 75

35. Pressure at Grid Point (2,1) for Two Phase Flow with r_j = 15μ and ϕ = 1.43% 76

36. Time History of Particle Concentration 77

37. Time History of Particle Free Zone 78

38. Particle Concentration Contour for Two Phase Flow with r_j = 1μ and ϕ = 1.43%. 88

39. Particle Concentration Contour for Two Phase Flow with r_j = 15μ and ϕ = 1.43% 89

40. Gas Velocity Vector for One Phase Flow 90

41. Pressure Distribution along the Wall and Centerline 91

42. Mach Number Contour for Two Phase Flow with r_j = 1μ and ϕ = 1.43% 92

43. Mach Number Contour for Two Phase Flow with r_j = 15μ and ϕ = 1.43%. 93

FIGURE PAGE

44. Gas Velocity Profile for One Phase Flow and Two Phase Flows with ϕ = 1.43% 96

45. Displacement Thickness for One Phase Flow and Two Phase Flows with ϕ = 1.43% 97

46. Shape Factor for One Phase Flow and Two Phase Flows with ϕ = 1.43% 99

47. Momentum Thickness for One Phase Flow and Two Phase Flows with ϕ = 1.43% 100

48. Friction Coefficient for One Phase Flow and Two Phase Flows with ϕ = 1.43% 101

49. Particle Concentration Contour for Two Phase Flow with r_j = 15μ and ϕ = 1.43% 102

50. Particle Concentration Contour for Two Phase Flow with r_j = 1μ and ϕ = 1.43%. 103

51. Pressure Distribution along the Wall 105

52. Computer Program Flow Diagram 140

LIST OF SYMBOLS

A	Term in Equation (10)
a	Sonic velocity
B	Term in Equation (10)
C	Term in Equation (10)
C_D	Drag coefficient
C_{D_o}	Term in Equation (13)
$C_{D_{Stokes}}$	Stokes law of drag coefficient
C_f	Friction coefficient
C_j	Particle heat capacity
C_P	Gas specific heat at constant pressure
C_v	Gas specific heat at constant volume
D	Term in Equation (10) or shear-work integral
$\vec{D}$	Total drag force exerted on a volume V of gas
$\vec{D}_j$	Drag force exerted on a particle
e_j	Particle total energy per unit mass
F_c	$[1 + (\gamma-1) \frac{Me^2}{2}]^{\frac{1}{2}}$
$\vec{f}$	Drag force per unit mass of gas
f_j	$\frac{C_D}{C_{D_{Stokes}}}$
$\bar{H}$	Incompressible shape factor
$H_{\delta*}$	Shape factor based on $\delta*$
$H_{\delta**}$	Shape factor based on $\delta**$
$H_{\theta*}$	Shape factor based on $\theta*$
h_c	Convection heat transfer coefficient

K	Molecular thermal conductivity
M	Mach number
M_j	$\frac{\left\|\vec{V} - \vec{V}_j\right\|}{a}$
m_j	Particle material density
$\vec{N}$	Characteristic normal
N_j	Number of particles per unit volume of gas
Nu_j	Nusselt number
P	Gas pressure
Pr	Prandtl number
P_T	Total pressure
R	Gas constant
Re_j	$\frac{\rho \left\|\vec{V} - \vec{V}_j\right\| (2r_j)}{\mu_g}$
$R_{e\theta}$	Reynolds number based on momentum thickness
r_j	Particle radius
r_{co}	Recovery factor
T	Temperature
T_T	Total temperature
u	Velocity component in x direction
v	Velocity component in r direction
x,r,t	Physical space coordinates
y	Coordinate normal to wall
ζ,η,τ	Computational space coordinates
σ	Stefan-Boltzmann constant
γ	Ratio of specific heats

δ	Axisymmetric flow (1), planar flow (0)
ε	Emissivity
θ	Momentum thickness or angle of wall
μ_g	Molecular viscosity
υ	$\frac{\mu_g}{\rho}$
ρ	Density or concentration
ϕ	Particle mass fraction ($\frac{\text{mass of particles}}{\text{mass of mixture}}$)

Subscripts

c	Centerline
e	Boundary edge
j	Particle
w	Wall
oe	Initial and boundary edge
L,M	Grid points

Superscripts

$\overline{}$	Incompressible value or predicted value
N	Time step

CHAPTER I

INTRODUCTION

Two Phase Solid Rocket Nozzle Flow

There are many problems of engineering importance that require the numerical solution of compressible two phase exhaust flow in ducts and nozzles. One example of an important problem is the exhaust gas from a solid propellant rocket motor. Solid propellant rocket motors burn aluminized propellants that form particles of aluminum oxide which pass into the atmosphere with the exhaust gases by expanding through a nozzle. The aluminum powder in the combustion chamber increases the temperature and helps to stabilize high frequency combustion instability. However, an undesirable effect of the aluminum is the creation of aluminum oxide particles in the exhaust which contribute an inefficiency in the expansion process in the propulsive nozzle. The inefficiency is due to the condensed Al_2O_3 particles that do not accelerate at the same rate as the gaseous combustion products. Also, the temperature of the condensed particles do not decrease as rapidly as that of the flowing combustion gases. From the above discussions it is necessary to know the behavior of the particle laden gas expanding through the nozzle in order to predict, evaluate, or design solid rocket motor performance. This problem has received attention in the past, for example, a computer program (SPP) for predicting such flows, has been discussed by G. R. Nickerson et al [1]. However, the general problem still exists today, that of predicting such flows with a minimum amount of empiricisms, and with a sufficient degree of accuracy.

Two Phase Flow in CFFF

The problem of critical interest in the present study is a two phase flow that starts as a plasma generator in the primary combustor of the Coal Fired Flow Facility (CFFF) which is a coal fired, magnetohydrodynamic power generation system currently being developed by The University of Tennessee Space Institute for the United States Department of Energy. Schematically, the MHD open cycle test train at the CFFF is shown in Figure 1. The plasma generated by burning seeded (K_2CO_3) pulverized coal with preheated oxygen-nitrogen gas mixture, is hot (3000K) and contains vaporized and condensed slag material. In this combustion system, particles of slag form and pass down the flow train with the plasma expanding through a nozzle to high subsonic or low supersonic speeds. The flow rate of the combined coal/seed mixture for this facility is normally 1.0 to 2.0 lbm/s. The gas/slag mixture leaves the channel after doing work against the magnetic field, which work is partially extracted in the form of electrical energy, and then the gas enters a diffuser which slows the flow down to moderate, subsonic speeds and increases the gas static pressure to about 1 atmosphere.

In the above process, there are several areas of concern. First, for gas diagnostic purposes, it is necessary to provide theoretical estimates of the particle and gas fluxes and properties in the flow leaving the nozzle and entering the power extracting MHD channel. Second, it is necessary to understand how the gas-particle coupling affects the basic performance of the nozzle as a flow acceleration device. Third, it will be necessary to perform parametric studies of

a. Oxidizer
b. Vitiation Heater
c. Coal + Seed
d. Disperser Plate
e. Coal Fired Combustor
f. Nozzle
g. Power Conditioner
h. MHD Channel
i. Diffuser
j. Radiant Slagging Furnace
k. Secondary Combustor
l. Superheater
m. Airheater
n. Electrostatic Precipitator

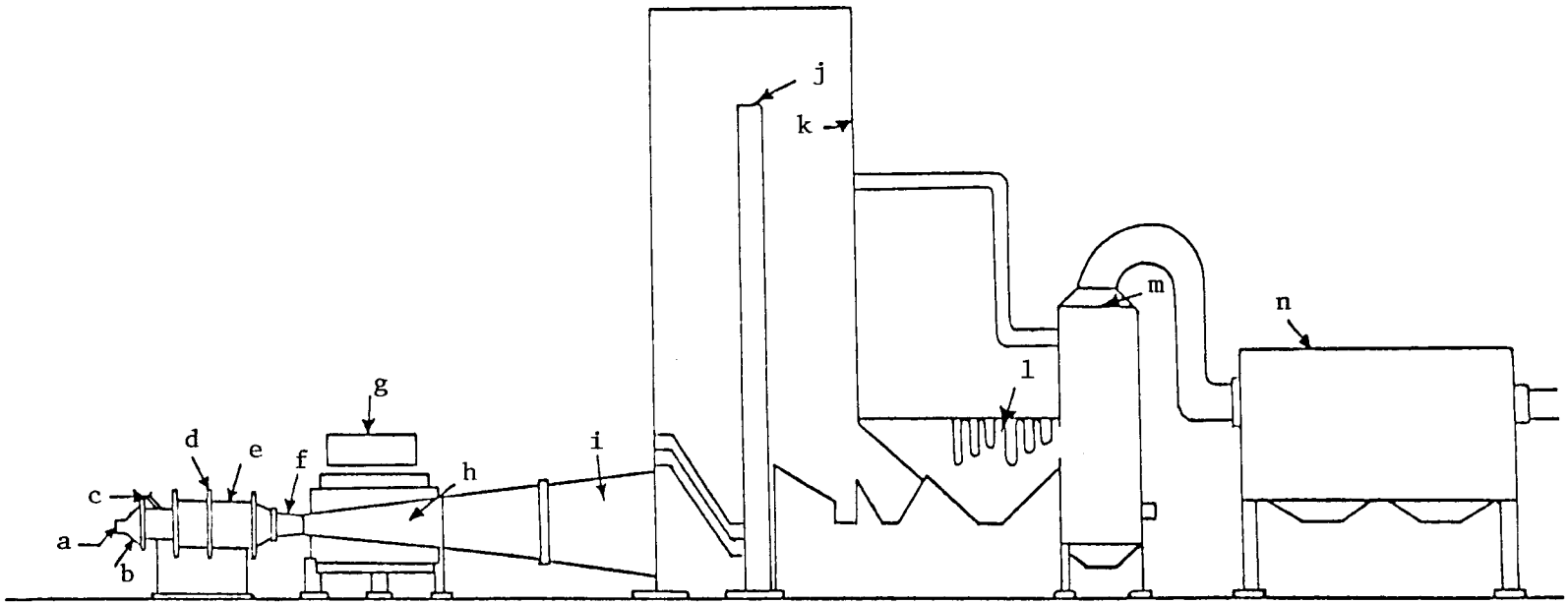


Figure 1. Schematic of the Low Mass Flow (LMF) Train in the Coal Fired Flow Facility (CFFF).

the effects of different nozzle inlet particulate concentrations and thermodynamic states on the flow in the channel for interpreting the MHD channel behavior. Fourth, it may be necessary to predict the performance of the diffuser where its integration with downstream equipment may cause problems due to the presence of particles that impinge with relatively high velocities on heat exchanger tubes.

Review of Previous Related Work

In order to understand previous research efforts on this problem, several research papers were studied and evaluated. A comprehensive review of gas-particle nozzle flows before 1962 was presented by Hoglund [2]. This paper presented the two phase flow theory, experimental studies, and discussed the one-dimensional approximations provided by early studies. Kliegel [3] calculated the coupled, one-dimensional gas particle behavior for an inviscid gas and obtained a particularly simple solution by a "constant lag" analysis. Improvements in the theory which overcame one-dimensional approximations were made by Kliegel and Nickerson [4] who showed that the inviscid two-dimensional, gas-particle equations are hyperbolic and can be solved by the method of characteristic in the supersonic region of nozzle. Other descriptions of two phase flows were provided by Rudinger [5], Zucrow [6] and Peters [7]. These papers contained comprehensive reviews. In recent years, numerical methods have been broadly applied to the complicated sets of governing equations for such flows. Regan, et al [8], and Jacques, et al [9] use an iterative technique to solve two-dimensional, axisymmetric flows. Both were limited by a numerical method based on the

assumption of fixed gas phase streamlines, which is not always true due to the particle effects and nozzle configurations. Chang [10] presented a time-dependent finite difference technique that solved both one and fully coupled two phase nozzle flows. The "conservative forms" of the conservation equations for the gas and particle phases were solved by a MacCormack finite difference scheme and coordinate stretching was used to achieve a "boundary-fitted-coordinate system" which generated a rectangular grid in a computational plane.

C. T. Crowe [11] has recently provided a complete review of numerical models for dilute gas-particle flows. Several different models have been mentioned in the literature and can be categorized according to coupling ("one-way" or "two-way"), dimension (one-dimensional, quasi-one-dimensional, or two dimensional) and approach (two-fluid or trajectory). For subsonic flows, both two-fluid and trajectory models are discussed. From the discussion of Crowe, the advantages and disadvantages of those two models are summarized as follows. The two-fluid model can be easily extended to multi-dimensional flows and incorporate particle diffusion effects. However, the treatment of the numerical instabilities, numerical diffusion and large storage requirements for multiple particle sizes are difficult to surmount. The trajectory approach can be thought of as the "natural" solution scheme, and storage requirements for multiple particle sizes are not excessive. However, particle dispersion must be incorporated through an empirical diffusion velocity or more expensive Monte Carlo methods. M. DiGiacinto, et al [12] used a two-fluid model to solve for dilute gas-particle flows. Two important

parameters (particle loading ratio and Stokes number) are used to parameterize the results. By using a time marching implicit scheme described in reference 12, the application to a sudden restriction duct flow was presented. From their study, one concludes that the one-way coupling may be appropriate for small values of loading ratio and large values of Stokes number. However, two-way coupling is necessary for the larger value of loading ratio and lower value of Stokes number.

Objective of the Present Work

The purpose of this study is to demonstrate a numerical procedure which can predict the physical properties and physical phenomena of gas-particle internal flow. Considering the work of previous authors, it was decided to formulate a fully coupled, gas-particle numerical model using a finite difference approach similar to the one Chang [10] had used. Although this method falls under the type of approach called "two-fluid", it is important to point out that the derivation of the governing equations only depends on sufficiently high particle number densities. The particle phase is not treated as a fluid (see Appendix A). The formulation of governing equations and several assumptions required to set up this model are given in Chapter II. All empiricisms, such as drag coefficient, Nusselt number and related turbulent boundary layer relations are explicitly addressed at the outset before any flow field is calculated. The details are described in Chapter II. The numerical treatment, which includes some special techniques to achieve numerical stability, identification of the "limiting particle streamline", and viscous-inviscid interaction ideas, is also presented

in Chapter III. After completing the theoretical formulation, two sets of geometrical configurations are studied in Chapter IV. The results of conical nozzle flow are compared to those of Chang's paper [10] in order to evaluate the present computer code. Several data are obtained for the two phase flow in CFFF. In the last chapter, concluding remarks and recommendations for future research are included.

In the present research program, the model is computationally intensive and therefore expensive to apply to certain problems, that is, to problems with difficult geometry, large particles, or both of these effects. Nevertheless, the method offers the possibility of achieving answers or solutions wherein both gas and particle mass, momentum and energy fluxes are resolved to any degree of precision and global conservation by merely running the program to more and more iterative solution steps. This is extremely important if nozzle thrust degradation is to be predicted accurately. As is the case for all computational fluid dynamic algorithms for complex flows, bigger and faster computers will eventually make such methods cost effective and hence very attractive as a design tool.

CHAPTER II

MATHEMATICAL MODEL

Inviscid Gas-Particle Flow

The mathematical formulation was developed to solve two sets of two phase flow problems. The first set of two phase flow problems is inviscid gas-particle flow, where the wall boundary layers are neglected. The second set of problems is viscous gas-particle flows. Due to the viscous boundary layer effects on the gas, application of boundary layer theory is necessary. A reasonable way to approach the present research problem is to treat the inviscid gas-particle flow first.

Basic Assumptions

In order to model the complicated, two phase internal flow, some simplifications were necessary and the following assumptions were employed.

1. Particles are spherical in shape; their internal temperature is uniform and the specific heat of each particle is constant.
2. The volume occupied by the particles is reasonably small, compared to the volume occupied by the gas, so that the ideal gas equation of state is satisfactory for the gas phase.
3. The particles do not interact with each other, so that collision, agglomeration and/or decomposition of the particles are neglected.

4. Particles that hit the physical wall do not stick, and they are assumed parallel to the wall. This assumption of parallel velocity is relaxed when the limiting particle streamline concept is introduced.
5. The gas is a perfect gas, with constant molecular weight and specific heats, although this assumption can be easily replaced by a real gas model of any degree of complexity.
6. The gas is inviscid. However, gas-particle interactions occur through particle drag.
7. No other external forces are applied to the flow except the gas pressure and the drag of the particles.
8. No mass transfer and phase changes are considered in this study.
9. The mixture flow is adiabatic, the total energy of mixture is constant; there is no heat transfer to the wall.
10. Energy exchange between particles and gas occurs through both convection and radiation.
11. Chemical reactions are not occurring in the gas, its composition is frozen, although this assumption can also be replaced, for example by a chemical equilibrium gas model.
12. At present, only one size of particle exists in this mixture, although this is only a computer size (storage) limitation imposed by the computer system used in the present study. The formulation is general enough to treat multiple size classes simultaneously.

Governing Equations

Based on the previous assumptions, the following set of governing equations was derived. The details of the particular derivation done by Dr. Roy J. Schulz is given in Appendix A. A search of the literature, such as references 1, 6 and 13, confirms that the set of governing equations obtained in his derivation is correct.

(a) Gas Phase

Continuity:
$$\frac{\partial \rho}{\partial t} + u \frac{\partial \rho}{\partial x} + v \frac{\partial \rho}{\partial r} + \rho \frac{\partial u}{\partial x} + \rho \frac{\partial v}{\partial r} + \delta \frac{\rho v}{r} = 0 \qquad (1)$$

X-Momentum:
$$\frac{\partial u}{\partial t} + u \frac{\partial u}{\partial x} + v \frac{\partial u}{\partial r} + \frac{1}{\rho} \frac{\partial P}{\partial x} = -A \frac{\rho_j}{\rho} (u-u_j) \qquad (2)$$

R-Momentum:
$$\frac{\partial v}{\partial t} + u \frac{\partial v}{\partial x} + v \frac{\partial v}{\partial r} + \frac{1}{\rho} \frac{\partial P}{\partial r} = - A \frac{\rho_j}{\rho} (v-v_j) \qquad (3)$$

Energy:
$$\frac{\partial P}{\partial t} + u \frac{\partial P}{\partial x} + v \frac{\partial P}{\partial r} - a^2 \left(\frac{\partial \rho}{\partial t} + u \frac{\partial \rho}{\partial x} + v \frac{\partial \rho}{\partial r}\right) = AB\rho_j \qquad (4)$$

Equation of State
$$P = \rho RT \qquad (5)$$

(b) Particle phase

Continuity:
$$\frac{\partial \rho_j}{\partial t} + u_j \frac{\partial \rho_j}{\partial x} + v_j \frac{\partial \rho_j}{\partial r} + \rho_j \frac{\partial u_j}{\partial x} + \rho_j \frac{\partial v_j}{\partial r} + \delta \frac{\rho_j v_j}{r} = 0 \qquad (6)$$

X-Momentum:
$$\frac{\partial u_j}{\partial t} + u_j \frac{\partial u_j}{\partial x} + v_j \frac{\partial u_j}{\partial r} = A(u-u_j) \qquad (7)$$

R-Momentum:
$$\frac{\partial v_j}{\partial t} + u_j \frac{\partial v_j}{\partial x} + v_j \frac{\partial v_j}{\partial r} = A(v-v_j) \qquad (8)$$

Energy:
$$\frac{\partial T_j}{\partial t} + u_j \frac{\partial T_j}{\partial x} + v_j \frac{\partial T_j}{\partial r} = D \qquad (9)$$

Where $A = \dfrac{9\ \mu_g\ f_j}{2\ m_j\ r_j^2}$

$$B = (\gamma-1)\ [(u-u_j)^2 + (v-v_j)^2 + \frac{2}{3}\ C\ (T_j-T) + \frac{3\sigma}{Am_j r_j}\ (\varepsilon_j T_j^4-\varepsilon T^4)]$$

$$C = \frac{Nu_j Cp}{2f_j\ P_r}$$

$$D = -\frac{2AC}{3C_j}\ (T_j-T) - \frac{3\sigma}{m_j r_j C_j}\ (\varepsilon_j T_j^4-\varepsilon T^4)$$

and

$$f_j = \frac{C_D}{C_{D_{Stokes}}} \quad . \tag{10}$$

Even though the numerical data which have been obtained in the present study are based on the axisymmetrical flow ($\delta = 1$), the problem also can be run for planar cases ($\delta = 0$). The drag coefficient and Nusselt number of the particles, C_D and Nu_j, are subject to debate. More information is given in the following description.

Drag Coefficient and Nusselt Number

Two important relations which show the interaction between gas phase and particle phase are drag coefficient and Nusselt number. Several different forms of C_D and Nu_j have been presented in the literature. In the present work, two different sets of C_D and Nu_j were employed. In order to reduce computations, the following simple empirical expressions of C_D and Nu_j were mainly used:

$$C_D = \frac{24}{Re_j}\ [1+0.15\ Re_j^{0.687}] \tag{11}$$

$$Nu_j = 2+0.459\ Re_j^{0.55}\ Pr^{0.33} \quad . \tag{12}$$

Equation (11), which shows the correction of Stokes law for inertial effects, was presented by Torobin and Gauvin [14]. Equation (12), which is the continum Nusselt number, was used by Drake [15]. The expressions (11) and (12) form a simple basis for the initial study of this research program. More completely and hopefully correct mathematical relations are given in the following discussion.

D. J. Carlson and R. F. Hoglund [16] gave a detail of description and mathematical form of C_D and Nu_j. They modified the relations (11) and (12) by considering some other effects, such as compressibility and rarefaction. G. R. Nickerson et al. [1] used a modified form of the Crowe drag law [17] in the improved "SPP" Code. They also compared the computing execution time, core storage and error analysis with those of models which were presented by Kliegel [19], Crowe [17,18] and Henderson [20]. According to the discussion of G. R. Nickerson et al., their formulations were in good agreement with those of Crowe and Henderson and saved computation time like that of Kliegel. Thus, the drag coefficient presented by G. R. Nickerson [1] is applied in this study and is shown as follows:

$$C_D = (C_{D_o} - 2)\, e^{-3.07\sqrt{\gamma}\,\frac{M_j}{Re_j}}\, g(Re_j) + \frac{h(M_j)}{\sqrt{\gamma}\, M_j}\, e^{-\frac{Re_j}{2M_j}} + 2 \qquad (13)$$

where

$$C_{D_o} = \frac{24}{Re_j} \qquad \text{for } 0 < Re_j \leq 0.34$$

$$C_{D_o} = 0.48 + 28\, Re_j^{-0.85} \qquad \text{for } 0.34 < Re_j \leq 10^5$$

$$h(M_j) = \frac{5.6}{M_j+1} + 1.7\,\sqrt{T_j/T}$$

and

$$g(Re_j) = \frac{1 + Re_j(12.278 + 0.584\ Re_j)}{1 + 11.278\ Re_j} \qquad \text{for } Re_j < 10^3.$$

The heat transfer term Nu_j given by Drake-Kavanaugh [21] is used in the present work. The expression of Nu_j is calculated from the incompressible value of Nusselt number Nu_{o_j} which was given by Ranz and Marshall [22]. The relation between the compressible and incompressible forms of the Nusselt number is given below:

$$Nu_j = \frac{Nu_{o_j}}{1 + 3.42 \frac{M_j}{Re_j Pr} Nu_{o_j}}$$

where $Nu_{o_j} = 2.0 + 0.60\ Re_j^{0.5}\ Pr^{0.33}$. (14)

Until now, the basic ideas of the inviscid gas-particle flow have been discussed. The next topic of discussion is the investigation of viscous gas-particle flow.

Viscous Gas-Particle Flow

In this topic, the viscous effect is not only considered as gas-particle drag forces but also the stress between gas and wall. In order to simplify the study, the effect of gas turbulence on particle drag and heat transfer was neglected. Two principal approaches to complex turbulent flow problem are in usage today. One approach is the well known approach of solution of the time-dependent, ensemble-averaged, Navier Stokes equations. In this method, different turbulence models, such as constant viscosity, mixing length, one equation and two equation, are employed to formulate the effective turbulence viscosity distributions.

Significant progress has been made in this approach as a vast, current literature will confirm. However, except for constant viscosity models, these turbulence models are very expensive to use. A second method to treat turbulent shear layers near walls is a viscous-inviscid interaction procedure in which integral methods of turbulent boundary layer analysis are used to match the common boundary between boundary layer and inviscid core flow. This approach is not expensive, but it needs a lot of empirical input relations such as velocity profile, shape factor, and wall shear stress distributions to start the calculation of the turbulent boundary layer. The accuracy of the integral method is restricted by those factors. To tentatively treat the effects of wall turbulent boundary layer on coupled gas-particle nozzle flow, two methods were employed: (1) simple effective viscosity model and (2) viscous-inviscid integral boundary layer analysis. Based on preliminary results of this simplified treatment, suggestions for future work have been formulated.

Simple Effective Turbulent Viscosity Approach

The effective turbulent viscosity model has been applied to many types of flow calculations. The present study uses a constant effective viscosity model to simulate low Reynolds number, thick boundary layer effects. In this model, the governing equations are the same as the form for laminar flow, except the molecular viscosity is replaced by an effective turbulent viscosity. The effective viscosity and thermal conductivity are assumed to be proportional to the molecular viscosity and thermal conductivity. The numerical treatments and discussions are given in the following two chapters.

Viscous-Inviscid Interaction Technique

Because of particle separation from the nozzle walls due to inertia effects, as the flow accelerates through the converging-diverging nozzle, a gas-only boundary layer calculation can be applied without significant error for the boundary layer downstream of the nozzle throat. The particles do affect the boundary layer edge conditions, however, and this is taken into account. For the gas-only flow, several research works have been devoted to this fluid dynamic problem. One summary of a current solution procedure for steady, unsteady, direct and inverse turbulent boundary calculation was given by Tracy Donegan [23]. The theory for steady, attached boundary layer was used in the present research, in the form of steady, direct integral method, even though the core flow treatment was by time-dependent finite difference methods.

The turbulent boundary layer calculation method presented herein is the method given by Whitfield [24]. In his work, an analytical expression of a velocity profile that depends on the local values of skin friction, shape factor, and Reynolds number based on momentum thickness was utilized. Velocity-temperature relations, which are the modified Crocco relation for an adiabatic wall, were also formulated as an analytical expression. The shear-work integral shown in the boundary layer integral equations is evaluated directly from a shear-stress distribution rather than by empirical relations. The shear-stress distribution is specified in three regions across the boundary layer. Several shape factor correlations have been derived. Based on Whitfield's work, the following turbulent boundary layer integral equations, from reference 24,

can be solved completely

$$\frac{1}{r_w^{\delta}\,\rho_e u_e^2}\frac{d}{dx}\left(r_w^{\delta}\rho_e u_e^2\theta\right) + H_\delta^*\,\frac{\theta}{u_e}\frac{du_e}{dx} = \frac{C_f}{2} \tag{15}$$

$$\frac{1}{2r_w^{\delta}\rho_e u_e^3}\frac{d}{dx}\left(r_w^{\delta}\rho_e u_e^3\theta H_\theta^*\right) + H_\delta^{**}\,\frac{\theta}{u_e}\frac{du_e}{dx} = \frac{C_f}{2}D \tag{16}$$

where x is a boundary fitted coordinate lying along the wall.

In the present viscous-inviscid iteration process, the "surface source" model which simulates boundary layer displacement effects was applied to keep fixed the computational mesh used in the inviscid gas-particle flow. It is convenient to use this model because a surface mass flux is imposed as a boundary condition in the inviscid calculation at the physical body surface, hence the surface source model avoids the necessity of making mesh adjustments such as would be needed for an effective displacement model. In this method, the slip wall condition in the inviscid calculation is replaced by the following normal wall condition which can be derived from the conservation of mass in the turbulent boundary layer [23].

$$v_n = \frac{1}{\rho_e r_w^{\delta}}\,\frac{d(\rho_e u_e r_w^{\delta}\delta^*)}{dx}\,. \tag{17}$$

The numerical results and detail of the treatment are shown in the following two chapters.

CHAPTER III

NUMERICAL METHOD

This chapter describes the numerical method used to solve the governing equations given in Chapter II. The numerical treatment of boundary conditions, initial conditions and instability problems will be discussed. In order to successfully simulate the physical phenomena, the accuracy, stability and reliability of the method is addressed. In this study, the numerical scheme is similar to that of the so-called VNAP program developed by Cline [25]. Two principal topics, inviscid gas-particle flow and viscous gas-particle flow, are discussed in terms of the solutions obtained by the numerical procedure.

Inviscid Gas-Particle Approach

The governing equations describing the inviscid gas-particle flow have been given in Chapter II. There are no second order diffusion terms in those equations. The procedures to solve this set of equations are presented below.

Coordinate Transformation

To apply the numerical solution procedure to general physical domains, it is convenient to map the x,r,t physical domain into a rectangular ζ,η,τ computational domain by using a non-orthogonal, body-fitted coordinate transformation scheme. Typical coordinate

transformations of this type are:

$$\zeta = x; \eta = \frac{r - r_c(x)}{r_w(x) - r_c(x)} \; ; \; \tau = t \tag{18}$$

where $r_c(x)$, $r_w(x)$ denote the inner and outer wall distances from the system centerline. If there is no inner wall or no center body, $r_c(x)$ is set to zero. The mapping functions are single-valued, and the following relations between the derivatives in the physical domain and the computational domain are obtained by the chain-rule of calculus:

$$\frac{\partial}{\partial t} = \frac{\partial}{\partial \tau}$$

$$\frac{\partial}{\partial x} = \frac{\partial}{\partial \zeta} + \alpha \frac{\partial}{\partial \eta}$$

$$\frac{\partial}{\partial r} = \beta \frac{\partial}{\partial \eta}$$

where $\alpha = \beta[(\eta - 1)\frac{dr_c}{dx} - \eta \frac{dr_w}{dx}]$, $\beta = \frac{1}{r_w - r_c}$. (19)

The computational domain grid shown in Figure 2 is rectangular and based on uniform spacing in the ζ and η direction. Note that $\Delta\zeta$ and $\Delta\eta$ are not necessarily equal. By using the coordinate transformation rules given above, the governing equation can be rewritten in the following form:

(a) Gas Phase

Continuity:
$$\frac{\partial \rho}{\partial \tau} + u \frac{\partial \rho}{\partial \zeta} + \bar{V} \frac{\partial \rho}{\partial \eta} + \rho \frac{\partial u}{\partial \zeta} + \rho\alpha \frac{\partial u}{\partial \eta} + \rho\beta \frac{\partial v}{\partial \eta} + \frac{\delta \rho v}{\overline{\eta}} = 0 \tag{20}$$

X-Momentum:
$$\frac{\partial u}{\partial \tau} + u \frac{\partial u}{\partial \zeta} + \bar{V} \frac{\partial u}{\partial \eta} + \frac{1}{\rho} \frac{\partial P}{\partial \zeta} + \frac{\alpha}{\rho} \frac{\partial P}{\partial \eta} = -A \frac{\rho_j}{\rho} (u - u_j) \tag{21}$$

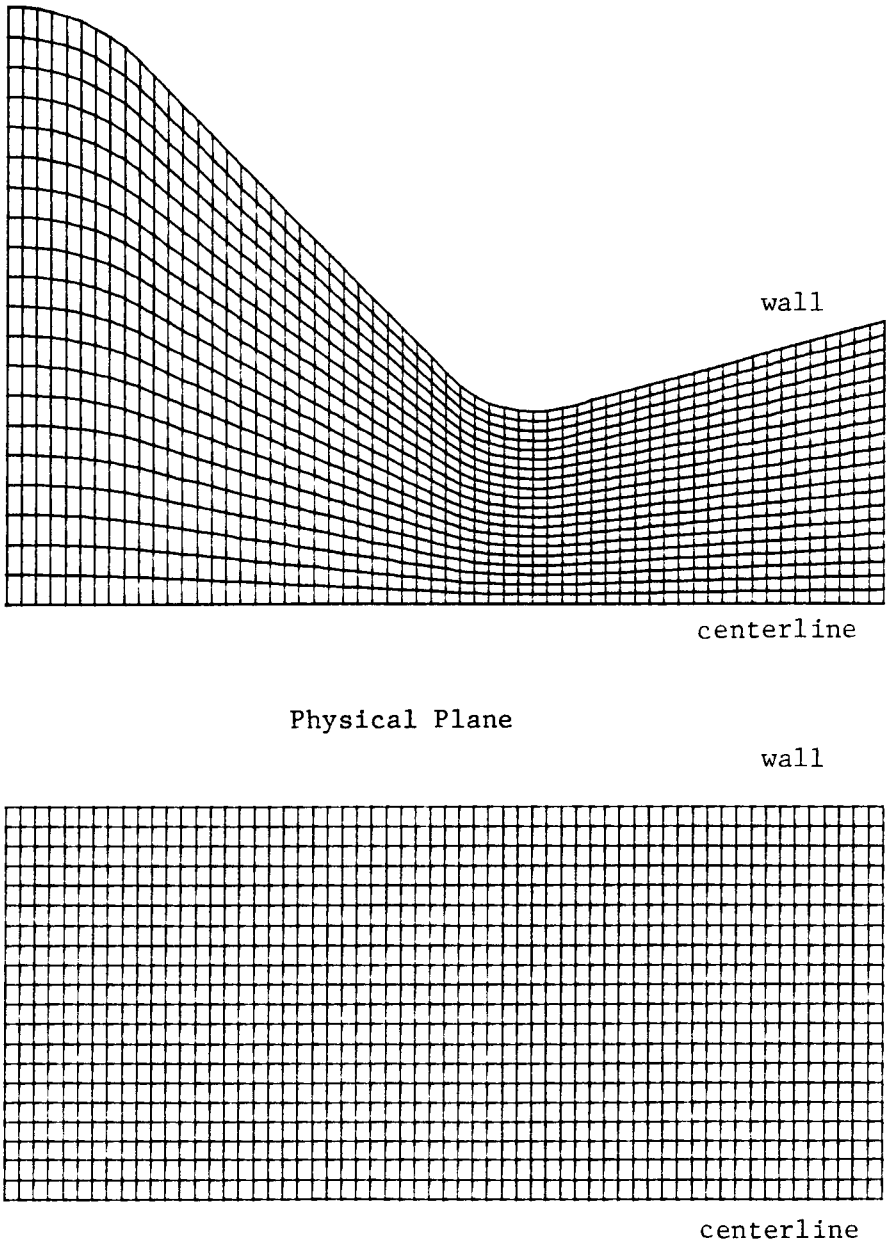


Figure 2. Physical Plane and Computational Plane.

R-Momentum: $$\frac{\partial v}{\partial \tau} + u \frac{\partial v}{\partial \zeta} + \bar{V} \frac{\partial v}{\partial \eta} + \frac{\beta}{\rho} \frac{\partial P}{\partial \eta} = -A \frac{\rho_j}{\rho} (v - v_j) \tag{22}$$

Energy: $$\frac{\partial P}{\partial \tau} + u \frac{\partial P}{\partial \zeta} + \bar{V} \frac{\partial P}{\partial \eta} - a^2 \left(\frac{\partial \rho}{\partial \tau} + u \frac{\partial \rho}{\partial \zeta} + \bar{V} \frac{\partial \rho}{\partial \eta}\right) = AB\rho_j \tag{23}$$

(b) Particle Phase

Continuity: $$\frac{\partial \rho_j}{\partial \tau} + u_j \frac{\partial \rho_j}{\partial \zeta} + \bar{V}_j \frac{\partial \rho_j}{\partial \eta} + \rho_j \frac{\partial u_j}{\partial \zeta} + \rho_j \alpha \frac{\partial u_j}{\partial \eta}$$

$$+ \rho_j \beta \frac{\partial v_j}{\partial \eta} + \frac{\delta \rho_j v_j}{\bar{\eta}} = 0 \tag{24}$$

X-Momentum: $$\frac{\partial u_j}{\partial \tau} + u_j \frac{\partial u_j}{\partial \zeta} + \bar{V}_j \frac{\partial u_j}{\partial \eta} = A(u - u_j) \tag{25}$$

R-Momentum: $$\frac{\partial v_j}{\partial \tau} + u_j \frac{\partial v_j}{\partial \zeta} + \bar{V}_j \frac{\partial v_j}{\partial \eta} = A(v - v_j) \tag{26}$$

Energy: $$\frac{\partial T_j}{\partial \tau} + u_j \frac{\partial T_j}{\partial \zeta} + \bar{V}_j \frac{\partial T_j}{\partial \eta} = D \tag{27}$$

Where $$\bar{V} = \alpha u + \beta v, \quad \bar{\eta} = r = \frac{1}{\beta} \eta + r_c, \quad a^2 = \frac{\gamma P}{\rho}, \quad \gamma = \frac{C_P}{C_v}$$

$$\bar{V}_j = \alpha u_j + \beta v_j$$

$$a = \beta\left[(\eta - 1)\frac{\partial r_c}{\partial x} - \eta \frac{\partial r_w}{\partial x}\right], \quad \beta = \frac{1}{r_w - r_c} . \tag{28}$$

Finite Difference Approximation

At present, many numerical methods have been developed for solving problems in non-linear continuum mechanics. But finite difference methods available for solving fluid flow problems are more popular, more developed, and often preferred to those based on finite element theory. In the present research work, the 1969 explicit, unsplit MacCormack [26] predictor-corrector finite difference scheme was applied to solve the

governing equations. The computational plane grid points are divided into interior and boundary points. The boundary grid points can be further identified depending on whether they are inlet boundary, exit boundary or wall boundary points.

The interior grid points are computed using the MacCormack second-order, noncentered, unsplit, two-step, finite difference scheme. Backward and forward differences are used in the respective predictors and corrector steps. As an example of the basic scheme, the finite difference equation for the predictor step in equation (21) is given

$$\overline{u^{N+1}_{L,M}} = u^{N}_{L,M} - \Delta\tau\left[u^{N}_{L,M}\left(\frac{u^{N}_{L,M}-u^{N}_{L-1,M}}{\Delta\zeta}\right) + \bar{V}^{N}_{L,M}\left(\frac{u^{N}_{L,M}-u^{N}_{L,M-1}}{\Delta\eta}\right)\right.$$

$$+ \frac{1}{\rho^{N}_{L,M}}\left(\frac{P^{N}_{L,M}-P^{N}_{L-1,M}}{\Delta\zeta}\right) + \frac{\alpha^{N}_{L,M}}{\rho^{N}_{L,M}}\left(\frac{P^{N}_{L,M}-P^{N}_{L,M-1}}{\Delta\eta}\right)$$

$$\left. + A^{N}_{L,M}\frac{\rho j^{N}_{L,M}}{\rho^{N}_{L,M}}\left(u^{N}_{L,M}-u j^{N}_{L,M}\right)\right] , \tag{29}$$

the finite-difference form for the corrector step in equation (21) is

$$u^{N+1}_{L,M} = 0.5\left\{u^{N}_{L,M}+\overline{u^{N+1}_{L,M}} - \Delta\tau\left[\overline{u^{N+1}_{L,M}}\left(\frac{\overline{u^{N+1}_{L+1,M}}-\overline{u^{N+1}_{L,M}}}{\Delta\zeta}\right) + \overline{\bar{V}^{N+1}_{L,M}}\left(\frac{\overline{u^{N+1}_{L,M+1}}-\overline{u^{N+1}_{L,M}}}{\Delta\eta}\right)\right.\right.$$

$$+ \frac{1}{\overline{\rho^{N+1}_{L,M}}}\left(\frac{\overline{P^{N+1}_{L+1,M}}-\overline{P^{N+1}_{L,M}}}{\Delta\zeta}\right) + \frac{\overline{\alpha^{N+1}_{L,M}}}{\overline{\rho^{N+1}_{L,M}}}\left(\frac{\overline{P^{N+1}_{L,M+1}}+\overline{P^{N+1}_{L,M}}}{\Delta\eta}\right)$$

$$\left.\left. + \overline{A^{N+1}_{L,M}}\frac{\overline{\rho j^{N+1}_{L,M}}}{\overline{\rho^{N+1}_{L,M}}}\left(\overline{u^{N+1}_{L,M}} - \overline{u j^{N+1}_{L,M}}\right)\right]\right\} , \tag{30}$$

where the subscripts L and M denote axial and radial grid points respectively; the superscript N denotes the time step, the bar denotes

the temporary time step between N and N + 1. If no centerbody exists in the computational plane, the centerline or midplane grid points are forced to be symmetric. The L'Hopital's rule, and a one-sided finite difference scheme in the η direction are used to connect those points to interior points.

Boundary Conditions

Due to the importance of the treatment of boundary conditions, many authors have attempted to deal with this problem. Roache [27] devotes a significant part of his monograph to this topic. H. C. Yee [28] presented a technical report in which the well-posedness and stability analysis of difference approximation for initial and boundary value problems are discussed. In his report, the analytical boundary conditions of partial differential equation and the numerical boundary conditions formulated for the analogous finite difference equations are discussed. For the different types of inlet and exit conditions in gasdynamic problems, several possible well-posed conditions are proposed. In Yee's conclusions, spatial linear extrapolation as a boundary scheme can produce reasonable steady-state solutions. Another valuable discussion about the boundary treatment for multistep finite difference methods of time-dependent equation was presented by Eli Turkel and David Gottlieb [29]. In their study, the theory of Kreiss [30] was used to test the stability of various boundary treatments for both the Richtmyer and MacCormack methods. Six groups of methods for treating the boundary condition formulations were discussed. From their results, the use of a one-sided Euler method led to instabilities. Specifying

the analytically given variables at predictor and corrector steps for the MacCormack method improved the accuracy. These authors and many others have shown that formulation of the numerical boundary conditions for complicated problems like the present two phase compressible flow is difficult to analyze by methods of pure mathematics and analysts must often resort to numerical experimentation to formulate stable, accurate boundary or initial condition functions. Especially, in the present study, it was found that the boundary conditions for particle concentration were extremely important in terms of their effects on stability and global particle mass conservation accuracy. Based on extensive analysis and numerical experimentation, the following boundary treatments were described.

Inlet grid points. Because the entrance flow is subsonic in the present study, two different boundary condition options are available. The first option was proposed by Serra [31]. He specified the total pressure P_T, total temperature T_T and flow angle θ at the inlet grid points. The second option, which was discussed by Oliger and Sundstrom [32], specified u, v, and ρ. A discussion of the relative merits of boundary conditions was given by Cline [33]. He felt that both boundary conditions were correct and that the best choice was problem-dependent.

In order to satisfy the numerical boundary requirement, Moretti and Abbett [34] suggested that all the unspecified dependent variables be computed using a second-order accurate, reference-plane characteristic scheme. In this scheme, the partial derives with respect to η are computed in the initial-value and solution surfaces using noncentered

differencing as in the MacCormack scheme. The gas-particle interaction terms and their derivatives are treated as source terms, and the resulting system of equations is solved, in the η = constant reference plane using a two-step, two-independent-variable characteristic scheme. A procedure was developed for deriving the characteristic relations that couple the interior points to the boundary points for the two phase flow in the present study and is similar to the method of Cline [25]. It is shown in Appendix D. The characteristic relation is written as:

$$dP - \rho a du = (a^2\psi_1 - \rho a\psi_2 + \psi_4)\, d\tau$$

$$\text{on the curve } d\zeta = (u - a)d\tau, \tag{31}$$

where the first equation is called the compatibility equation and the second is called the characteristic curve equation.

For the boundary condition scheme in which u, v and ρ are specified, the pressure can be calculated from equation (31). If P_T, T_T and θ are specified, the solution procedure is as follows: local Mach number, M, is assumed, P and T are calculated from P_T and T_T; ρ is calculated from the equation of state, u is calculated from equation (31), v is calculated from the specified flow angle θ. Then a new M is calculated from u, v, P and ρ, and the process is continued until the change in M has converged to 10^{-3}.

After the gas phase inlet variables have been obtained, the velocity and temperature of the particle phase can be calculated by assuming they are proportional to those of the gas phase. In particular, for example, they can be selected as equal to the gas phase values. The concentration of particle phase is calculated from the specified particle mass fraction. On the other hand, the data defining the particle

inlet conditions may be available. Thus prescribed boundary conditions for the particle phase can be directly input from known data and easily handled by the computer program. Even though the present study does not cover cases of supersonic inflow, the specified boundary conditions for this inlet condition have been set up in the program.

Exit grid points. The numerical treatment of exit boundary values in the present study is the same as that of VNAP developed by Cline [25]. Even though the results in the following chapter are restricted to the cases of supersonic outflow, the exit boundary can be a subsonic outflow/reverse flow, or a supersonic flow or mixed. For subsonic flow, a reference-plane characteristic scheme similar to the inlet scheme can be used. The characteristic relations that relate the interior points to the exit points are shown in Appendix D. They can be written as:

$$\left.\begin{aligned} dP - a^2 d\rho &= \psi_4 d\tau \\ dv &= \psi_3 d\tau \end{aligned}\right\} \text{on } d\zeta = u d\tau \qquad (32)\ (33)$$

and

$$dP + \rho a du = (a^2\psi_1 + \rho a \psi_2 + \psi_4)d\tau \quad \text{on } d\zeta = (u + a)d\tau. \qquad (34)$$

The static pressure is specified and u, v and ρ are calculated from the above equations. If subsonic reverse flow occurs at the exit plane, inflow boundary conditions must be specified across the region of reverse flow. In the present work, this is accomplished by leaving p equal to the specified exit pressure, setting ρ equal to the average of the wall and centerline, and setting v equal to zero. The arbitrary

conditions for the ρ and v can be easily changed by modifying subroutine EXITT.

For supersonic flow, the exit points are computed by extrapolation from upstream interior field points. Linear, space extrapolations for gas phase variables (ρ,u,v,P) and particle phase variable (ρ_j,u_j,v_j,T_j) are applied to supersonic outflow cases. As an example, the finite difference form for axial velocity, u, was taken as:

$$u_{i,j} = 2u_{i-1,j} - u_{i-2,j} \tag{35}$$

where (i-1,j) and (i-2,j) are the interior points which relate to the exit point (i,j).

Wall grid points. For the impermeable and adiabatic wall, slip conditions for both gas phase and particle phase were applied to calculations of inviscid gas-particle flow. All flow variables, except particle concentration, were computed by a reference-plane characteristic scheme. The characteristic relations that relate the interior flow to the wall are derived in Appendix C, and can be written as:

$$\left.\begin{aligned} dP - a^2 d\rho &= \psi_4 d\tau \\ \beta du - \alpha dv &= (\beta\psi_2 - \alpha\psi_3)d\tau \end{aligned}\right\} \text{for } d\eta = \bar{V}d\tau \tag{36, 37}$$

$$dP + \frac{\rho\alpha a du}{\alpha^*} + \frac{\rho\beta a}{\alpha^*} dv = (\psi_4 + a^2\psi_1 + \frac{\rho\alpha a\psi_2}{\alpha^*} + \frac{\rho\beta a\psi_3}{\alpha^*})d\tau \tag{38}$$

$$\text{for } d\eta = (\bar{V} + a\alpha^*)d\tau$$

$$\left.\begin{aligned} du_j &= \psi_6 d\tau \\ dT_j &= \psi_8 d\tau \end{aligned}\right\} \text{for } d\eta = \bar{V}_j d\tau. \tag{39, 40}$$

These equations can be written in finite difference form in the same way as those for the inlet or exit schemes. By using the slip condition and the characteristic relations, the variables (u,v,P,ρ) for the gas and (u_j,v_j,T_j) for the particles can be specified on the wall.

For gas-particle flow in a conical nozzle, two approaches, the particle continuity equation, and an extrapolation technique, were used to calculate the particle concentration on the wall. For small particle sizes, such as 1μ, the continuity equation for the particle concentration was written in finite difference form in which a backward-forward difference in x-direction and backward difference in r-direction were applied. The results obtained by this approach were very good. However, strong oscillations appeared in particle concentration for the cases with larger size particles. These oscillations make the solution unstable. In order to cancel these oscillations, the following two methods were tried which produced unacceptable results. The first attempt specified concentration on the wall as the average value taken from points which surround the wall grid point. The oscillations disappeared, but physically implausible distributions began to form in the interior points. The second attempt was to throw out the assumption of slip condition for the particle on the wall. The continuity, momentum and energy equations for the particle phase were rewritten using a finite difference scheme which was backward in η direction and backward-forward in ζ direction. When this method was applied, the numerically computed results became worse. Based on further analysis, space extrapolation for the wall particle concentration (which was similar to

groups I and V in reference 29) and the slip wall, tangent velocity conditions were reintroduced. By using this kind of treatment, the numerical oscillations were suppressed. To illustrate the effects of different boundary treatments for wall particle concentration, space extrapolation and continuity equation, the mass, momentum and energy flux through inlet, throat and exit were studied and the results were presented in Table 1. It is easy to see that the numerical differences between those two boundary treatments are small. In other words, the numerical accuracy is preserved by using the extrapolation scheme for the particle concentration. In this study, therefore, a space extrapolation scheme was applied to overcome numerical oscillation problems.

Initial Conditions, Stability and Convergence Criteria

Several discussions about the initial conditions have been presented by previous authors, such as Roache [27], Moretti [35] and Cline [33]. According to the discussion of Roache, the initial condition problems seem to be more critical in supersonic flow than in low speed flow. Several examples in the literature have shown that a poor guess of the initial condition can cause the numerical instability. If only the steady state solutions are of interest, Roache [27] suggested three methods to reduce the affects of poor guesses for initial conditions. For subsonic flow, Moretti [35] claimed that the initial data surface and boundary conditions must be matched so that the transient part of a steady state calculation follows the true transient solution. Cline [33] felt that this is generally not sufficiently economical, even though the treatment of Moretti is the most correct way to formulate

Table 1

Data Analysis for Two Phase Flow with Different Wall Conditions[a]

Station of Calculation	Type of Conditions	$\int \rho u dA$[b]	$\int \rho_j u_j dA$[c]	$\int_{inlet} (p+\rho u^2+\rho_j u_j^2)dA + \int_{inlet}^{x} P_w \frac{dA}{dx} dx$[d]	$\int (h+1/2 \mid \vec{v} \mid^2)\rho u dA + \int (h_j+1/2 \mid \vec{v}_j \mid^2)\rho_j u_j dA$[e]
Inlet	Continuity[f]	4.1011	1.7576	2956.41	1625.28
	extrapolation	4.0924	1.7539	2956.35	1621.83
Throat	Continuity[f]	4.1133	1.6944	383.52	1594.33
	extrapolation	4.1251	1.6583	383.97	1585.57
Exit	Continuity[f]	4.1596	1.7158	445.3	1600.18
	extrapolation	4.1695	1.6912	445.5	1594.63

[a]Two phase flow (1μ, 30%) passing through the conical nozzle is treated by different wall conditions about the particle concentration.

[b]Gas mass flow rate across the section.

[c]Particle mass flow rate across the section.

[d]Force.

[e]Energy.

[f]The continuity equation of particle phase is applied in this type of condition.

problems. In the present study, one dimensional relations were selected as the initial conditions of 2-D gas flow. After the steady state solution of gas phase flow has been obtained by the MacCormack method, the initial condition for the two phase flow was assumed according to the idea of Chang [10]. The relations are written as:

$$\rho_j = \rho \frac{\phi}{1-\phi} \ , \ u_j = \lambda_v u, \ v_j = \lambda_v v, \ T_j = \frac{T}{\lambda_T} \ . \tag{41}$$

Because the unsplit MacCormack method, which is used in the present work, is conditionally stable, the time step $\Delta\tau$, which is based the Courant-Friedrich-Lewy (CFL) criterion [36,37] must satisfy the restriction

$$\Delta\tau \leq \left(\frac{|u|}{\Delta\zeta} + \frac{|v|\beta}{\Delta\eta} + a \sqrt{\frac{1}{(\Delta\zeta)^2} + \frac{\zeta^2}{(\Delta\eta)^2}} \right)^{-1} \tag{42}$$

where a is the local speed of sound, and $\Delta\rho$, $\Delta\eta$ are the mesh intervals.

Many ideas on convergence criteria have been discussed by Roache [27]. He concluded that no satisfactory objective criterion exists for interactive convergence. In this study, the relative error criterion is used, such as

$$\underset{L,M}{\text{Max}} \left| \frac{u_{L,M}^{N+1} - u_{L,M}^{N}}{u_{L,M}^{N}} \right| < \varepsilon \tag{43}$$

where u represents the velocity component in x direction for the two phase flow. (L,M) are the grid points in the flow field and N is the time step. For most results shown in the following chapter, ε is equal to 10^{-4} and the convergence tolerance was satisfied on three consecutive time steps.

As mentioned earlier, the centrifugal forces acting on the particles as they accelerate through the nozzle tend to separate the particles from the walls into regimes of very high concentrations. This produces regimes where the particle concentration gradients are very large and they cannot be resolved with a single mesh system obtained by one transformation. This problem is similar to attempting to resolve a shock wave without artificial viscosity; that is, it leads to numerical oscillations and instability as the particle sizes increase.

In order to attempt to devise methods for handling this phenomenon with the present numerical scheme, three special techniques were developed and tested in the present study. The first thing tried was a fourth-order smoothing scheme similar to that proposed in reference 38. Also, it was decided to define the particle concentration as equal to zero once it had fallen below 1 percent of the inlet particle concentration values used for reference conditions. This kept negative particle concentrations from occurring in the calculation. Implementing these two ideas, some calculations were done. However, although the oscillation behavior was avoided, relatively large errors in global particle mass flux were incurred, some as great as about 11 percent particle mass flux deficits. The problem was traced to the fact that the differencing scheme for the interior points still was being applied to zones where the particle concentration was going from large values to zero. Thus the high gradient problem in particle concentration, even with smoothing, was leading to particle concentration errors. The way to cure this problem was found to be that one must limit the use of the

MacCormack scheme for the particle phase to the region inside or interior to the "limiting particle streamline", and not completely out to the wall. Thus, a routine, which sought out and identified the radial location of the limiting streamline for the particle phase at each axial location, was programmed. This streamline became the "wall" condition in the MacCormack scheme for the particle phase applied to all points interior to this streamline. For the gas phase, of course, the MacCormack scheme was continued out to the physical wall location. For the limiting particle streamline used as a moving pseudo-wall condition for the particle phase, the MacCormack scheme was modified to calculate the particle pseudo-wall boundary conditions. Based on the developing spatial definition of the limiting particle stream, one-sided backward, one-sided forward or backward-forward differences were used. The tangential velocity condition was not applied on the limiting particle streamline because the limiting particle streamline was only approximately located in the mesh.

Finally, by use of these three methods, fourth order smoothing, defining zero particle mass concentration zones, and using the pseudo-wall (limiting streamline) as a boundary for the application of the MacCormack scheme to particle phase, good solutions were obtained that preserved global particle mass flux and prevented unwanted numerical oscillations. These results are presented in a following chapter.

For several cases computed, time oscillation in the flow variables happened in the subsonic flow region (inlet conditions). In order to deal with this kind of problem, Cline [33] has introduced time smoothing procedures into VNAP2, a later version of his code. In his approach to

time smoothing, the flow variables at the present time step are weighted by those of last time step. By applying Cline's time smooth procedure in the present study, the time oscillation was damped and convergence was accelerated. The numerical effects of this kind of smoothing will be shown in the next chapter.

Viscous Gas-Particle Approach

The previous discussions concerned the numerical formulation for inviscid gas-particle flow. In order to study the viscous effects on two phase flow, additional numerical treatments were required.

Simple Effective Turbulent Viscosity Model

In this approach, the finite difference method is the same as that of inviscid gas-particle flow except for the inclusion of viscous terms. The second-order viscous terms for the interior grid points were calculated using centered difference in the initial-value plane only. Because the viscous terms were calculated only in the initial-value plane, they are second-order accurate in space but first-order accurate in time. To achieve second-order accuracy in time, the viscous terms should be re-evaluated by using the values from the results of the first time. Such a procedure for the calculation requires much larger amounts of computing time per time step. For most problems, this greater accuracy in time does not seem worth the increase effort, unless the transient solution is important.

Following the algorithm structure of the VNAP [25] code, the viscous terms were neglected on the inlet grid points for the subsonic

inflow condition. The reference-plane characteristic scheme is applied to inlet and exit plane if the flow is subsonic. On the exit plane, the η derivatives of the viscous terms were calculated using centered differences in the initial-value plane only.

A big difference between the inviscid and viscous codes is the numerical treatment on the wall conditions, where a no-slip condition is applied to the viscous gas phase. The wall density and pressure for the gas are calculated from the continuity equation and energy equation. The η derivatives, except in the viscous terms, are calculated using backward difference on both time steps. A reflection scheme is used to formulate the viscous terms on the wall. The energy equation which contains the temperature terms is applied such that the normal temperature gradient is set equal to zero on the wall, for simulating adiabatic conditions.

The slip condition and characteristic scheme for the particle phase are still used. Experience gained in the present study is that the velocity of the particle on the wall should be small. If the velocity of particles on the wall is too high, numerical instability can happen. This kind of numerical problem is caused by large values of the interaction terms between gas and particle which show up in the governing equation as $A(u-u_j)$. This is thought to be a problem due to too coarse a mesh, not able to resolve the physics near the walls.

Viscous-Inviscid Interaction Model

As mentioned before, the direct integral boundary layer method of Whitfield [24] was applied in this study. The computational method is a

combination of interior flow (governed by the inviscid equation) with boundary layer flow (governed by integral turbulent boundary layer equations). The governing equation for the turbulent boundary layer can be rewritten as:

$$\frac{d}{dx}\left(\frac{r_w\rho_e u_e^2\theta}{\rho_{oe}u_{oe}^2}\right) = 0.5\,\frac{r_w\rho_e u_e^2}{\rho_{oe}u_{oe}^2}\,C_f - \frac{r_w\rho_e u_e^2\theta}{\rho_{oe}u_{oe}^2}\,H_\delta^*\,\frac{1}{u_e}\frac{du_e}{dx} \tag{44}$$

$$\frac{d}{dx}\left(\frac{r_w\rho_e u_e^3\theta H_\theta^*}{\rho_{oe}u_{oe}^3}\right) = \frac{r_w\rho_e u_e^2}{\rho_{oe}u_{oe}^2}\,\frac{u_e}{u_{oe}}\,C_{fD} - 2.0\,\frac{r_w\rho_e u_e^2\theta}{\rho_{oe}u_{oe}^2}\,\frac{u_e}{u_{oe}}\,H_\delta^*\,\frac{1}{u_e}\frac{du_e}{dx}\ , \tag{45}$$

where the subscript o means the initial or starting point of turbulent boundary layer and e is the edge of the boundary layer. The method used to solve equations (44) and (45) is the predictor-corrector method used by Nash [39], with a constant value for the dx step size used in this study.

For the interaction between inviscid gas or gas-particle core flow and the turbulent boundary layer flow, an interation procedure was applied. It is shown in Figure 3. During the calculation of the inviscid core flow, the characteristic scheme for the gas on the wall was replaced by a modified MacCormack scheme. In this modified scheme, the variables u, ρ and P were calculated using the governing equations, in which the η derivatives were expressed as one-sided difference in the η direction and backward-forward difference in the ζ direction. The velocity component v was calculated from the following relation:

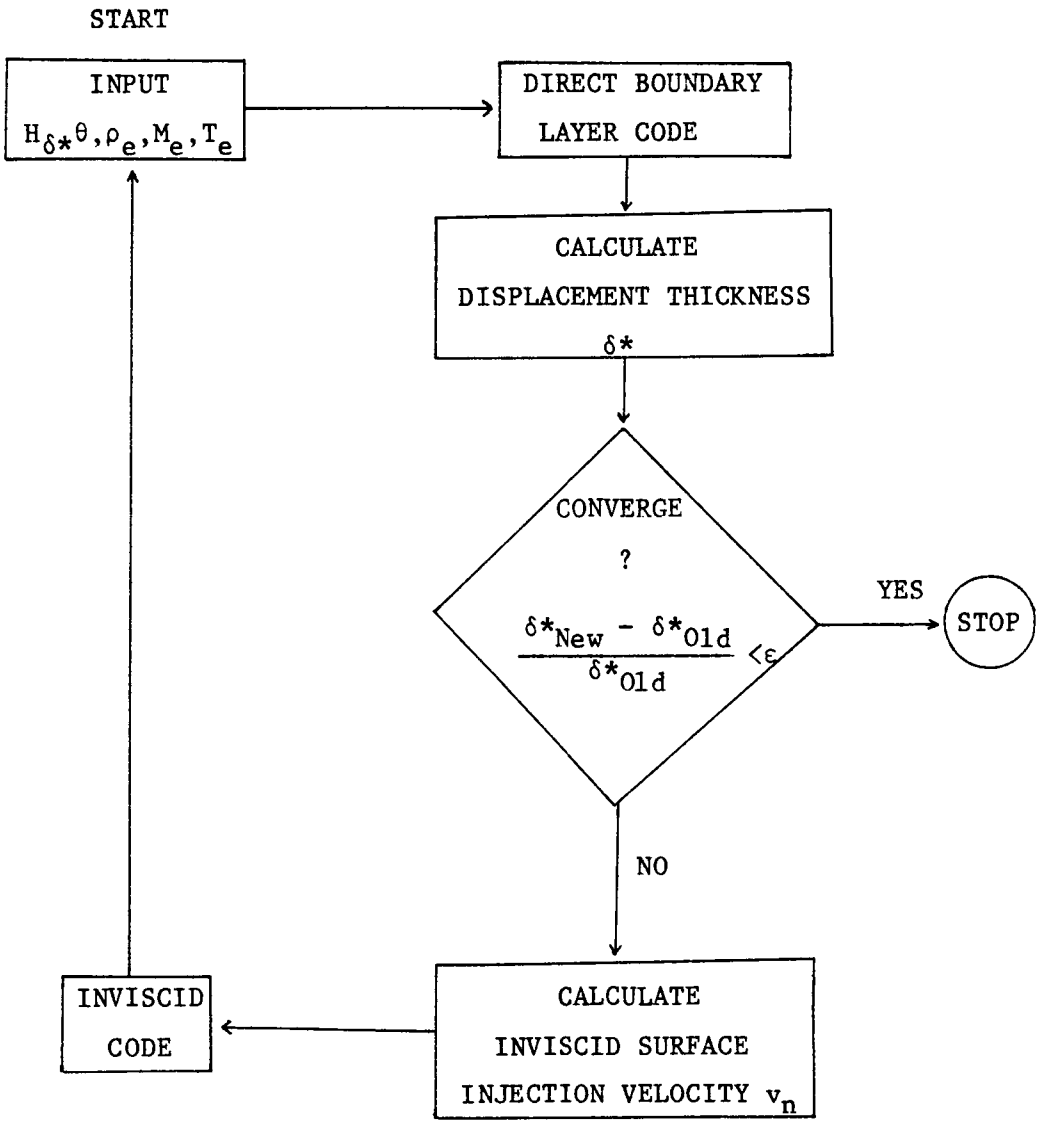


Figure 3. Iteration Procedure for Viscous-Inviscid Interaction Technique.

$$v = u\tan\theta - \frac{v_n}{\cos\theta} \tag{46}$$

where θ is the angle of wall and v_n a "displacement" velocity created by the presence of the turbulent boundary layer.

Because no experimental data were available for use as initial conditions for the turbulent boundary layer, an analytical formula deduced from the 1/7th power velocity distribution law for the smooth flat plate was applied. The mathematical forms provided by Schlichting [40] were used as follows:

$$\text{momentum thickness, } \theta(x) = 0.036 \times \left(\frac{u_e x}{\nu}\right)^{-1/5} \tag{47}$$

$$\text{shape factor, } H_\delta^* = \frac{9}{7} \, . \tag{48}$$

For the gas phase flow in CFFF, the effective length x is calculated from the inlet of the combustor, so that the initial value of x is equal to 7.5 inches in this calculation. In order to suppress numerical instability near the nozzle inlet contraction section, the above analytical expressions were applied at the wall from the inlet grid point to grid point 13. For two phase flow problems, the turbulent boundary layer effect is treated only downstream of the throat. The time-varying, converging values of gas phase flow at the throat were chosen as the initial conditions of two phase boundary layer calculations.

CHAPTER IV

NUMERICAL RESULTS AND DISCUSSIONS

Two Phase Flow in Conical Rocket Nozzle

The first step taken was to verify the code by setting it up to predict a flow reported in the literature by Chang [10]. Since Chang reported results for several configurations, one nozzle, which was similar to a JPL nozzle given in his paper, was adopted in the present study. This geometry is a circular-arc, conical nozzle (44.88-15 degrees) shown qualitatively in Figure 4. The coordinates of inlet, throat and exit are respectively (0.31, 2.50), (2.554, 0.8) and (4.05, 1.1832) in which the first numbers per number pair stand for axial coordinates in inches, and the second number is the radial coordinates. Also shown in Figure 4 is the numerical mesh used to develop the flow field. Because the nozzle was symmetrical, only the mesh in the upper half plane was actually used in the calculation.

The two phase flow data for Chang's case are as follows:

Gas Phase	Particle Phase
$C_p = 198.39 \frac{ft\text{-}lb_f}{lbm\text{-}^\circ R}$	$C_j = 256.74 \frac{ft\text{-}lb_f}{lbm\text{-}^\circ R}$
$\mu_o = 0.0559 \times 10^{-5} \frac{lb_f\text{-}sec}{ft^2}$	$m_j = 250 \frac{lbm}{ft^3}$
$\gamma = 1.4$	$r_j = 1\mu$ (radius)
$R = 53.35 \frac{ft\text{-}lb_f}{lbm\text{-}^\circ R}$	$\varepsilon_j = 0.1$
$Pr = 0.74$	$\phi = 30\%$

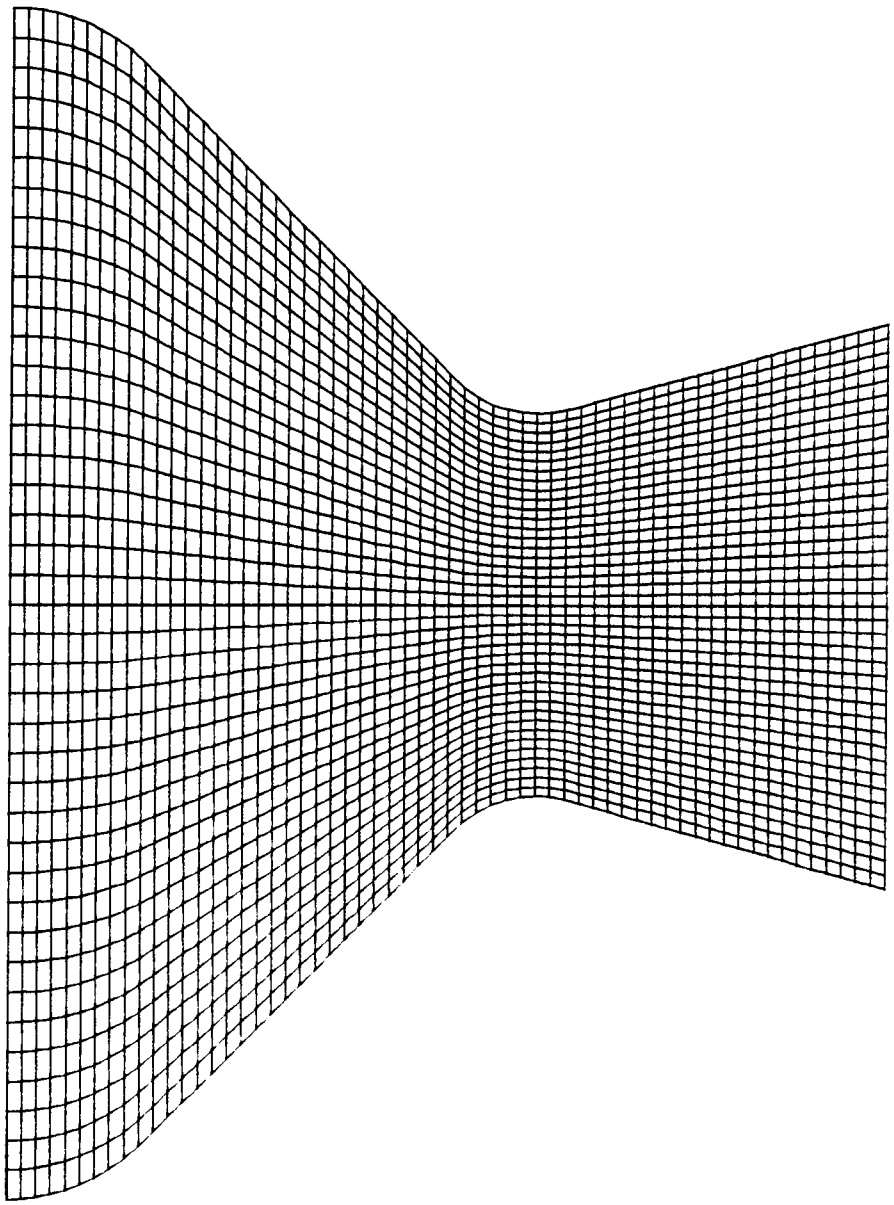


Figure 4. Grid for Conical Rocket Nozzle.

$A'' = 0.6$

$T_T = 1000.0°R$

$P_T = 150.0$ psia

$\mu = \mu_o \left(\frac{T}{T_T}\right)^{A''} \frac{lb_f\text{-sec}}{ft^2}$

$\varepsilon = 0.05$

Discussion of the Results

The results of the calculated flow through the conical nozzle are presented in Figures 5 - 17, where both particle laden and particle free (one phase) flows are compared for the same gas phase inlet conditions.

The gas density shown in Figure 5 is defined as the mass of gas per unit volume of gas, so that the gas concentration in Figure 6 is the mass of gas per unit volume of mixture. Because the volume of the particle phase in the mixture is neglected, the gas concentration is equivalent to the gas density in the two phase flow. The particle concentration distribution is shown in Figure 7 and it is easy to see that the mass of particles near the wall in the nozzle flow downstream of the throat is lower than anywhere else in the flow field. For the gas density shown in Figures 5 and 6, the distribution of gas density near the downstream wall is relatively uniform. The reason for the above phenomena is that the particle cannot adjust like the gas, thus the particles concentrate near the centerline in the downstream region because of centrifugal separation. Due to the existence of particle free zones,

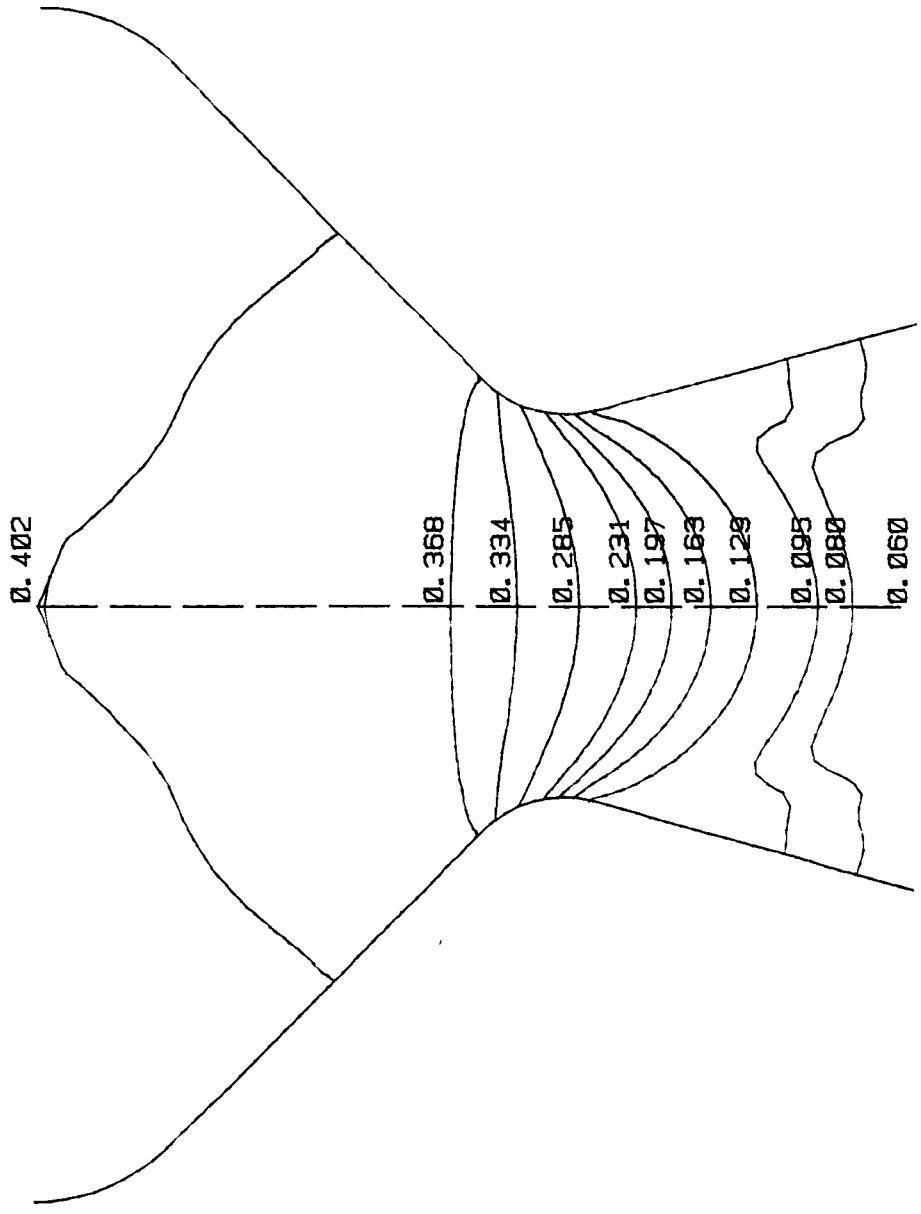


Figure 5. Gas Density Contour for One Phase Flow.

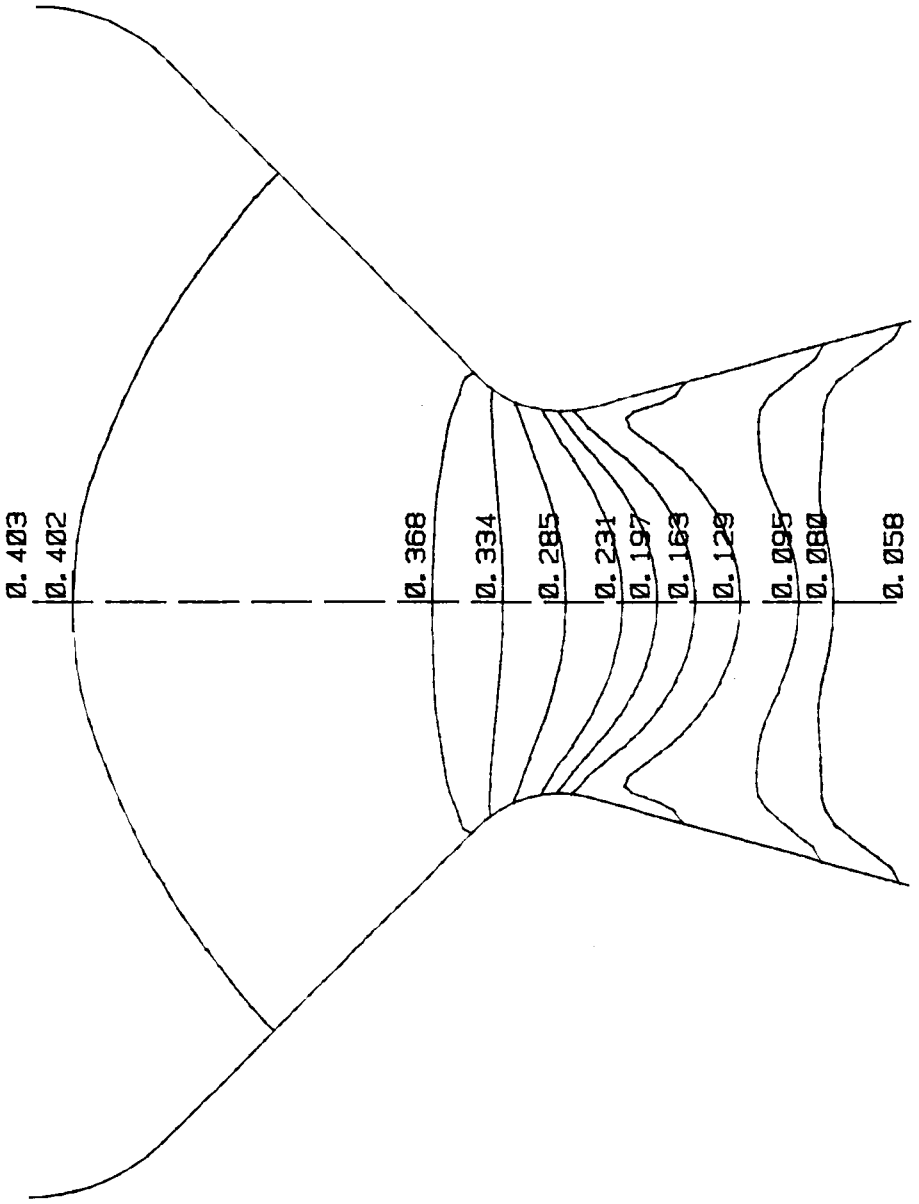


Figure 6. Gas Concentration Contour for Two Phase Flow.

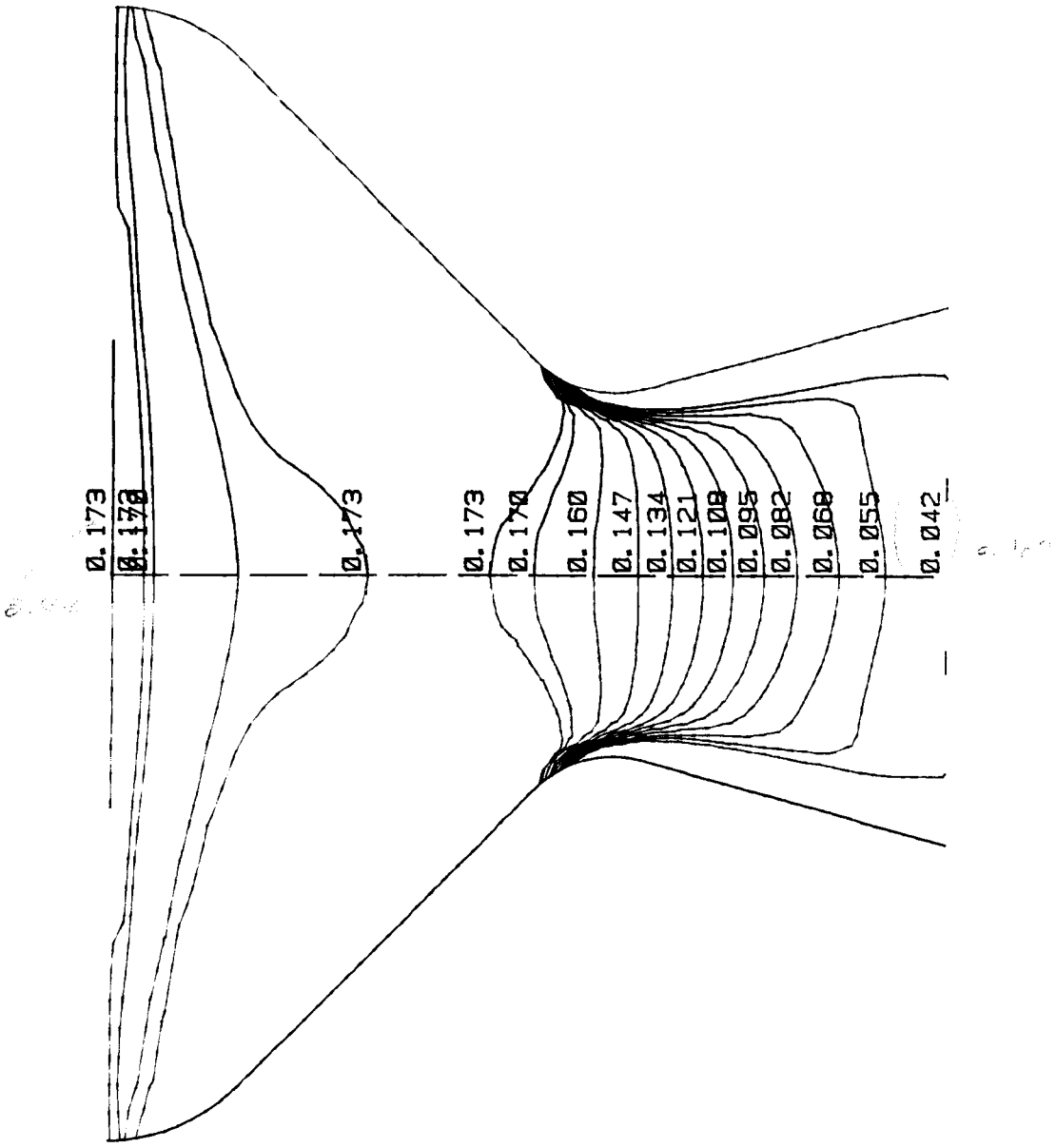


Figure 7. Particle Concentration Contour for Two Phase Flow.

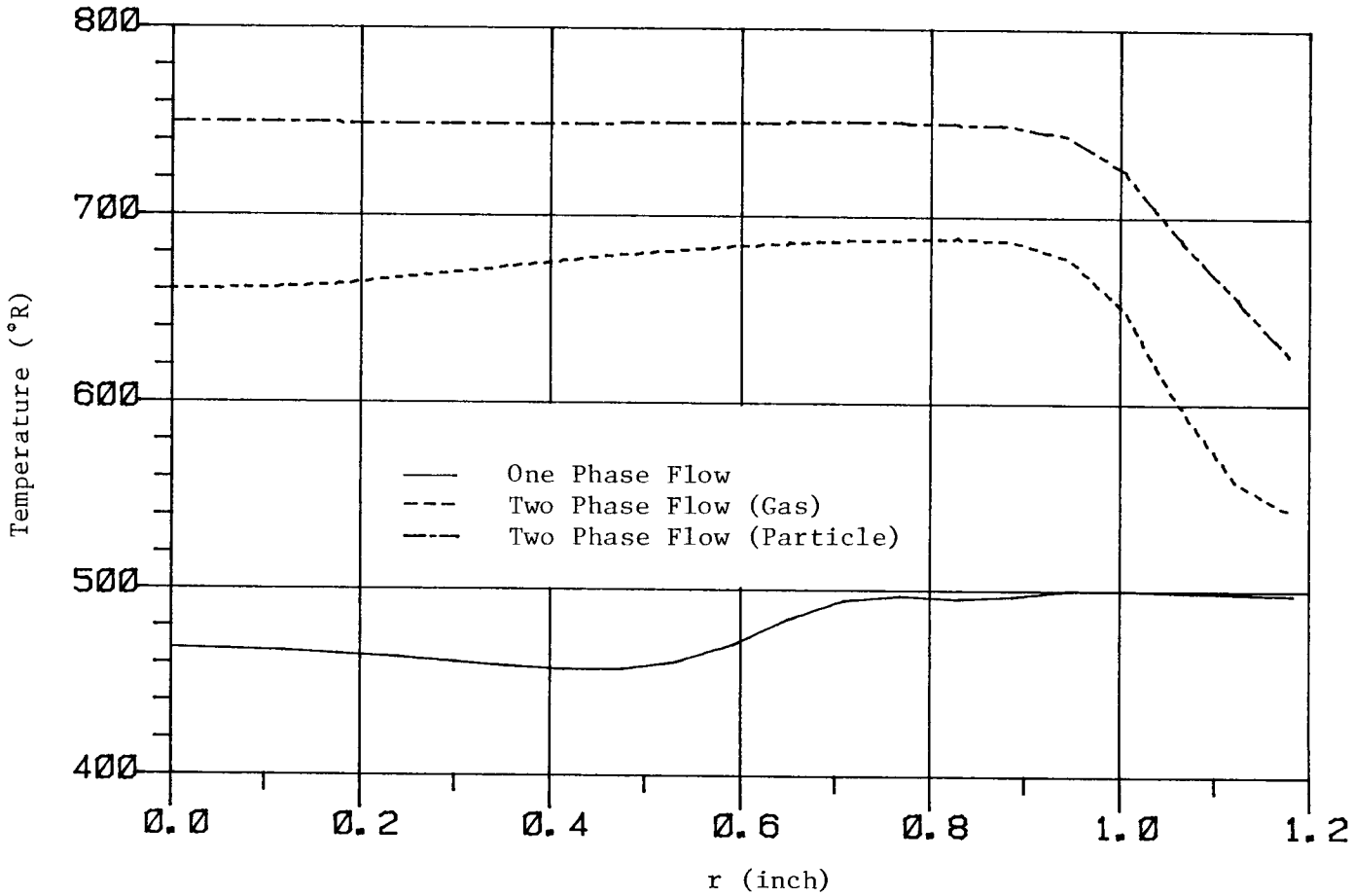


Figure 8. Temperature Distribution at the Nozzle Exit Plane.

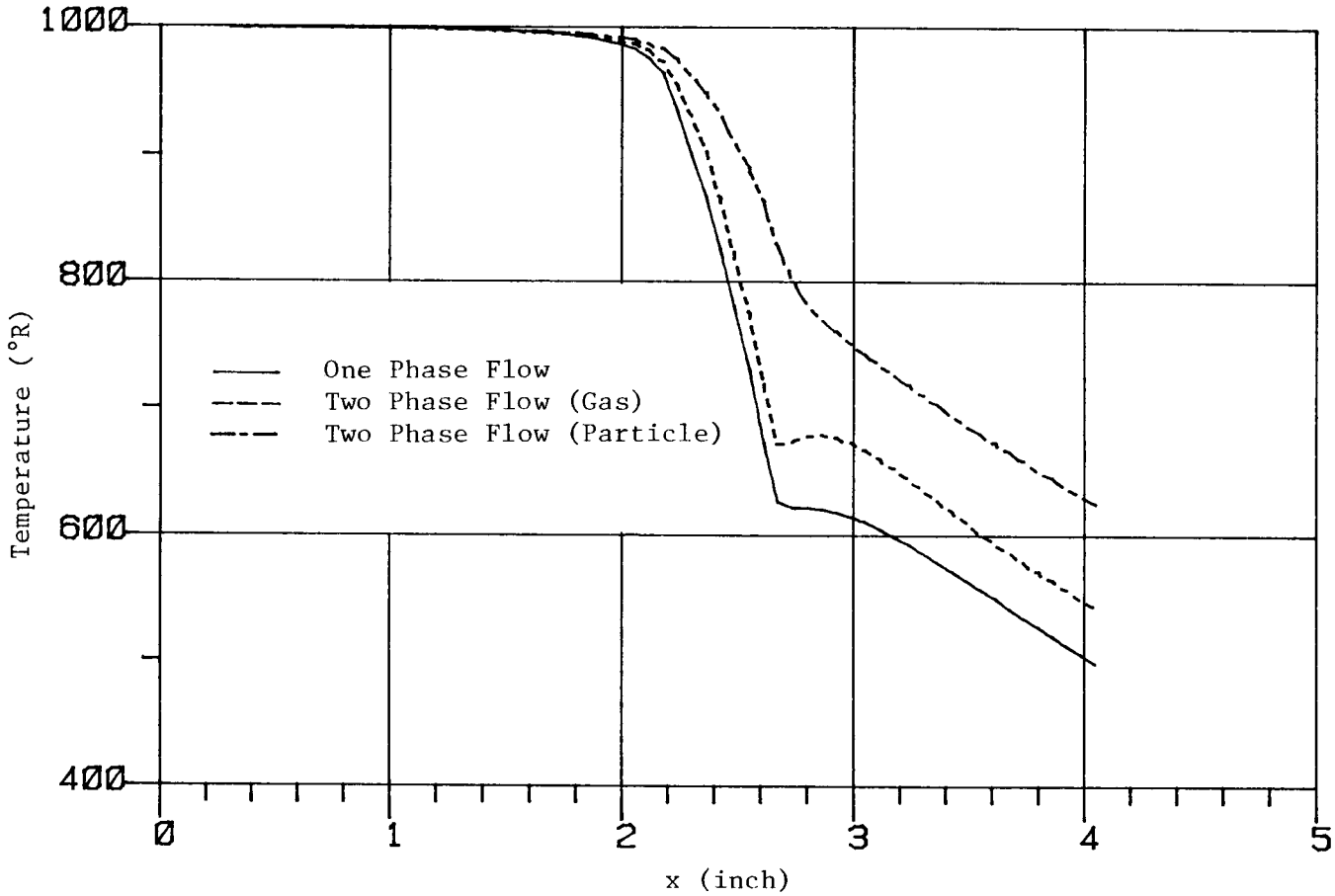


Figure 9. Temperature Distribution at the Nozzle Wall.

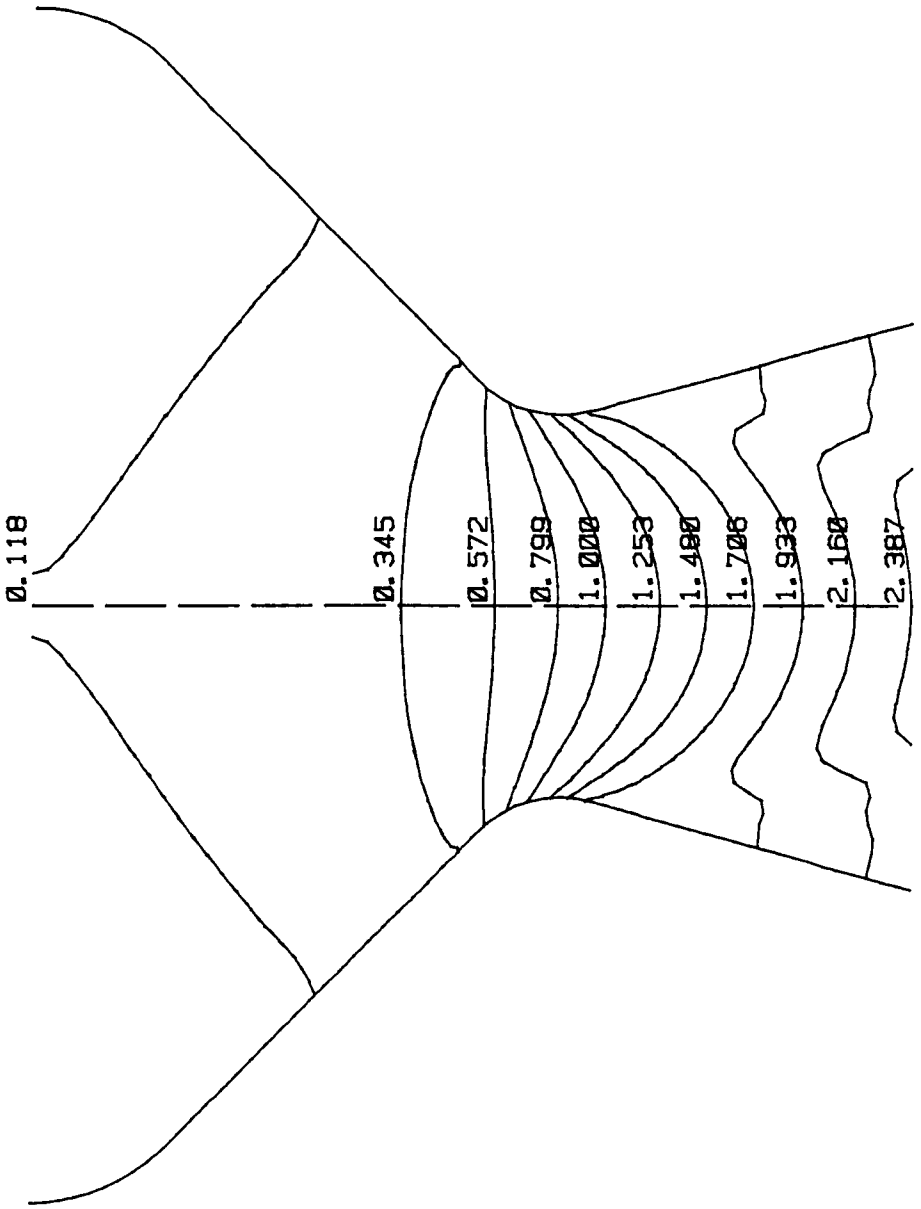


Figure 10. Mach Number Contour for One Phase Flow.

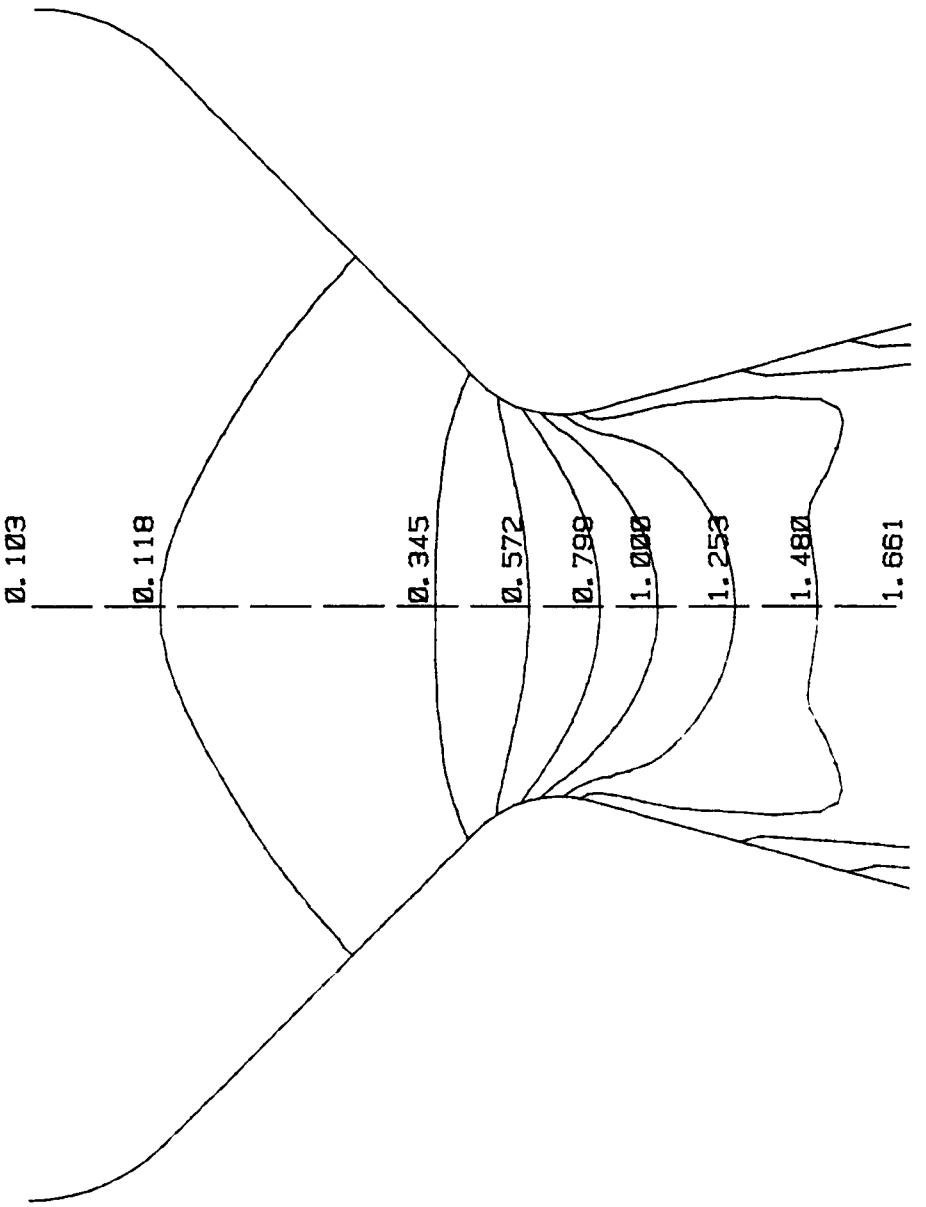


Figure 11. Mach Number Contour for Two Phase Flow.

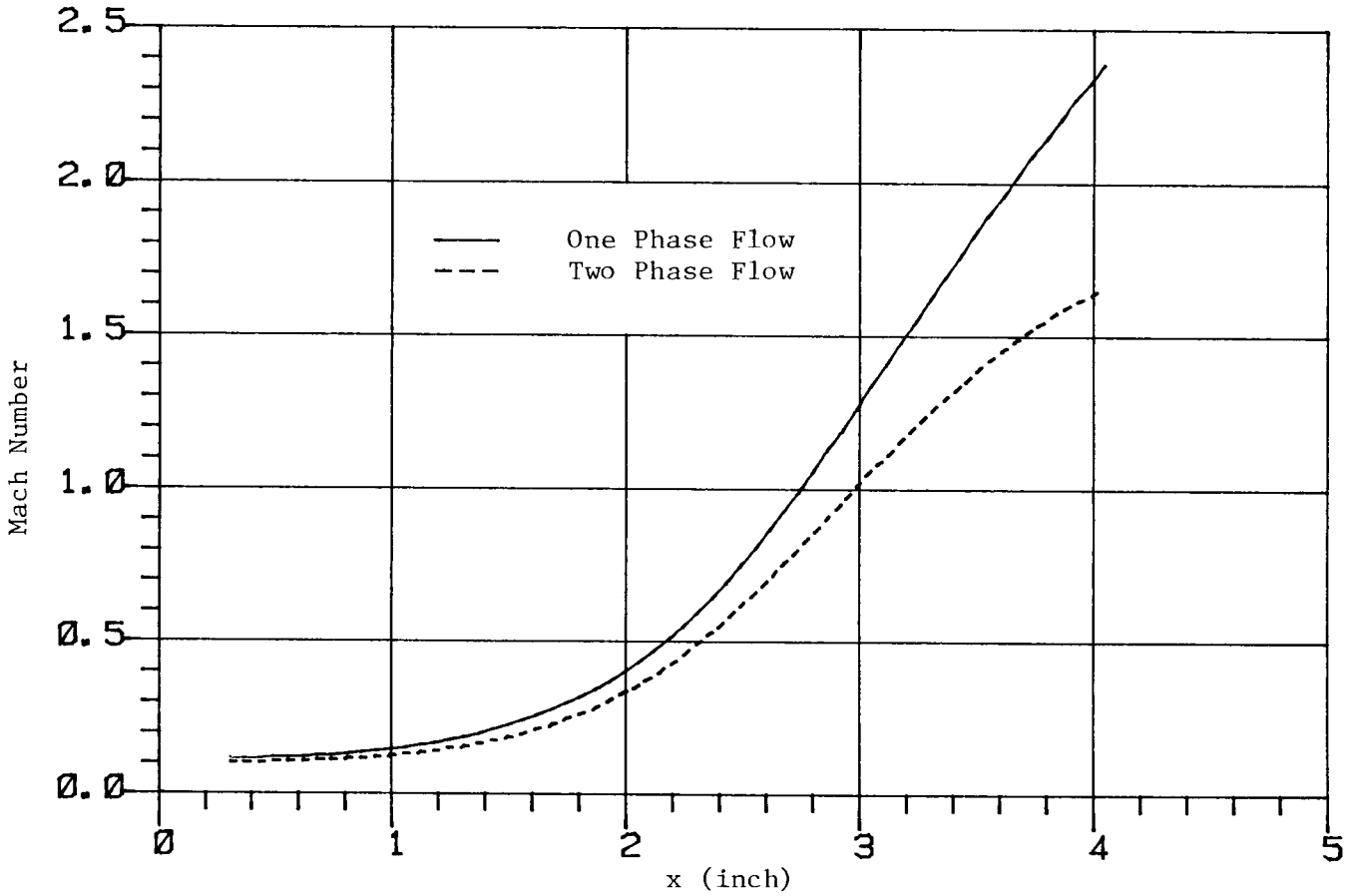


Figure 12. Mach Number Distribution at the Nozzle Centerline.

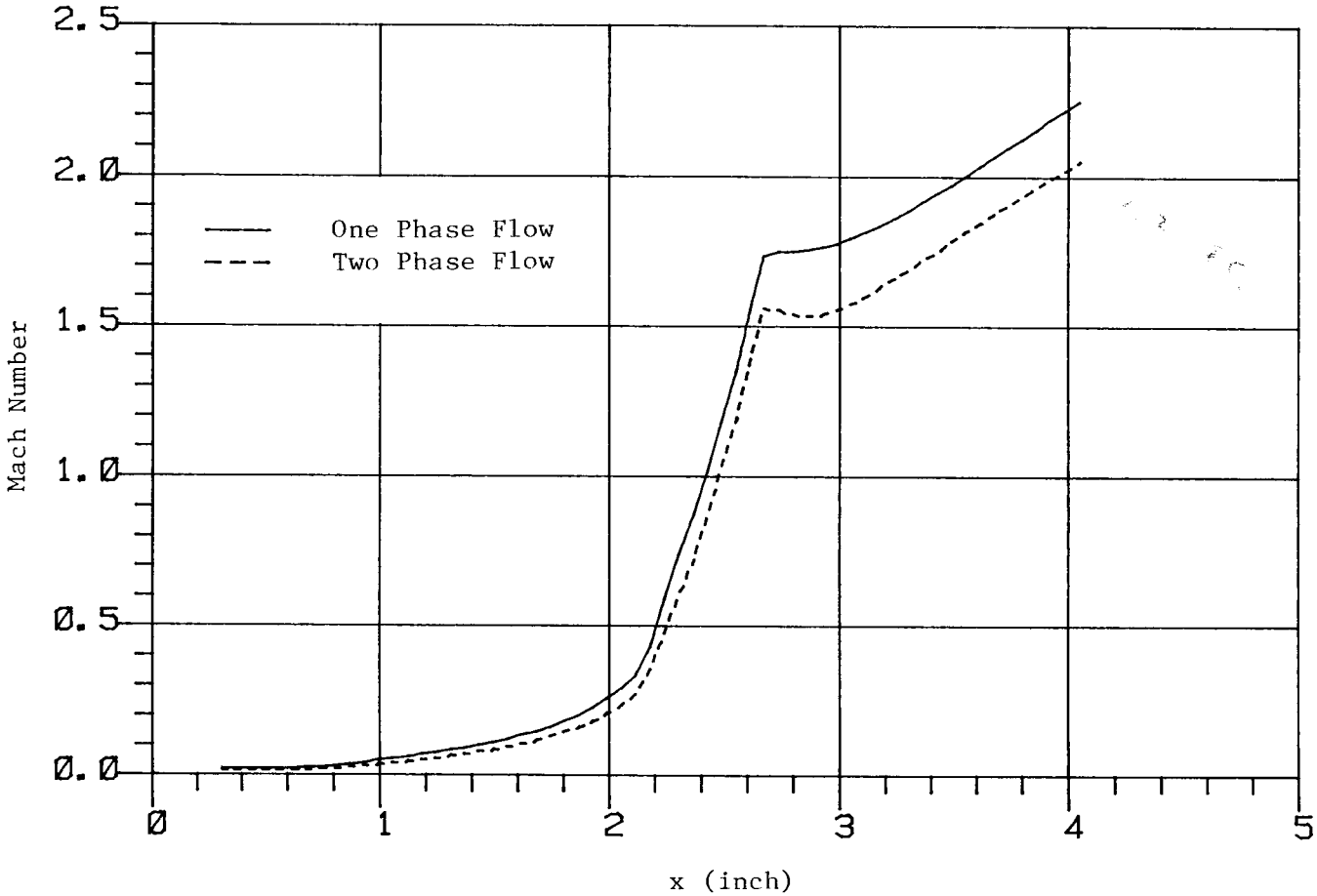


Figure 13. Mach Number Distribution at the Nozzle Wall.

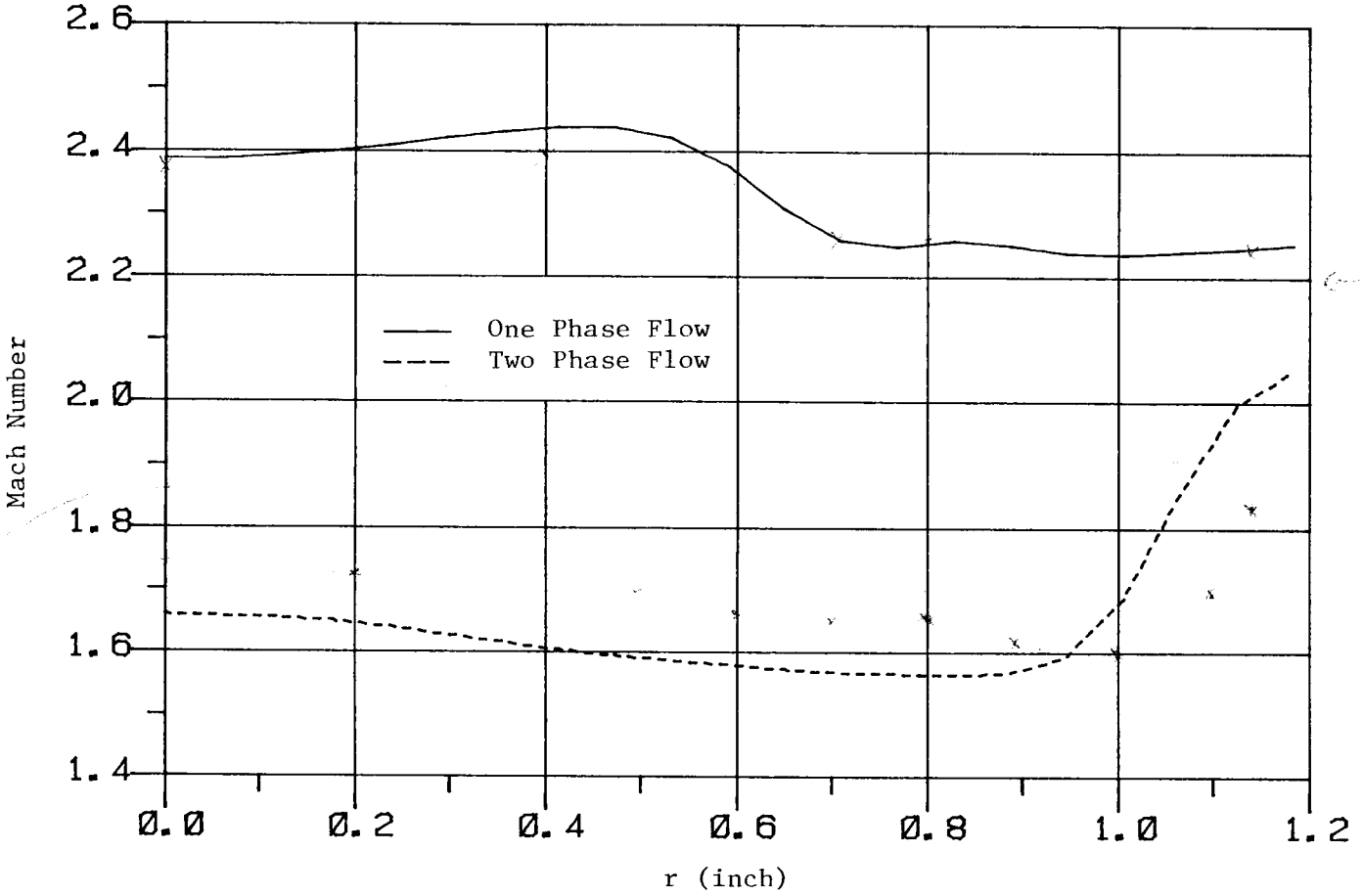


Figure 14. Mach Number Distribution at the Nozzle Exit Plane.

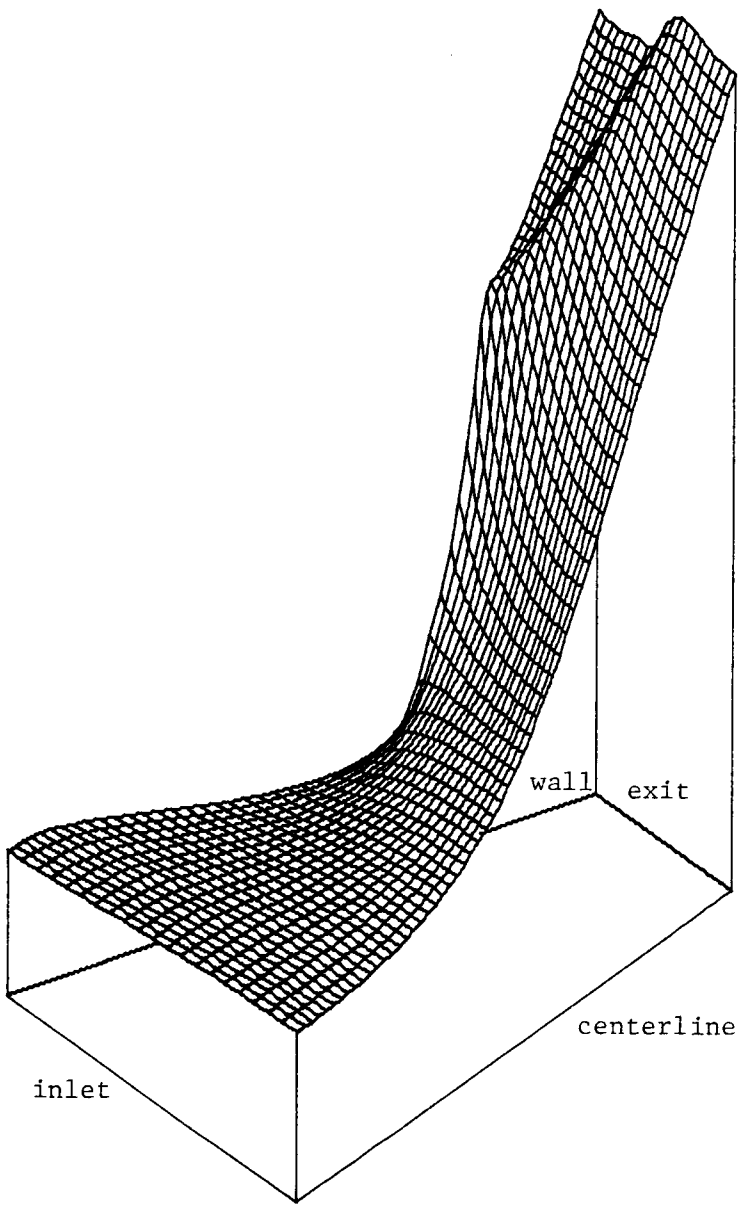


Figure 15. Mach Number Distribution for One Phase Flow.

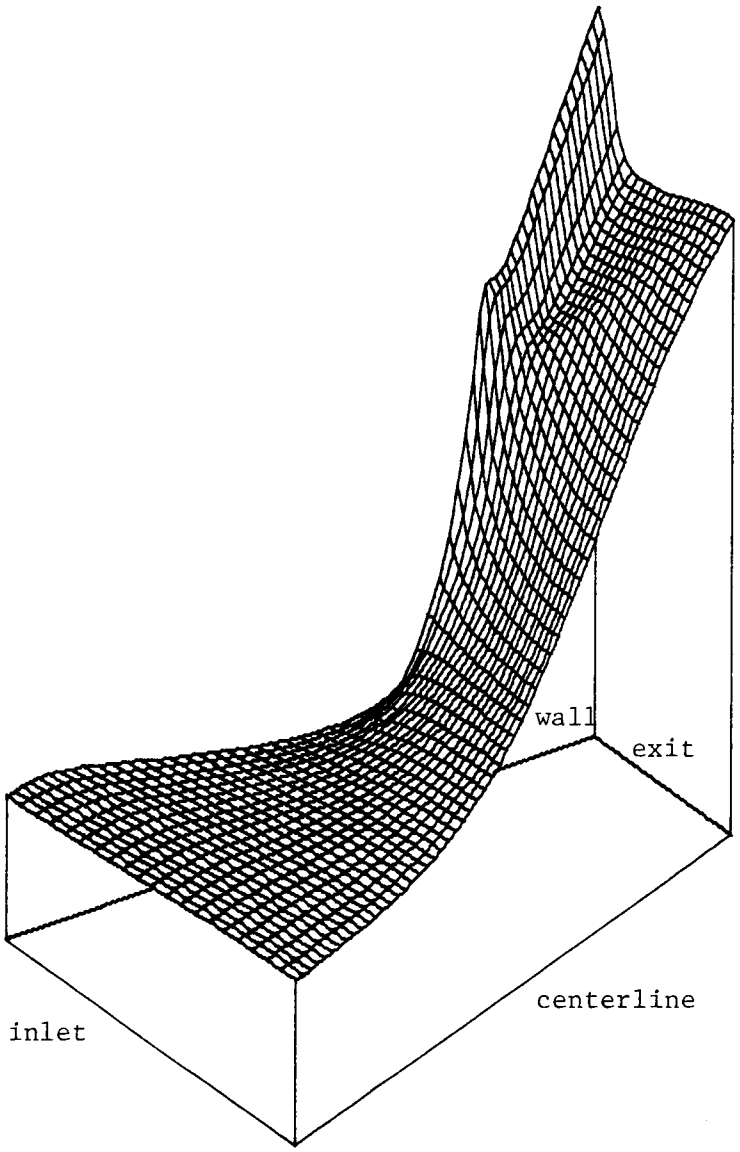


Figure 16. Mach Number Distribution for Two Phase Flow.

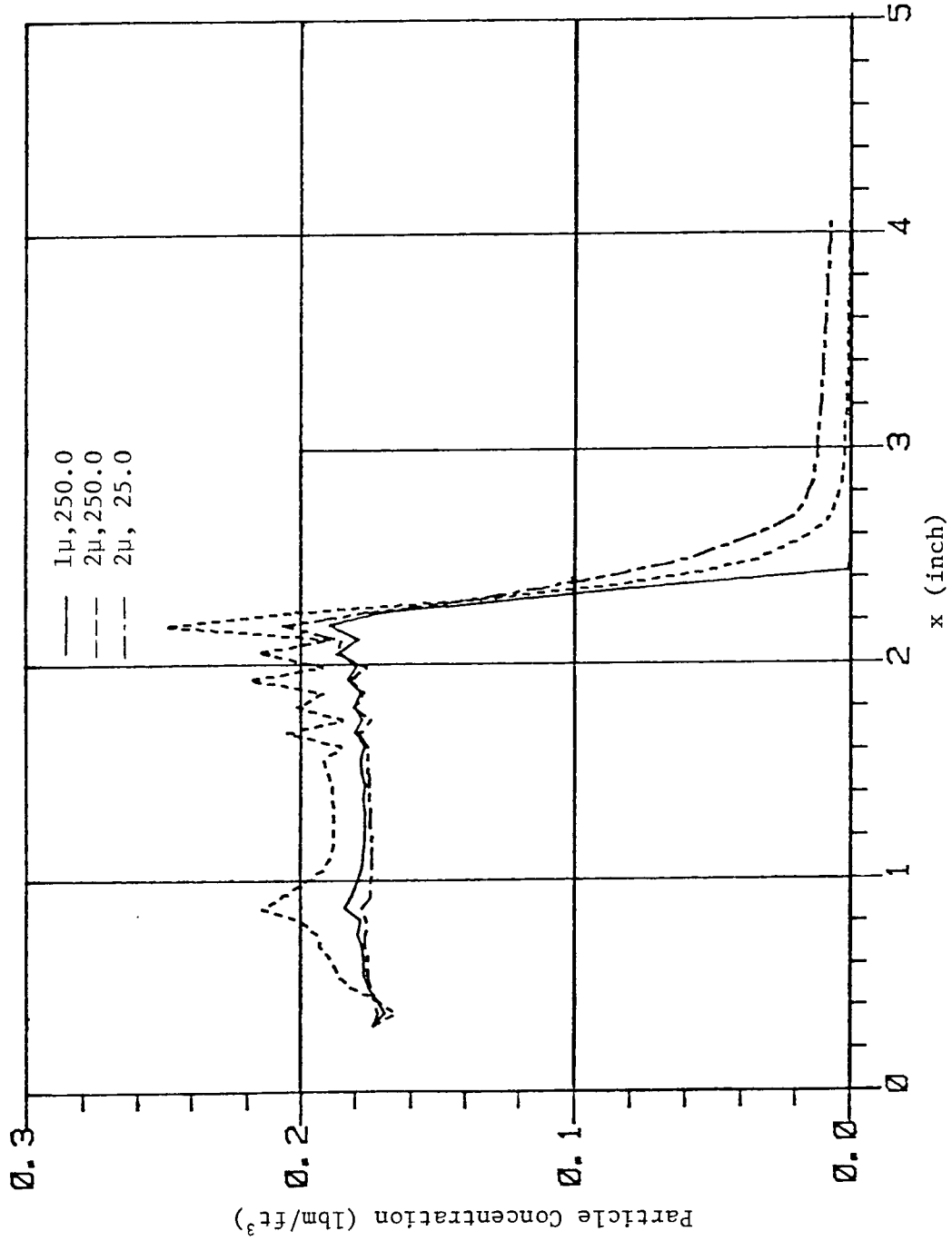


Figure 17. Particle Concentration Distribution at the Nozzle Wall.

the calculated results for the temperature in Figures 8 and 9, and Mach numbers shown in Figures 10-14, become understandable.

Temperature is an important thermodynamic property. In order to examine the difference between one phase flow and two phase flow, the numerical solutions are plotted and compared in Figures 8 and 9. In the nozzle exit plane, the temperature distributions near the wall for the two phase flow indicate high gradients, much different than that of the one phase flow. (See Figure 8). At the same time, the difference in the gas temperature between one phase flow and two phase flow is greater on the centerline of the nozzle than at the wall. The reason for this result is that the affect of the particles on the gas temperature is less at the wall regions because there are so few particles there. The temperature distribution along the wall is provided in Figure 9. A sharp temperature decrease near the throat appears. Because the total temperature is constant (1000°R) and the wall is adiabatic, the sharp decrease in temperature is due to the increase in Mach number along the wall given in Figure 13. One important fact is also shown in Figure 9. This fact, which has been mentioned in the Chapter I, is that the temperature of the particle phase does not decrease as rapidly as that of the flowing gas.

To show the behavior of the Mach number of the flow, two contours (Figures 10 and 11) and five distributions (Figures 12-16) are presented. In this test case, the gas is subsonic in the inlet and is supersonic in the exit. From gas dynamic theory, the sonic line is very near and slightly downstream of the throat for one phase flow. Because of particle drag effects, the sonic line moves farther downstream for

two-phase flow. These results are shown in Figures 10 and 11. This behavior has an impact on the nozzle discharge coefficient. In Figures 12 and 13, the Mach number difference between one phase flow and two phase flow is smaller upstream of the throat than downstream. Also the Mach number difference is larger on the centerline than on the wall which comes from the effect of particle free zone. The particle free zone effect is clearly observed in the results presented in Figures 14, 15 and 16.

In order to validate further the theoretical solution method, the numerical results shown in Figures 10, 11, 12, 13 and 15 were compared with related data presented by Chang [10]. From this comparison, the similar profiles for both one and two phase flows confirm that the present study is reliable. To assess the accuracy of the numerical solution, the mass, momentum and energy fluxes of the flow have been checked. By integrating across the inlet, throat and exit planes, the mass, energy fluxes conserve to within 3% for a two phase flow, and within 2% for a single phase. The momentum is conserved to about 4%. Therefore, from the view of numerical conservation of the physical flow variables, the present solution procedure is excellent.

As mentioned in Chapter I, the particles will contribute an inefficiency in the expansion process in the propulsive nozzle. To prove this physical phenomenon, the ratio of thrust function of one phase flow to that of two phase flow, and the ratio of specific impulse of one phase flow to that of two phase flow at the vacuum environment are calculated, and the values are 0.98 and 1.14 respectively. From these

results, the total thrust for one phase flow is lower than that of two phase flow. However, the specific thrust is higher for one phase flow.

For the calculations previously discussed, the continuity equation was applied on the wall to provide particle wall concentrations for boundary conditions. When the particle size and particle material densities were increased, strong oscillations occurred in the numerical solution. From the results shown in Figure 17, it is apparent that a large, heavy, article makes numerical oscillation more serious. In order to reduce this kind of numerical problem associated with a shock-like behavior in the particle wall concentrations, an extrapolation technique for the particle wall concentration, and fourth order smoothing, which were mentioned in Chapter III, were introduced to overcome such oscillations. The solutions for the two phase flow in CFFF are discussed next where use was made of such procedures.

Two Phase Flow in CFFF

The Coal Fired Flow Facility has been developed at UTSI . The coal-fired combustor is a full-slag-carry-over design, so the plasma leaving the combustor is heavily particle laden. The approximate geometry and the grid configuration used to simulate it are shown in Figure 18. Because axisymmetric flow is assumed, only the upper half plane was used in the numerical calculation.

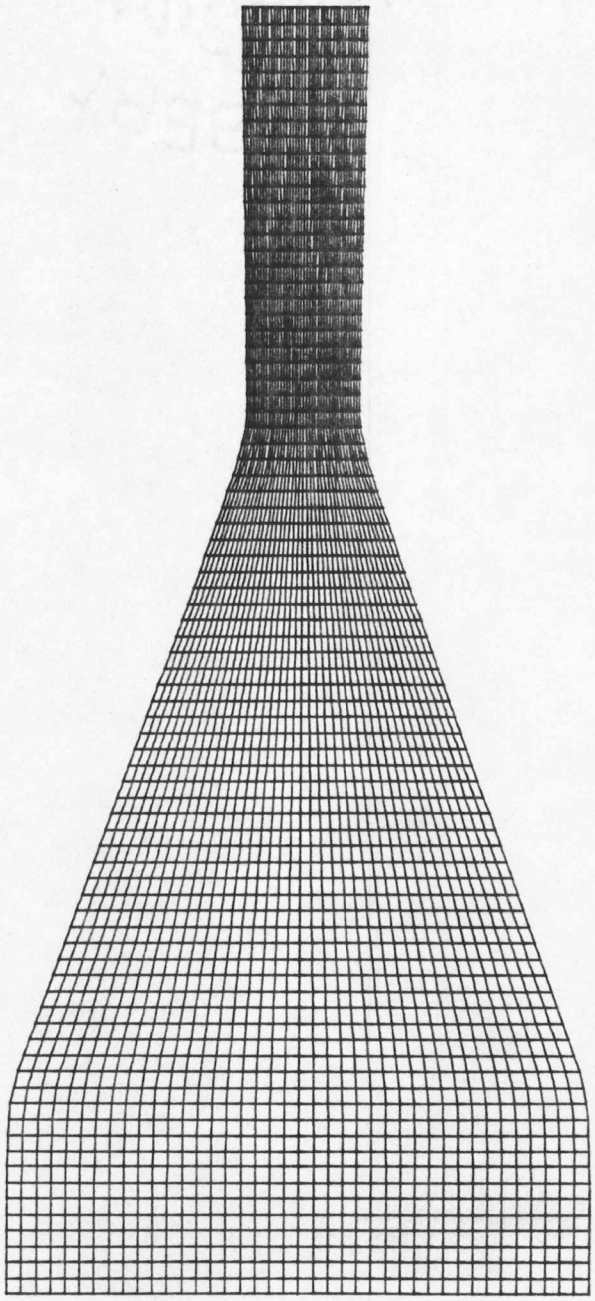


Figure 18. Grid for CFFF.

The two phase flow data used in the calculations for the CFFF are as follows:

Gas Phase

$C_p = 394.83 \frac{ft\text{-}lb_f}{lbm\text{-}°R}$

$\mu_o = 0.1653 \times 10^{-5} \frac{lb_f\text{-}sec}{ft^2}$

$\gamma = 1.15$

$R = 51.5 \frac{ft\text{-}lb_f}{lbm\text{-}°R}$

$Pr = 0.76$

$A'' = 0.6$

$T_T = 5400°R$

$P_T = 95.5$ psia

$\mu = \mu_o \left(\frac{T}{T_T}\right)^{A''} \frac{lb_f\text{-}sec}{ft^2}$

$\varepsilon = 1.0$

Particle Phase

$C_j = 778 \frac{ft\text{-}lb_f}{lbm\text{-}°R}$

$m_j = 26.0 \frac{lbm}{ft^3}$

$r_j = 1\mu, 15\mu$

$\varepsilon_j = 1.0$

$\phi = 1.43\%, 14.3\%$

Two numerical formulations for inlet condition, which were mentioned in Chapter III, were used in this case. For the calculation of one phase flow, the specified total temperature (5400°R), total pressure (95.55 psia) and parallel inlet flow condition were applied. The inlet condition for the two phase flow were based on the results of the one phase flow, and the assumption of kinetic and thermal equilibrium between gas and particles was applied. In order to satisfy well-posed condition and generalize the computer code, an option to specify arbitrarily, using experimental data, the velocities and concentrations

for the two phases has been provided. The particle free zones and the pseudo-wall concepts are applied for boundary conditions for the particle phase when the near wall particle concentrations are computed to be less than or equal to about 1% of inlet value during the calculation. The asymptotic steady solution is assumed to be reached when the values of $\left|\frac{\Delta u}{u}\right|$ and $\left|\frac{\Delta u_j}{u_j}\right|$ are everywhere less than 10^{-4} in three consecutive time steps.

Discussion of Results for the Inviscid Gas-Particle Flow

For the given inlet conditions, the results of the calculations are presented in Figures 19 - 37 and Tables 2 - 4. Limiting particle streamlines are shown in Figure 11. It is easy to see that the particle free zone is larger for larger particles. The reason is that the inertia for the larger particle is larger than that of the small one, so that the larger particles follow paths that are further from the gas streamlines than those of smaller particles. The results of Figure 20 show that the distribution of the particle concentration is more nonuniform near the wall than near the nozzle centerline. This phenomenon, the ununiform distribution of particles, has been mentioned in several papers. One valuable discussion about this topic is provided in reference 1 on the SPP code. To treat this kind of problem, in the SPP code, an extrapolation method was developed for the particle concentration at the wall based on the particle mass flow rate passing through a particle stream tube under the assumption of steady state conditions. However, in the present study, the special techniques which were mentioned in Chapter III were used to solve this problem. Because

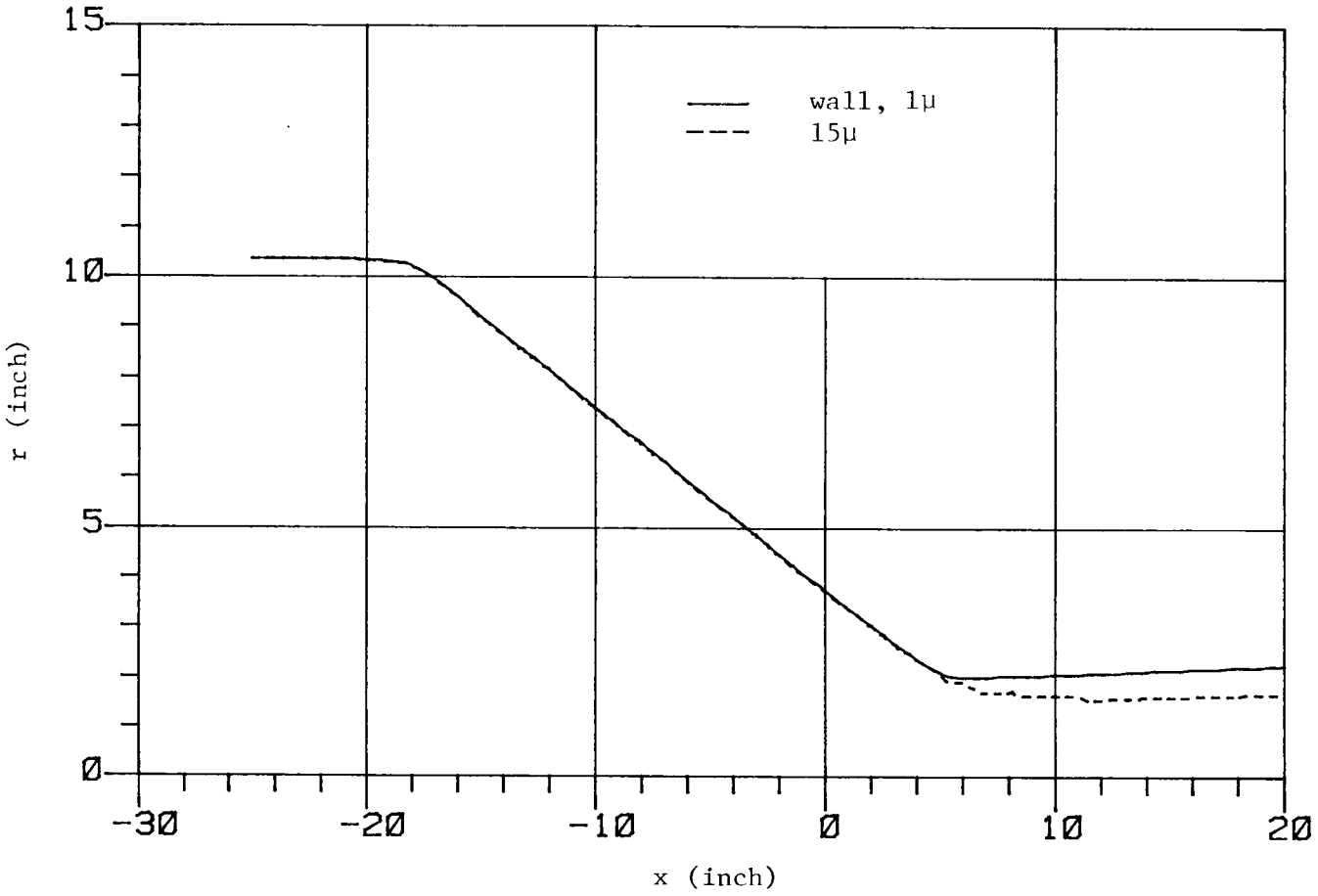


Figure 19. Limiting Particle Streamline for Two Phase Flows with ϕ = 1.43%.

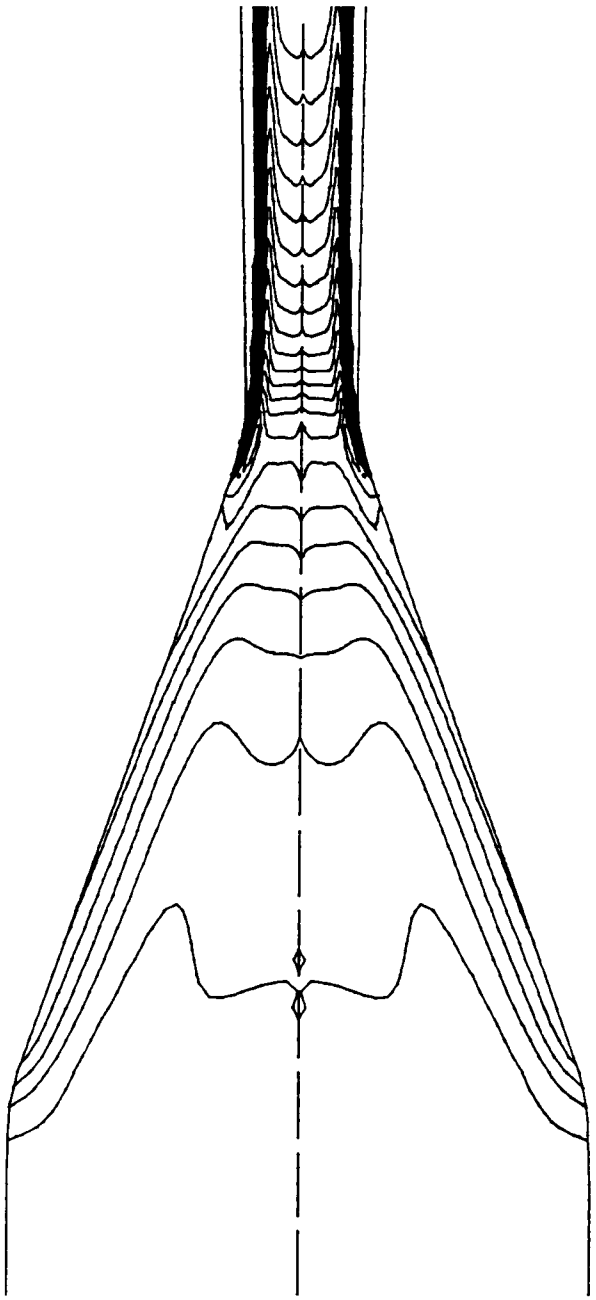


Figure 20. Particle Concentration Contour for Two Phase Flow with $r_j = 15\mu$ and $\phi = 1.43\%$.

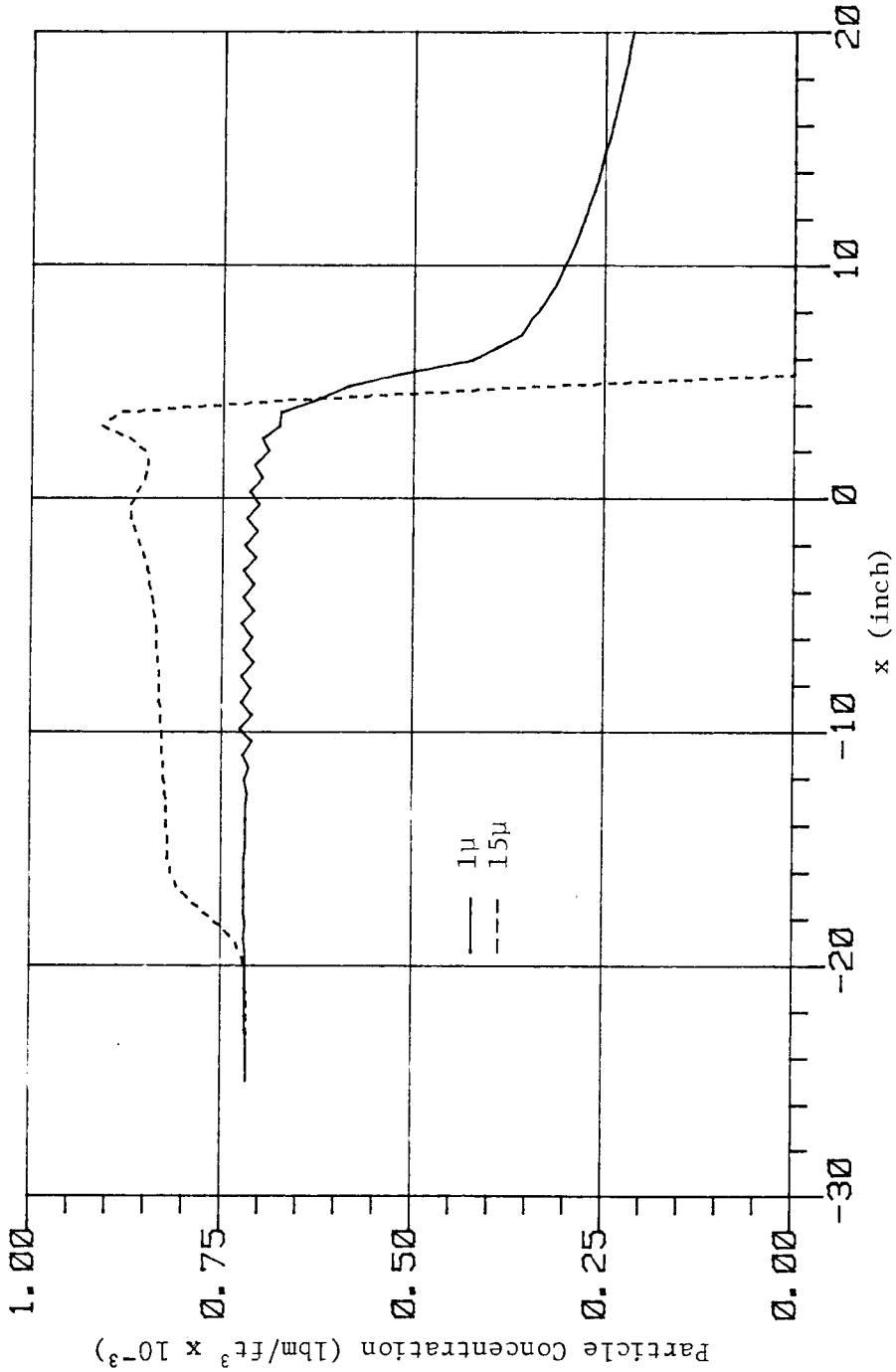


Figure 21. Particle Concentration Distribution at the Wall for Two Phase Flows with ϕ = 1.43%.

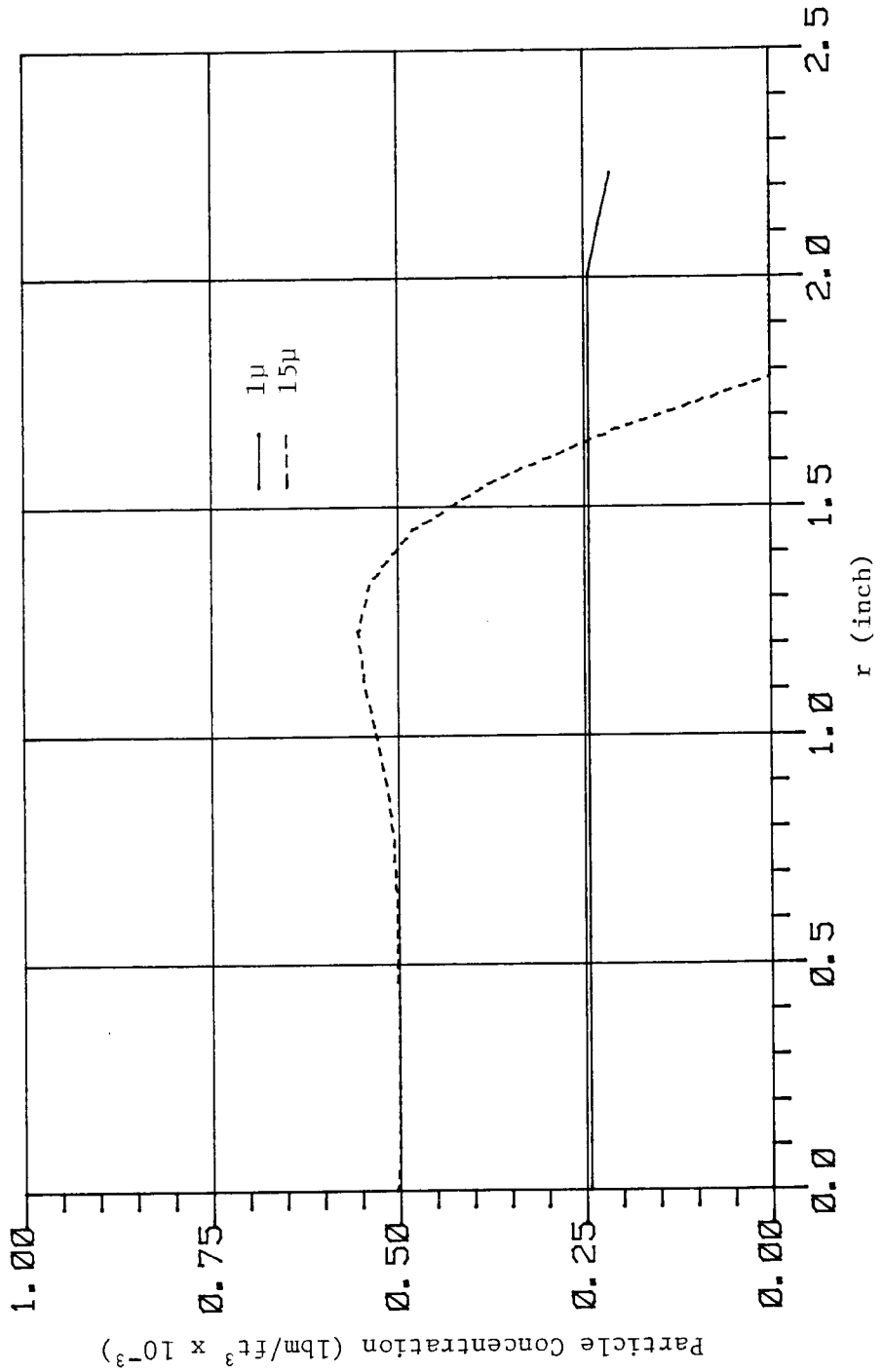


Figure 22. Particle Concentration Distribution at the Exit Plane for Two Phase Flows with ϕ = 1.43%.

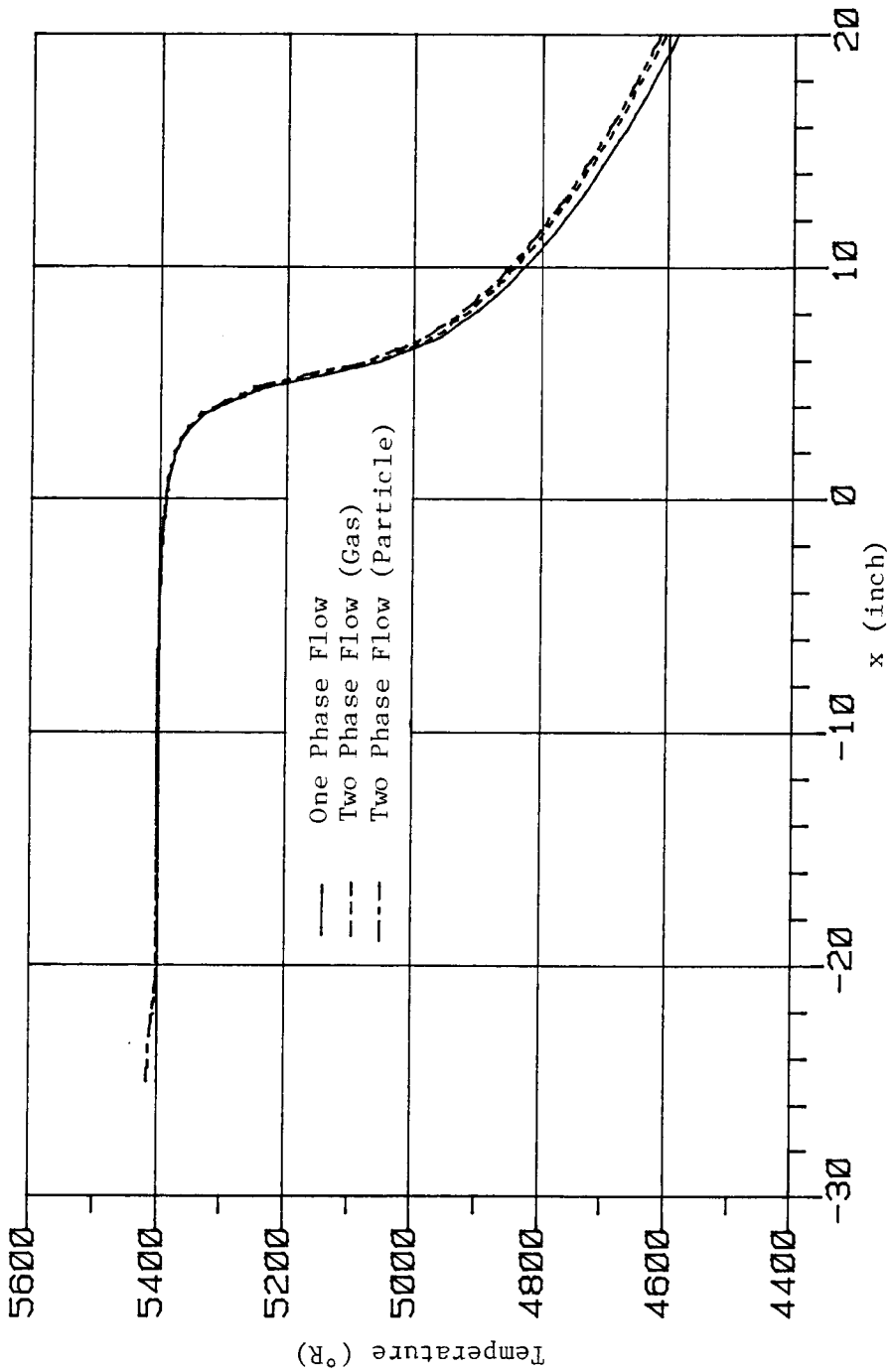


Figure 23. Temperature Distribution at the Wall for One Phase Flow and Two Phase Flow with r_j = 1μ and ϕ = 1.43%.

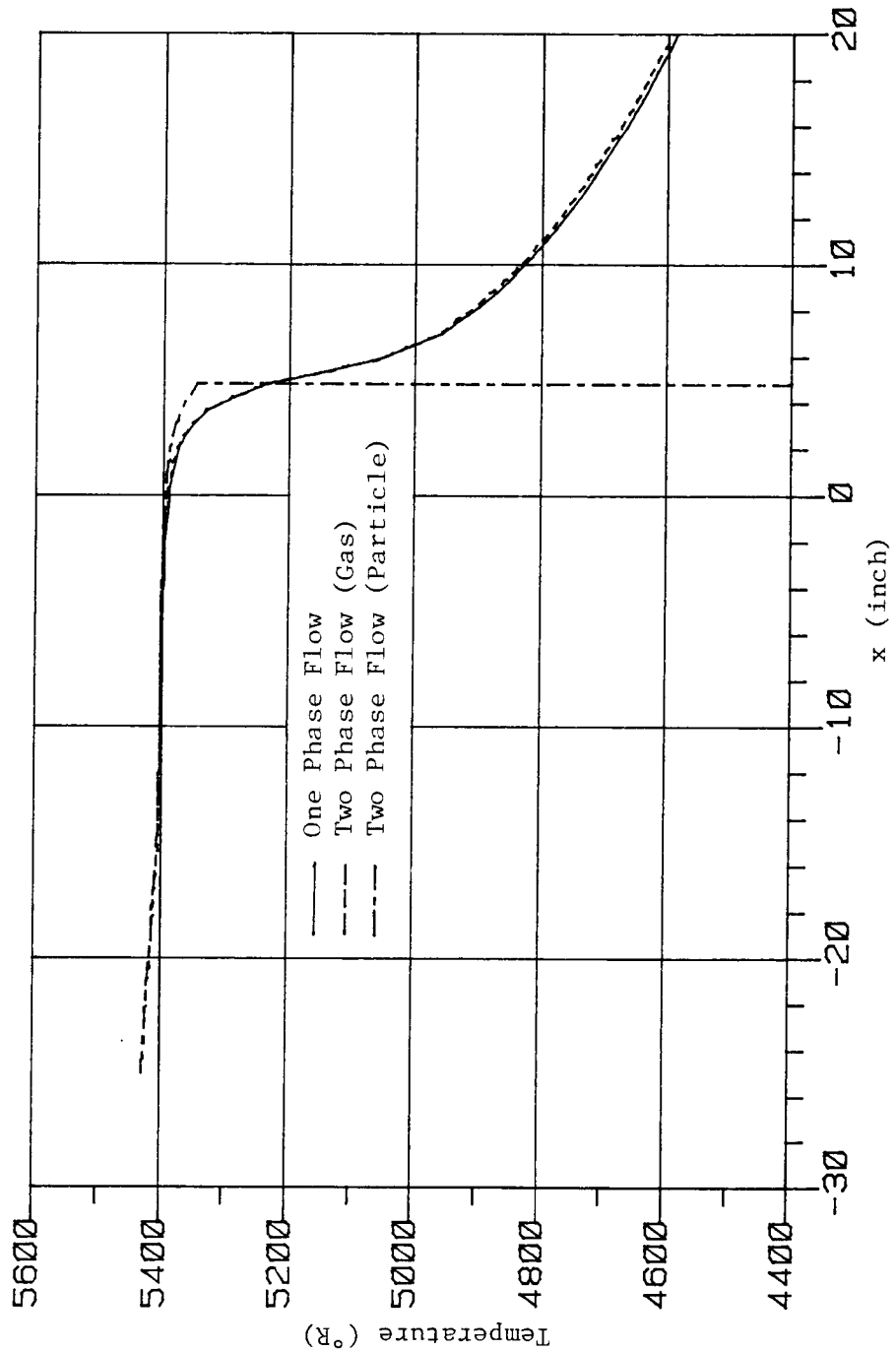


Figure 24. Temperature Distribution at the Wall for One Phase Flow and Two Phase Flow with r_j = 15μ and ϕ = 1.43%.

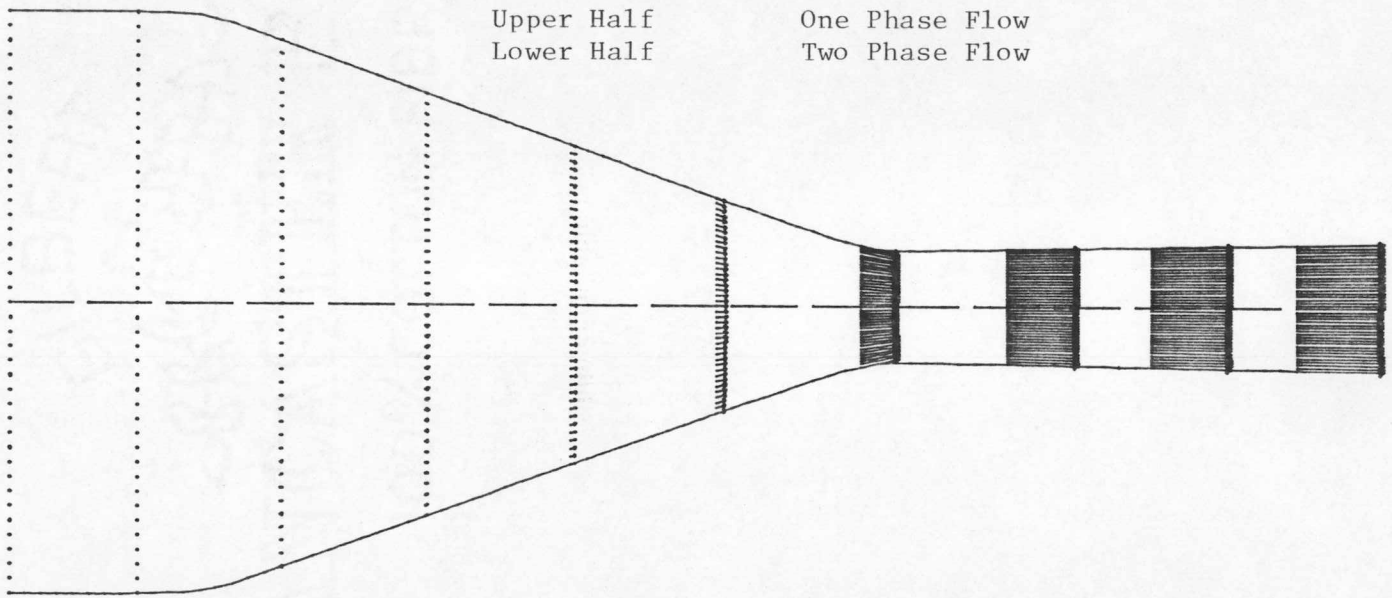


Figure 25. Gas Velocity Vector for One Phase Flow and Two Phase Flow with $r_j = 15\mu$ and $\phi = 1.43\%$.

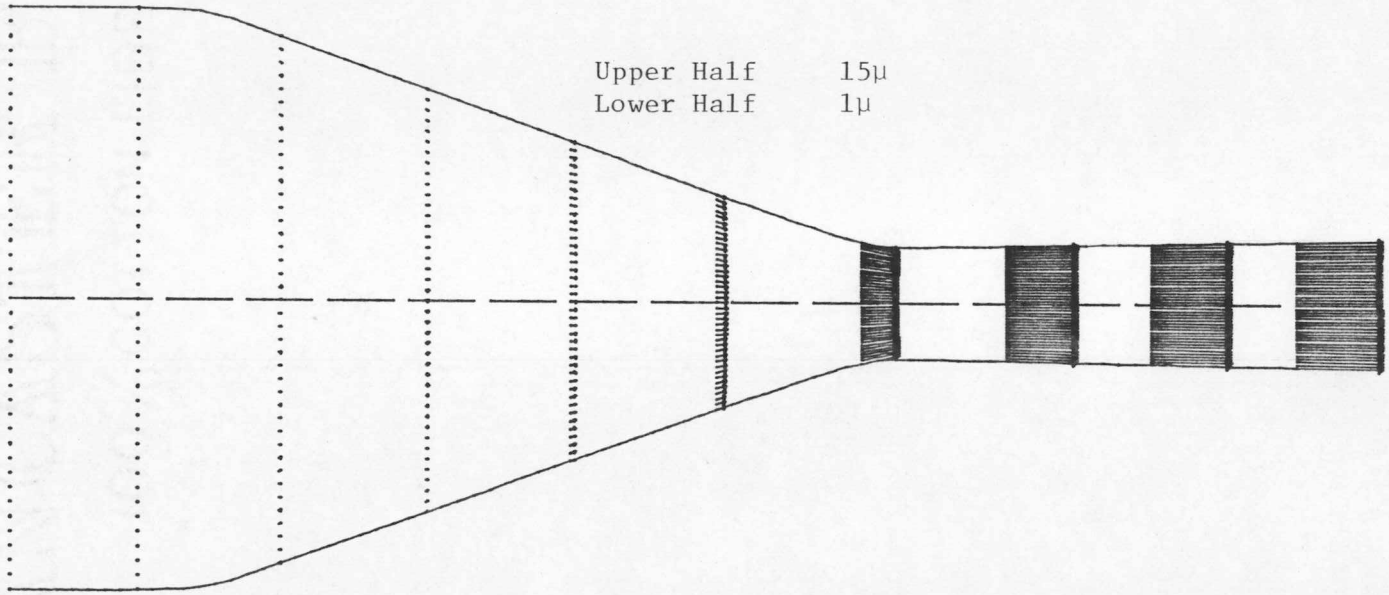


Figure 26. Gas Velocity Vector for Two Phase Flows with ϕ = 1.43%.

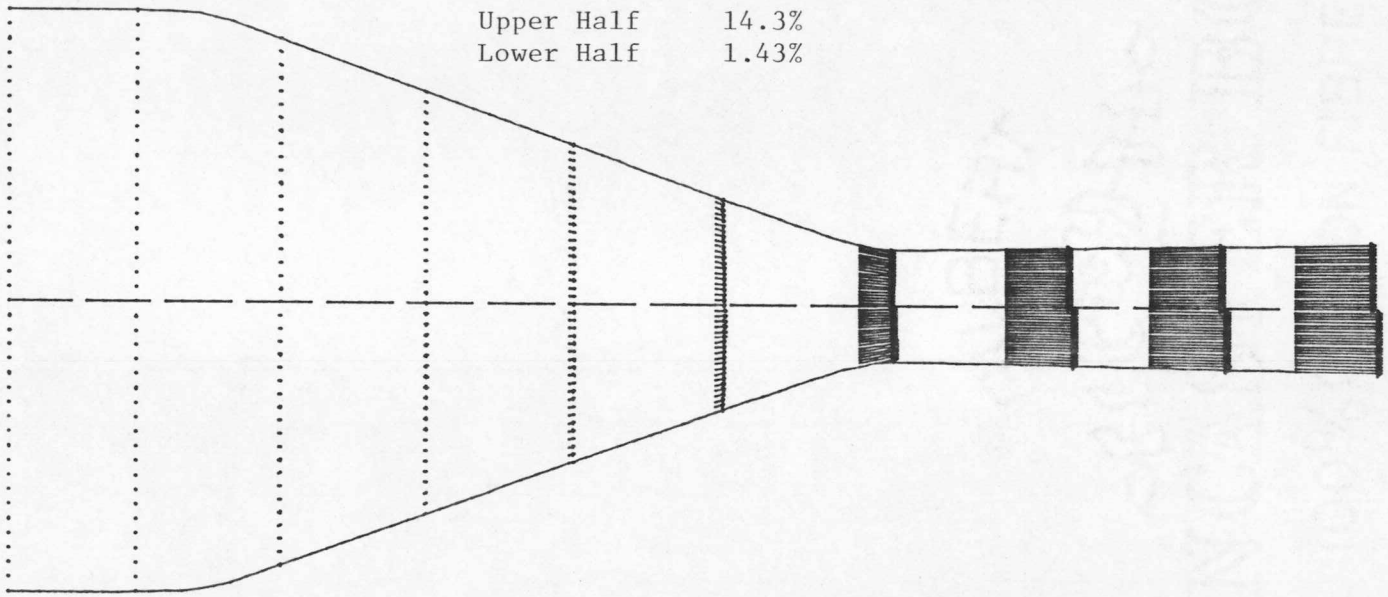


Figure 27. Gas Velocity Vector for Two Phase Flows with r_j = 1μ.

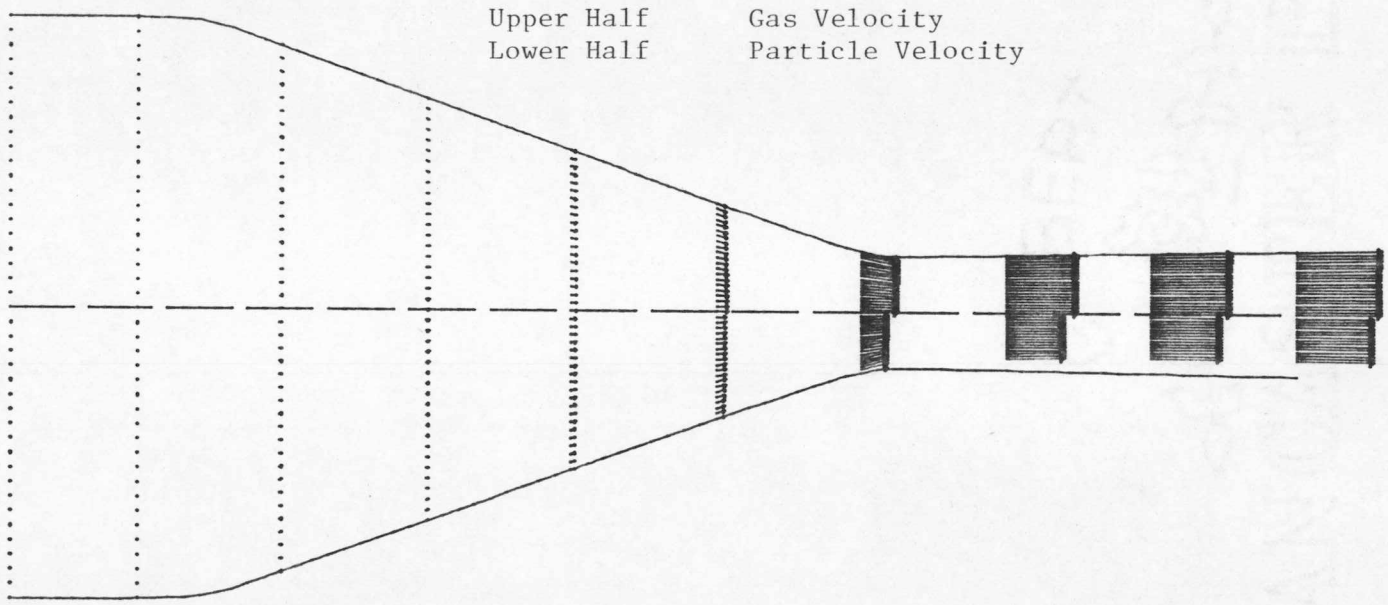


Figure 28. Velocity Vector for Two Phase Flow with r_j = 15μ and ϕ = 1.43%.

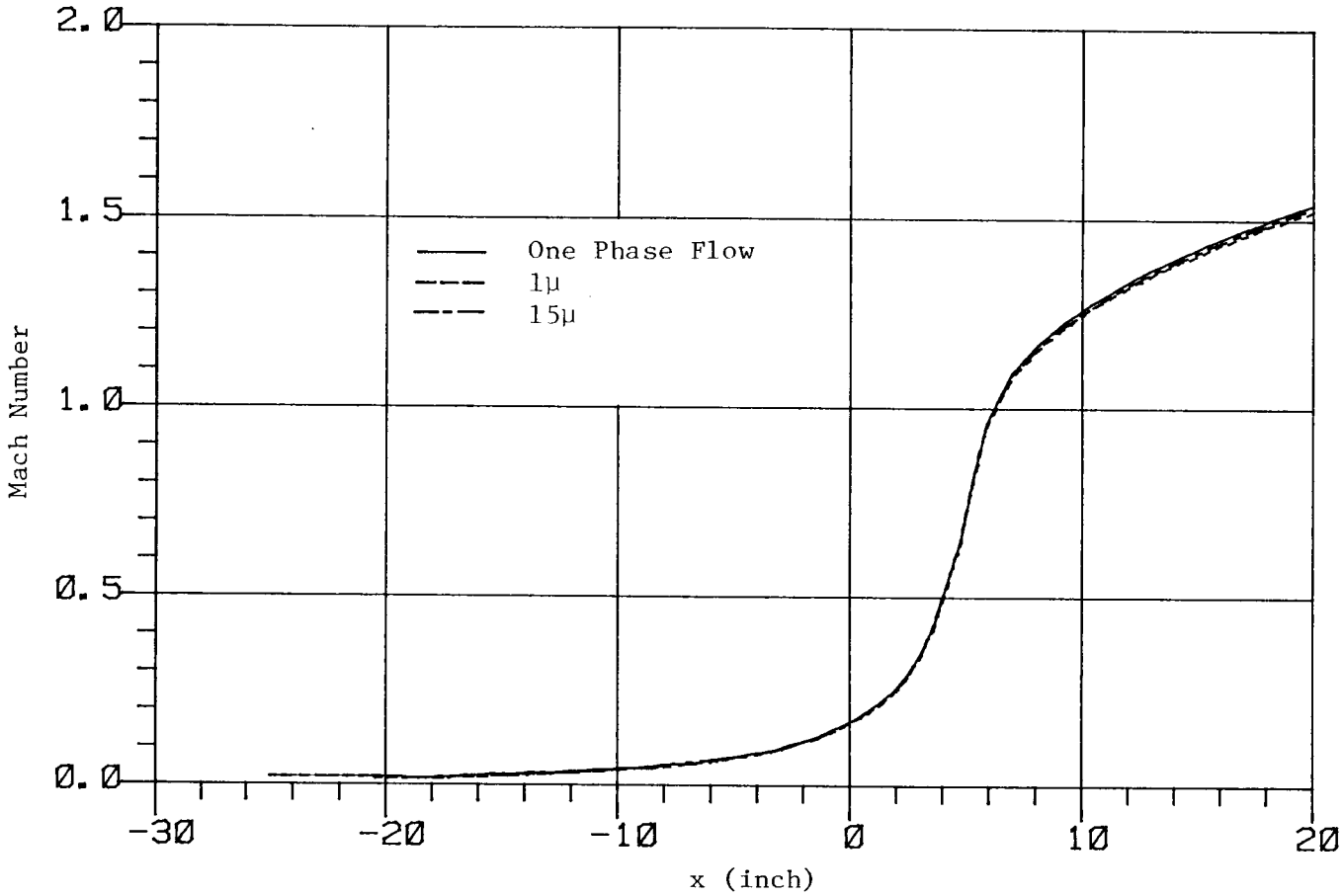


Figure 29. Mach Number Distribution at the Wall for One Phase Flow and Two Phase Flows with ϕ = 1.43%.

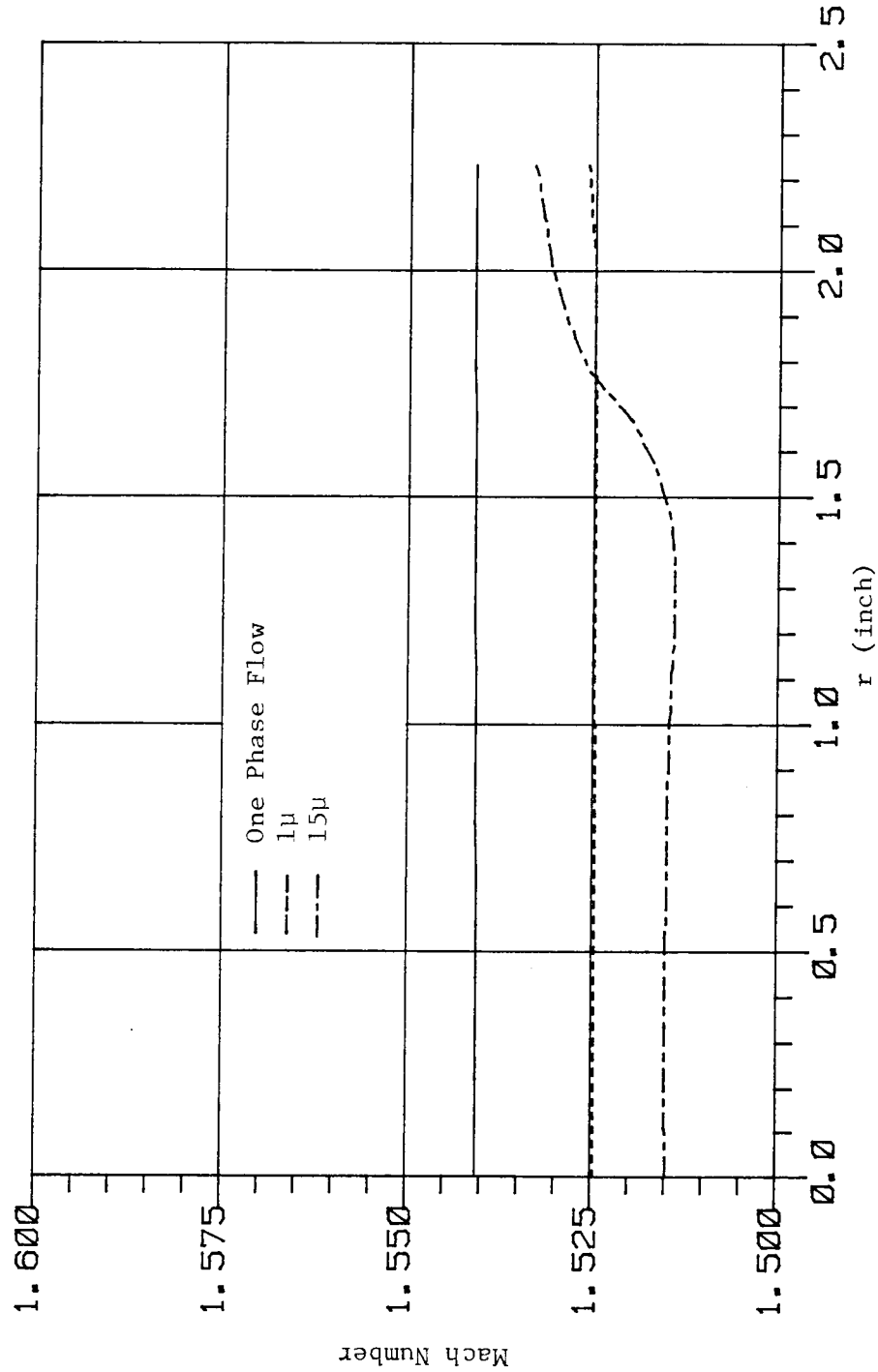


Figure 30. Mach Number Distribution at the Exit Plane for One Phase Flow and Two Phase Flows with ϕ = 1.43%.

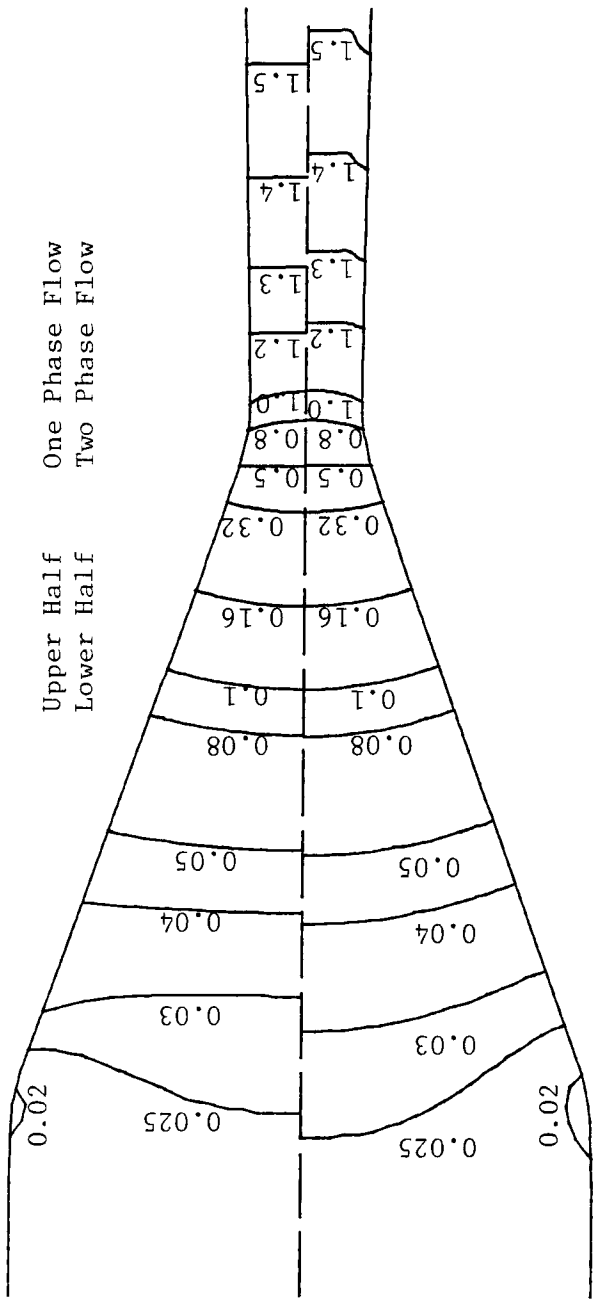


Figure 31. Mach Number Contour for One Phase Flow and Two Phase Flow with $r_j = 15\mu$ and $\phi = 1.43\%$.

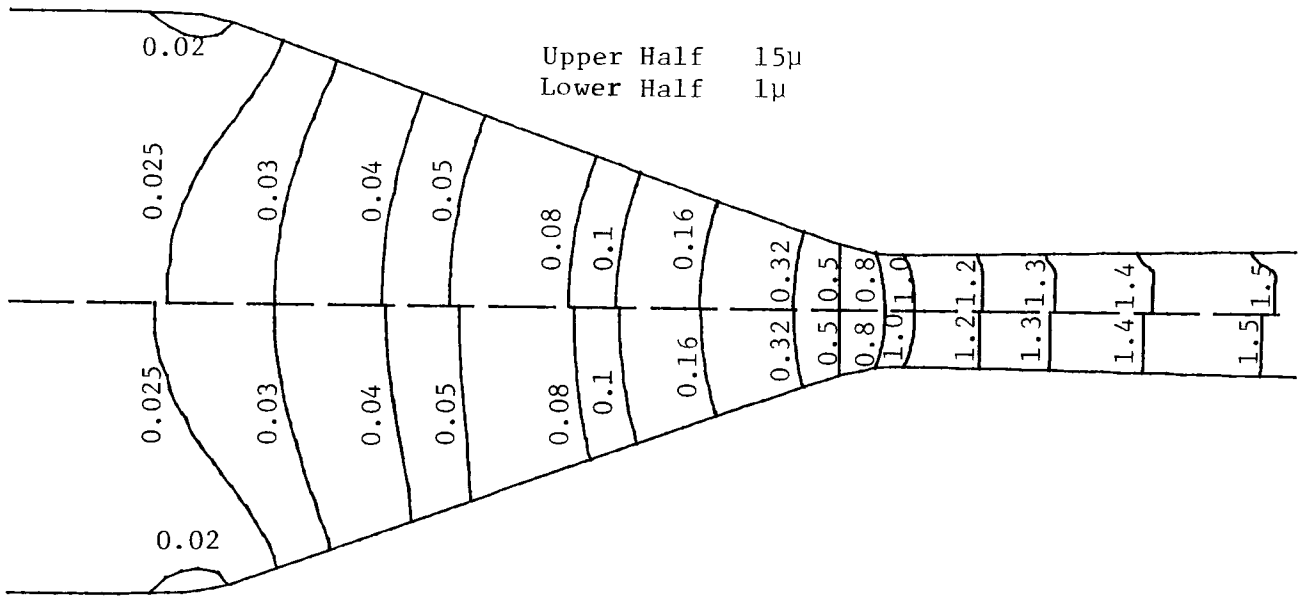


Figure 32. Mach Number Contour for Two Phase Flows with ϕ = 1.43%

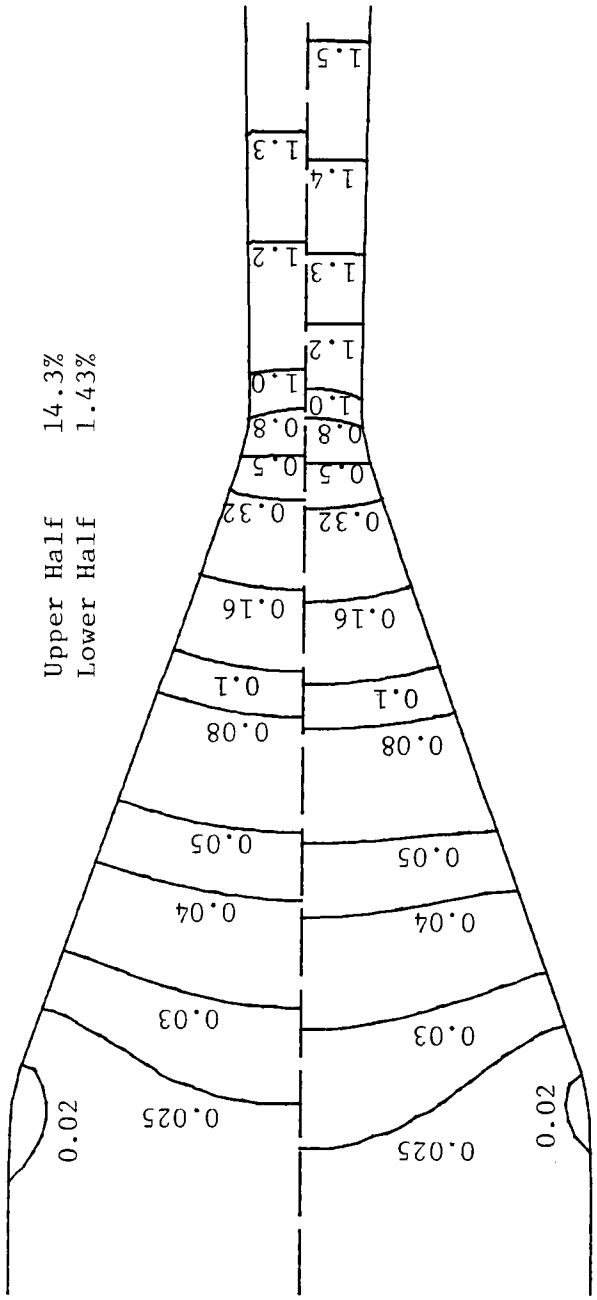


Figure 33. Mach Number Contour for Two Phase Flows with $r_j = 1\mu$.

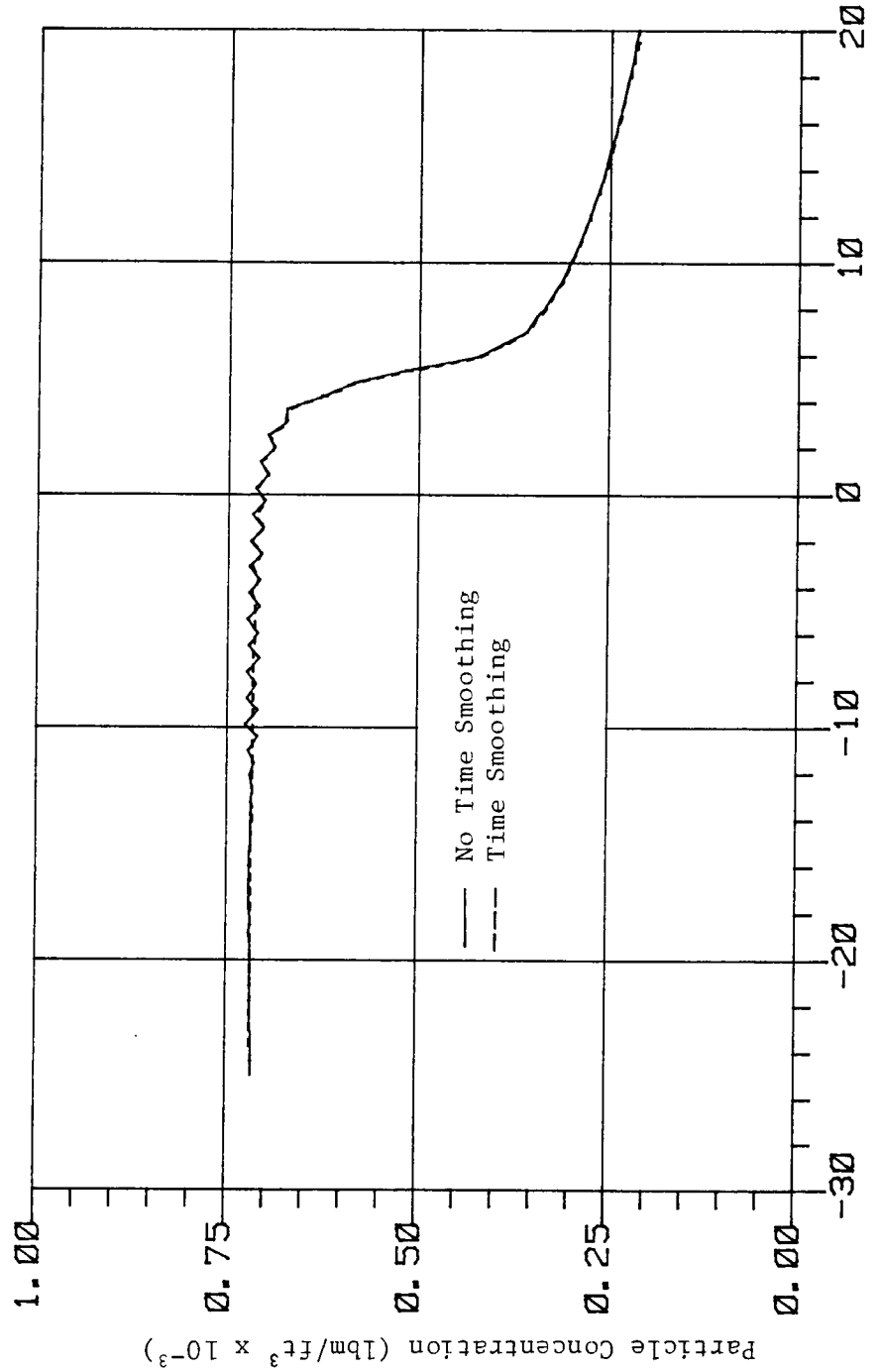


Figure 34. Particle Concentration Distribution at the Wall for Two Phase Flow with r_j = 1μ and ϕ = 1.43%.

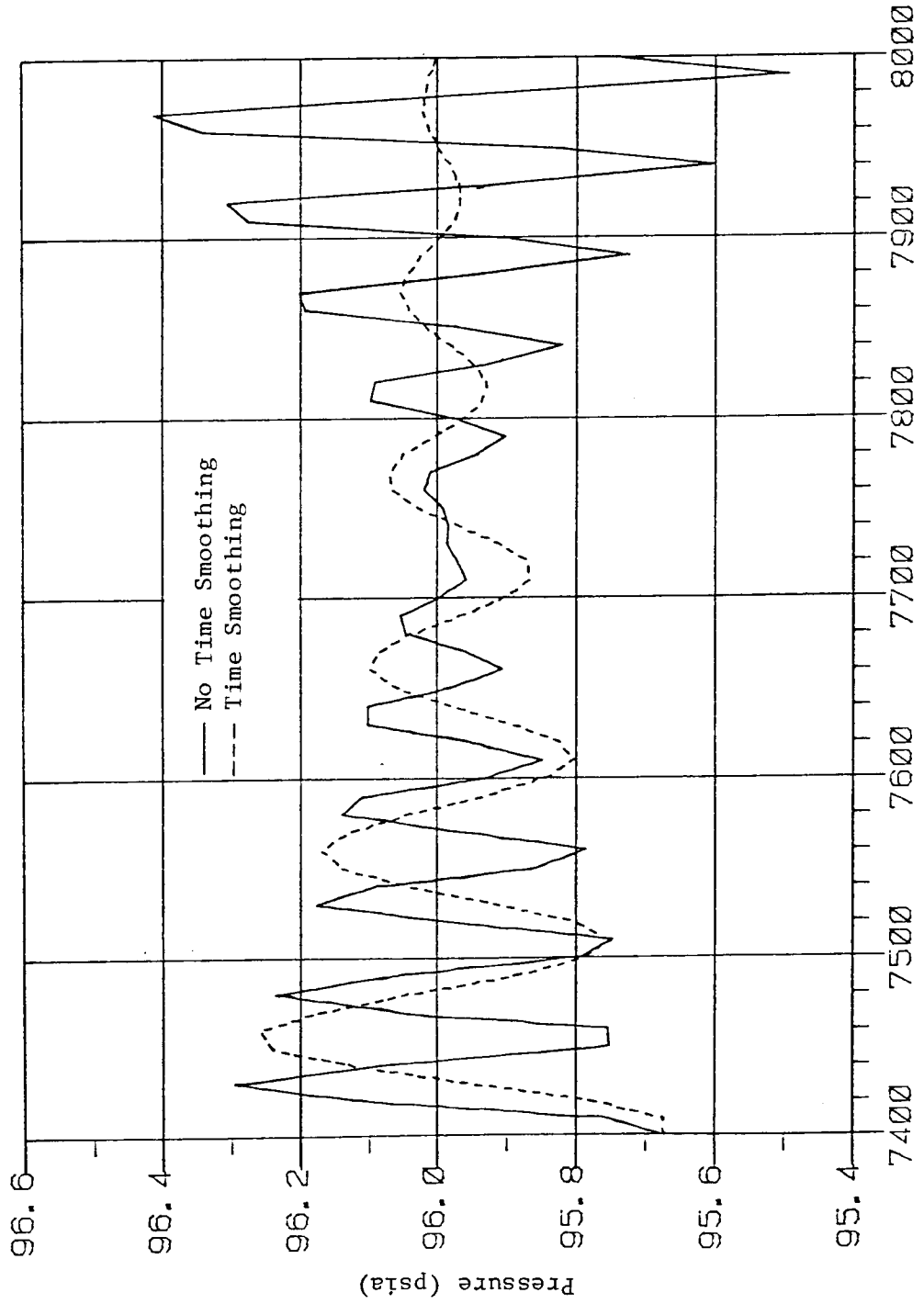


Figure 35. Pressure at Grid Point (2,1) for Two Phase Flow with $r_j = 15\mu$ and $\phi = 1.43\%$.

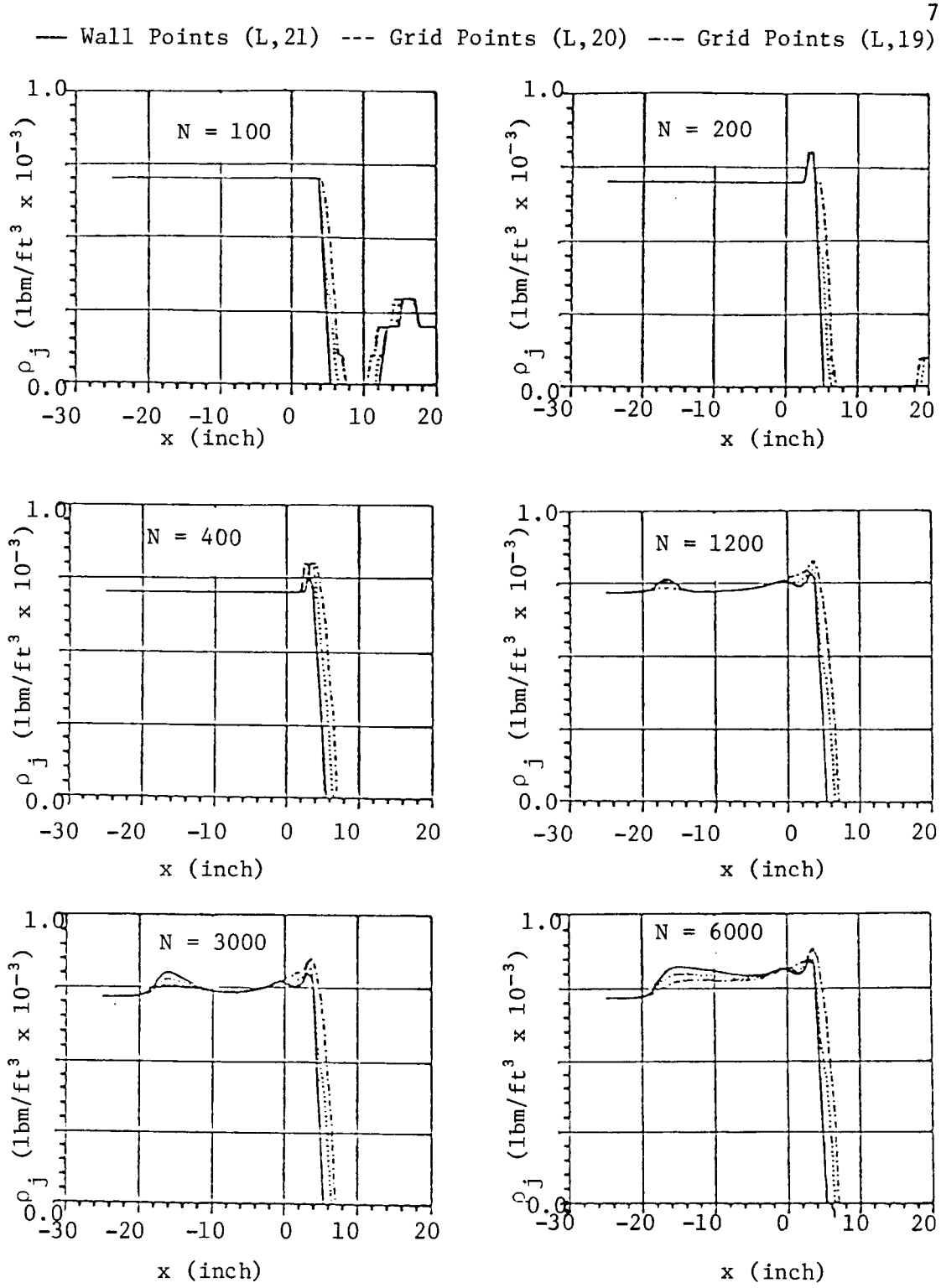


Figure 36. Time History of Particle Concentration.

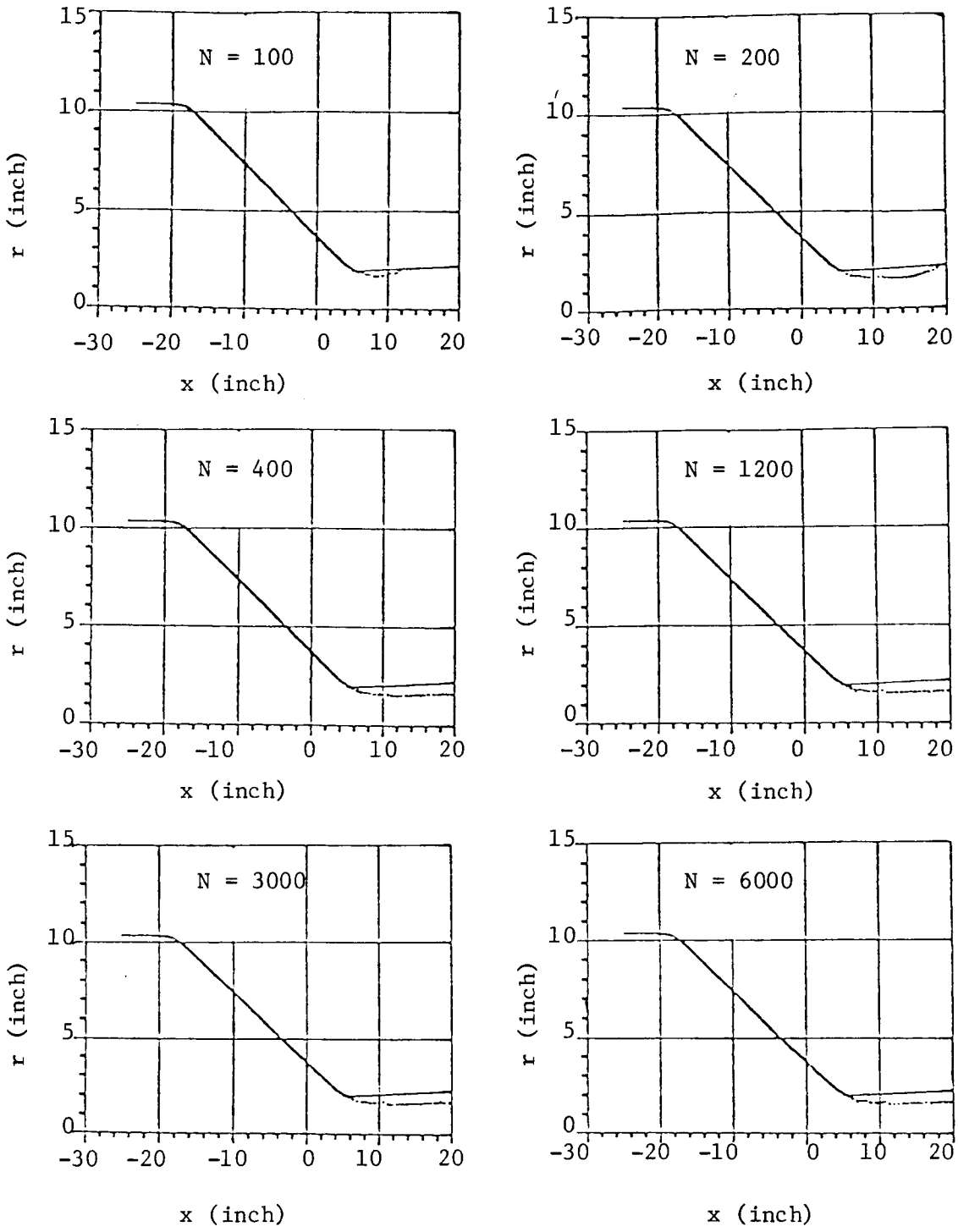


Figure 37. Time History of Particle Free Zone.

Table 2

Error Analysis of Mass Flow Rate between Inlet and Throat Planes[a]

Time Step	Throat Plane Mass Flow Rate (lbm/sec)		Error Analysis (%)[b]	
	Gas Phase	Particle Phase	Gas Phase	Particle Phase
600	8.137907	0.105704	1.728	13.62
1200	8.135301	0.109919	1.76	9.264
2000	8.140391	0.112396	1.697	6.856
3000	8.145347	0.113923	1.635	5.424
5000	8.156196	0.115325	1.5	4.142
6000	8.159970	0.116085	1.453	3.46
7000	8.164023	0.117304	1.403	2.385
8000	8.166869	0.118060	1.376	1.73
9223	8.169521	0.118643	1.334	1.23

[a]Two phase flow (15μ, 1.43%) passes through CFFF.

[b]Gas and particle mass flow rates across the inlet plane are 8.278529 and 0.120102, respectively.

Table 3

Error Analysis for One Phase Flow (CFFF)

Station of Calculation	$\int \rho u dA$ (lbm/sec)[a]	$\int (p+\rho u^2) dA$ (lb_f)[b]	$\int_{inlet}^{x} p_w \frac{dA_w}{dx} dx$ (lb_f)[b]	$\int (\rho+\rho u^2) dA - \int_{inlet}^{x} p_w \frac{dA_w}{dx} dx$ (lb_f)[b]	$\int (h+1/2 \vec{v}^2) \rho u dA$ (Btu/sec)[c]
Inlet	8.278527	32320.65039	0	32320.65039	22682.35352
Throat	8.199131	1474.38733	-30886.03320	32360.42	22470.30469
Exit	8.211707	1588.24939	-30774.09375	32362.343	22507.01953
Error Analysis					
	0.97%			0.13%	0.94%

[a]Gas mass flow rate across the section.

[b]Force

[c]Energy

Table 4

Error Analysis for Two Phase Flow (CFFF, 1.43%)

	$\int \rho u dA$ (lbm/sec)[a]	$\int \rho_j u_j dA$ (lbm/sec)[a]	$\int (\rho u + \rho_j u_j) dA$ (lbm/sec)[a]	$\int_x (p+\rho u^2+\rho_j u_j^2) dA - \int_{\text{inlet}}^{x} P_w \frac{dA_w}{dx} dx$ (lb_f)[b]	$\int (h+1/2 \vec{v}^2) \rho u dA + \int (h_j+1/2 \vec{v}_j^2) \rho_j u_j dA$ (Btu/sec)[c]
1μ	8.278529	0.120102	8.39863	32356.873	23356.739
15μ (inlet)	8.278529	0.120102	8.39863	32492.404	23454.6
1μ	8.115418	0.118367	8.233785	32360.597	22874.628
15μ (throat)	8.169521	0.118643	8.288164	32492.758	23035.695
1μ	8.147245	0.118457	8.265702	32366.303	22971.308
15μ (exit)	8.203670	0.123388	8.327058	32499.169	23163.579
1μ	2.0%	1.47%	2.0%	0.029%	2.1%
15μ (Error Analysis)	1.33%	4.00%	1.33%	0.021%	1.82%

[a] Mass flow rate

[b] Force

[c] Energy

of numerical dispersion in the MacCormack scheme, and the presence of high gradients in particle concentrations, numerical oscillations and the overshoot of particle concentrations appear: examples of which are shown in Figures 21 and 22. To correct for this numerical behavior, strong damping terms were applied to the cases with the larger particle sizes. If no damping terms were used in the calculations, it was not possible to obtain a converged solution. However, it must be understood that too strong numerical damping will destroy the physical meanings of the differential equation. From the aforementioned discussions, it is clear that the numerical damping terms must be used carefully to preserve accuracy and the conservation property. For flow variable profiles presented in Figures 21 and 22, it is confirmed again that a particle free zone appears near the downstream wall for larger size particles.

For an adiabatic wall, the temperature profiles along the wall are given in Figures 23 and 24. Comparing the numerical values of gas temperature in these two figures, one observes that the differences between wall temperatures in the downstream for one phase and two phase flow are smaller for larger particles. The reason is that the larger particles create a larger particle free zone and thus do not influence gas behavior in this region. In order to understand the direction and magnitude of gas and particle velocity, the corresponding velocity vectors are plotted in Figures 25, 26, 27 and 28. In order to clearly indicate the vector velocity field differences between one phase and two phase flow, the corresponding results are provided in Figure 25. The drag of the particles on the gas significantly reduced gas velocity near the nozzle

centerline. In the particle free zone, the gas velocity for the two phase flow is almost the same as that of the one phase flow. For the two phase flows with different sized particles, the gas velocities are plotted in Figure 26. From this result, it is obvious that the gas velocity for the 1μ size particle is distributed more uniformly than that of 15 μ size particle. The reason is that the particle concentration is more uniform for the smaller particle. If the particle loading is increased, magnitude of the gas velocity will be further reduced. Figure 27 shows this type of consistency in the numerical results. As mentioned in Chapter I, the particle cannot accelerate like the gas due to inertia. This fact is clearly shown in the plot which is presented in Figure 28. This figure shows clearly the particle free zone.

For the CFFF nozzle, Mach number distributions are important. The nozzle must mate to an MHD channel having prescribed design inlet Mach number. To investigate the effects of particle size and loading on the nozzle Mach number distributions, two distribution plots, Figures 29 and 30, and three contour plots, Figures 31, 32 and 33, are presented. The Mach number distributions on the wall for the one phase and two phase flows are presented in Figure 29. The differences in Mach number between one and two phase flow in the three cases is larger downstream of the throat of the nozzle than upstream of the throat. To further show particle size effect, the Mach number distributions across the exit plane of the nozzle are plotted in Figure 30. Because larger particles concentrate near the centerline region, the Mach number is lower than at the wall. According to the theory, for a particle laden gas, the sonic

line moves downstream of the throat. Three Mach number contours shown in Figures 31, 32 and 33 prove this physical phenomena. From the solutions given in Figure 31, the most significant differences in Mach number distributions are indicated near the centerline region. To illustrate the differences in the distribution of Mach number for different kinds of particle size and particle mass fraction, other results are presented in Figures 32 and 33. It is easy to see that the Mach number contours in the downstream nozzle flow are flat for small sized particles, and the sonic line moves farther downstream of the throat for higher particle loadings.

As mentioned in Chapter III, a time smoothing technique is introduced to accelerate the numerical convergence of the subsonic inlet flow. The details of the technique are presented in reference 33. The results shown in Figures 34 and 35 demonstrate the effects of this technique as applied in the present study. As shown in Figure 34, the space oscillations of particle concentration can be reduced. In the same way, the time oscillations of the pressure field shown at grid point (2,1), presented in Figure 35, is significantly suppressed.

Because the drag coefficient and Nusselt number formulations are not explicitly functions of time, the solution is not truely time-dependent. Even though the true unsteady solution is computationally expensive, it is worthwhile to attempt to predict the approximate time history of particle behavior. In order to approach this problem, two phase flow with 15μ particle size and 1.43% particle mass fraction was briefly studied. The results shown in Figure 36 are the particle concentrations for different time steps, plotted along the wall, grid

points (L,20) and (L,19), in which L represents the mesh numbers along the ζ direction from the inlet to exit. In the early time steps, the particles separate from the wall just downstream of the throat and gradually accumulate near the corner of the upstream inlet contraction. Finally, the particles become distributed more uniformly along the wall from the inlet corner to the throat. At the same time, the particle free zone reaches its asymptotic size. To prevent numerical over-damping, moderate damping was applied, which gave a solution with a small overshoot upstream of the throat. In this case, the damping coefficient was set equal to 0.015. To more clearly show the growth of the particle free zone, solutions for different time steps are presented in Figure 37. It is easy to see that the particle free zone develops and becomes stable very fast. To evaluate the stability and accuracy of the computer code, the integral or global mass flow rate and an error analysis for the same case are shown in Table 2. If a convergence criterion of 10^{-3} is accepted, the asymptotic steady state solution is achieved in only about 600 time steps. However, mass conservation for the particle phase is poor at this time step. To reduce the mass flux deficit, the convergence criterion was set equal to 10^{-4} for the entire flow region. But then, even when the convergence value was obtained for the flow downstream of the nozzle throat, for time steps less than 7400, numerical oscillation still existed in the subsonic inlet part of flow field. In order to accelerate the convergence, the time smoothing technique was applied after time step 7400 and the solution finally was converged at the time step 9223. From Table 2, it is apparent that the stability and accuracy requirements are satisfied.

To complete the accuracy analysis, two tables are given to check whether the code satisfies basic physical principles of conservation. The results are shown in Tables 3 and 4, where the mass, energy and momentum flux integrals across the inlet, throat and exit planes are compared. The error analysis is evaluated from the three values which were calculated at the different cross sections for mass, momentum and energy. For every case, the maximum deviation was used to examine the accuracy of the numerical results. The data shown in Table 4 show that solutions for flows with the larger particle size have the largest error for the particle mass flow rate.

The study of one inviscid gas-particle flow solution procedure was concluded at this point. From the aforementioned discussions, the computer code presented in this research is thought to be reliable and sufficiently accurate for some engineering design purposes although to achieve the low mass, momentum and energy flux errors requires many iteration steps.

Discussion of Results for the Effective Turbulent Viscosity Model

Even though the effective turbulent viscosity model is not accurate, it is easy to set up in the code for determining the effects of a thick boundary layer on the gas and particle flow in the nozzle. Because this model was applied to study the general flow behavior in a qualitative sense, an arbitrary effective viscosity was used. In this study, the value of effective viscosity was set to about 1000 times the molecular viscosity. Using an effective viscosity model, different cases were computed, one phase flow and two phase flows (1μ, 15μ).

The results are presented in Figures 38 - 43. To understand the particle concentration distribution under the effect of a thick boundary layer, two plots are shown in Figures 38 and 39. From the results shown in those two figures, it is easy to see that the distributions of particle concentrations in a gas with a thick boundary layer are different from that obtained previously. The contour curves have been shifted downstream by boundary layer effects. This can be explained by the conservation of mass and the reduction of velocity by to the viscous effect. Even though the particle free zone shown in Figure 39 appears to the eye to be almost the same, the regimes with high gradients in particle concentration are spread out and move down toward the centerline. The viscous thickening of the boundary layer and the dispersive effect on the particles explains those results.

The gas velocity profile in Figure 40 shows the magnitude and direction of velocity for the one phase flow with and without thick boundary layers. The differences are significant. Pressure is an important field variable. Pressure fields for the viscous and inviscid cases, for the one phase flow and two phase flow (1μ, 15μ), are presented in Figure 41. From these results, it is concluded that the nozzle pressures for the viscous cases are higher than those of inviscid cases and the pressure difference between centerline and wall is small for all cases. Mach number contours also show a significant difference between viscous and inviscid cases. The Mach number contours are displayed in Figures 42 and 43. It is apparent that the sonic line is moved downstream due to the viscous effect. As mentioned before, the physical accuracy for the results may be doubtful because the effective

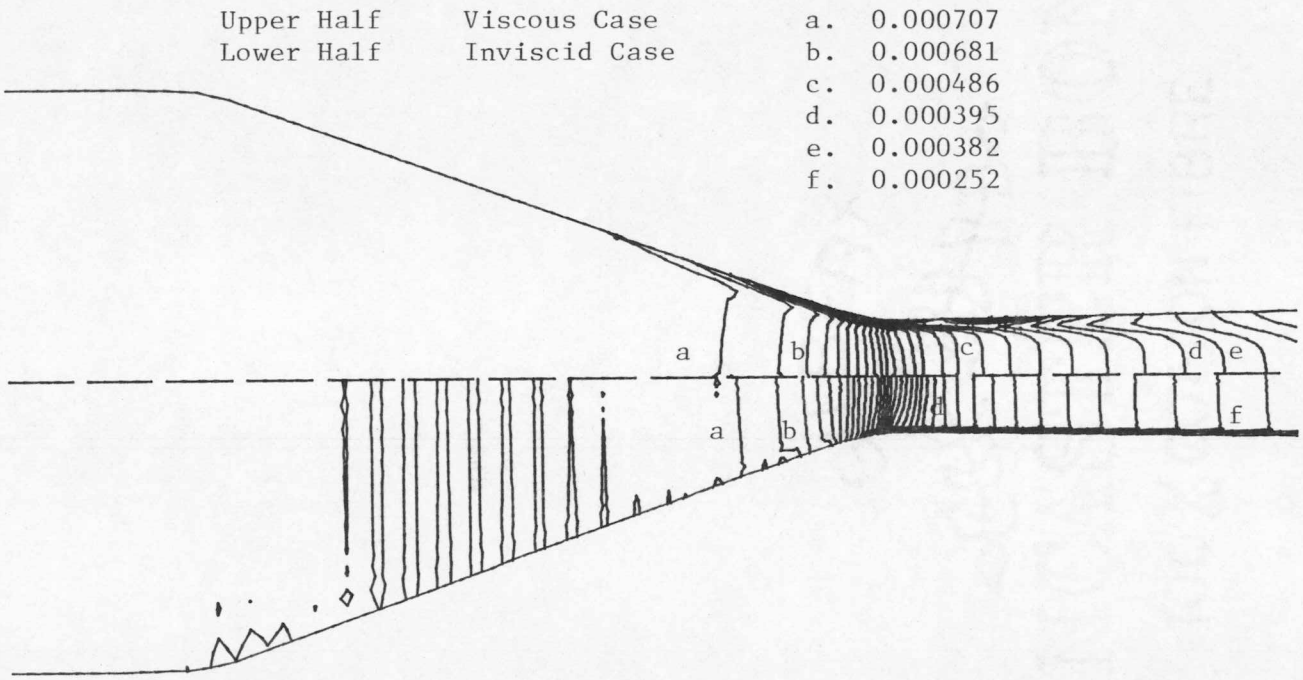


Figure 38. Particle Concentration Contour for Two Phase Flow with r_j = 1μ and ϕ = 1.43%.

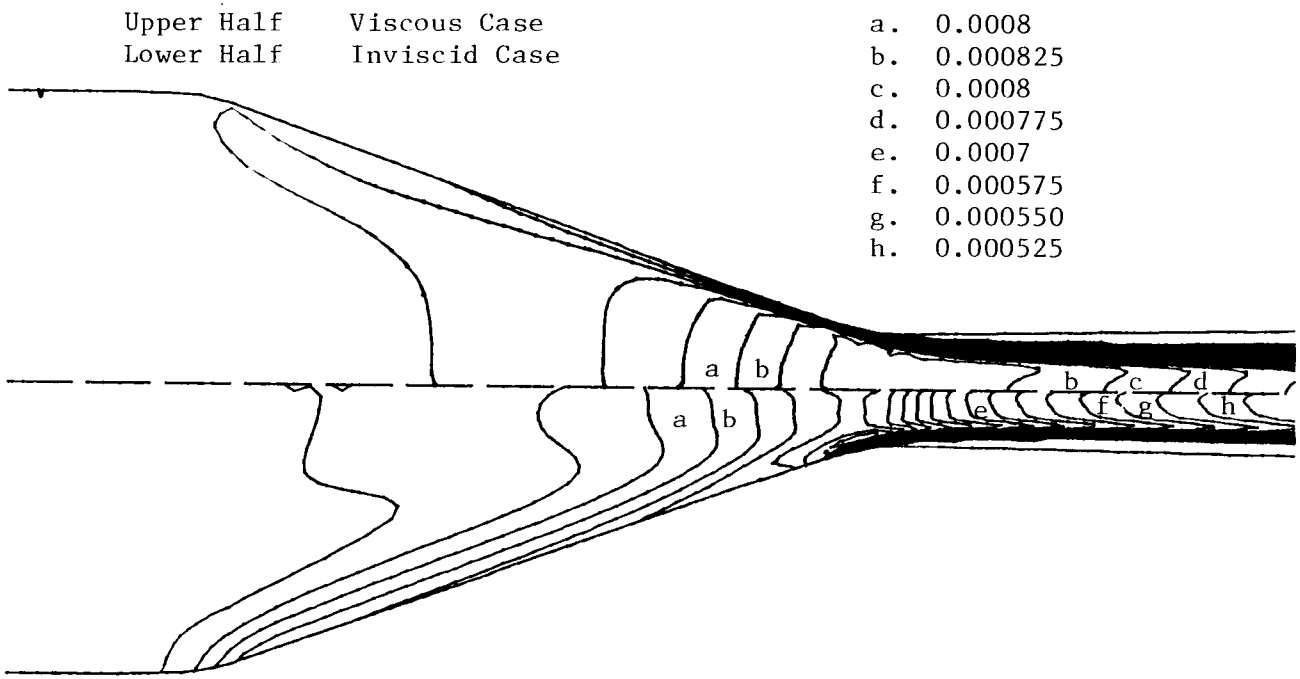


Figure 39. Particle Concentration Contour for Two Phase Flow with r_j = 15μ and ϕ = 1.43%.

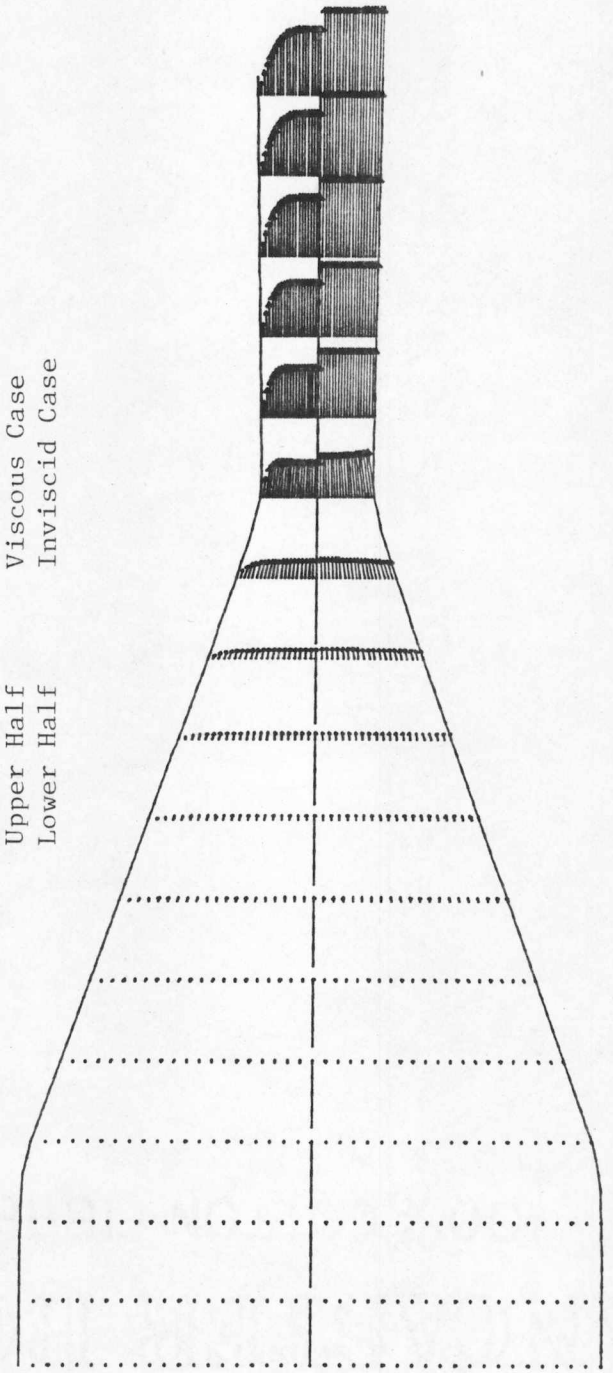


Figure 40. Gas Velocity Vector for One Phase Flow.

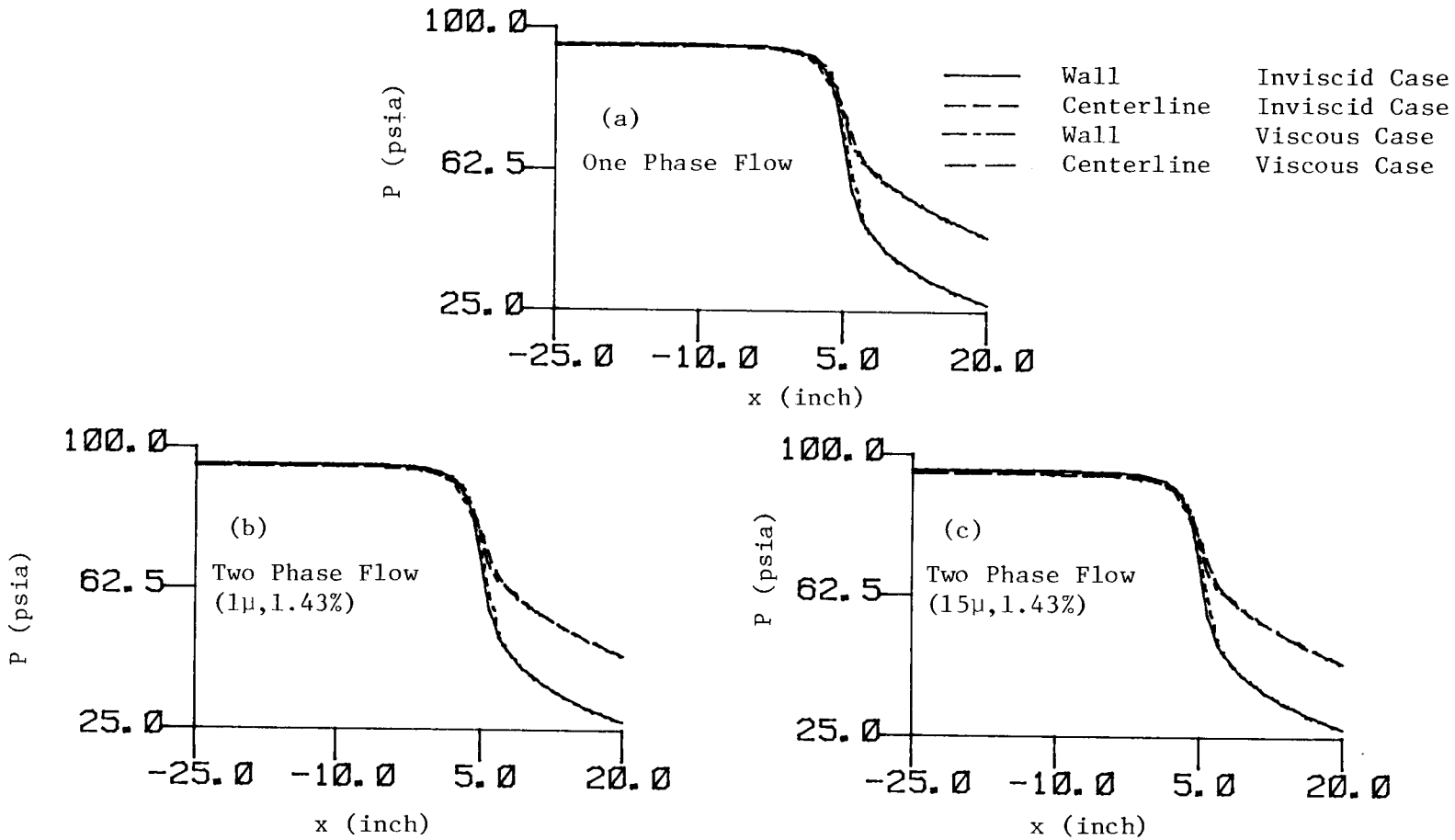


Figure 41. Pressure Distribution along the Wall and Centerline.

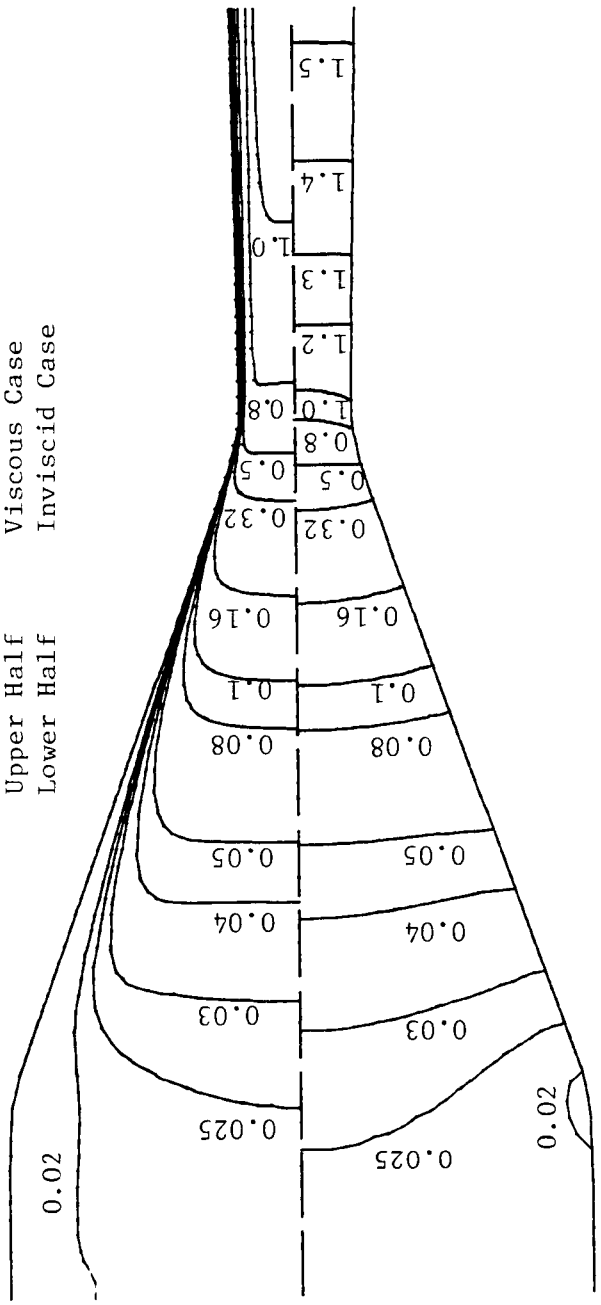


Figure 42. Mach Number Contour for Two Phase Flow with r_j = 1μ and ϕ = 1.43%.

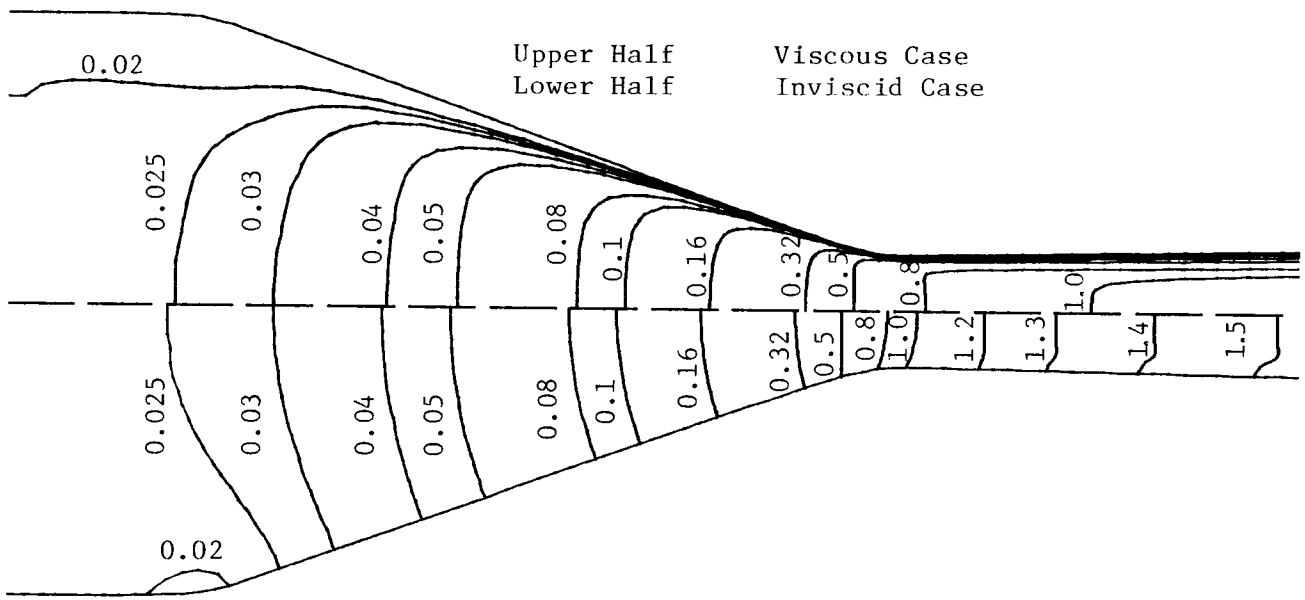


Figure 43. Mach Number Contour for Two Phase Flow with r_j = 15μ and ϕ = 1.43%.

viscosity model is arbitrary. It was important to confirm that this model could provide an easy way to check the effect of a thick boundary layer on the particle concentrations and flow behaviors in compressible nozzle flow. The previously discussed results provided the confirmation, in addition to being important in their own way.

Discussion of Results for the Viscous-Inviscid Interaction Model

In this attempt to study boundary layer effects on compressible gas-particle flow, the effect of particles inside the turbulent boundary layer is neglected. The integral equations of the turbulent boundary layer for the one phase flow were applied to study the effects of thin turbulent boundary layer on the internal two phase flow. The above assumption is justified for two phase flows with large particle sizes, high Reynolds numbers and/or for nozzle with large angle contraction and expansion sections. The reason is that extensive particle free zones exist downstream of the nozzle throat for these conditions. To simplify this type of analysis, the turbulent boundary displacement effect was applied only downstream of the throat. If such a study is to apply to all the flow regions (upstream and downstream), such a complete set of integral equations for the two phase turbulent boundary layer flow must be derived from the governing equations which were presented in Chapter II. Moreover, the velocity profiles and all the empirical relations would require modification.

Under the aforementioned asumption, three different cases, which include one phase and two phase flow with different particle sizes

(1μ, 15μ), were studied in the present research. As mentioned, the turbulent boundary layer velocity profile, which was presented by Whitfield [24], was utilized in the study.

The numerical results for the velocity profile for the one and two phase flow are shown in Figure 44. It is easy to see that the velocity distributions for the two phase flow are not very smooth. The reason may be that the effects of particles on the gas phase inside the turbulent boundary layer were neglected, and, the surface source model which is used to simulate the boundary layer displacement effect was only applied to the gas phase. In order to analyze this problem, further study is required to develop a two phase gas-particle integral boundary layer analysis. Note also that if the boundary layer extends far enough into the flow, it will be interacting with the high particle concentration zones, so the outer regime of the velocity profile will probably have to be modified to incorporate particle drag effects.

Even though several problems may reduce the accuracy of this study, the results given in the following figures present valuable information which shows the difference in flow properties between one and two phase flow with thin turbulent boundary layers. As mentioned before, the particles try to move to the centerline after the throat due to the inertial effect. Thus, particles tend to drag the boundary layer to the centerline. The displacement thickness for the case of larger size particles is larger than that for small particles. One expects then, that the displacement thickness of one phase flow should be smaller than that of both two phase flows. This is confirmed in Figure 45. Whitfield [41] has mentioned that the turbulent boundary layer velocity profile

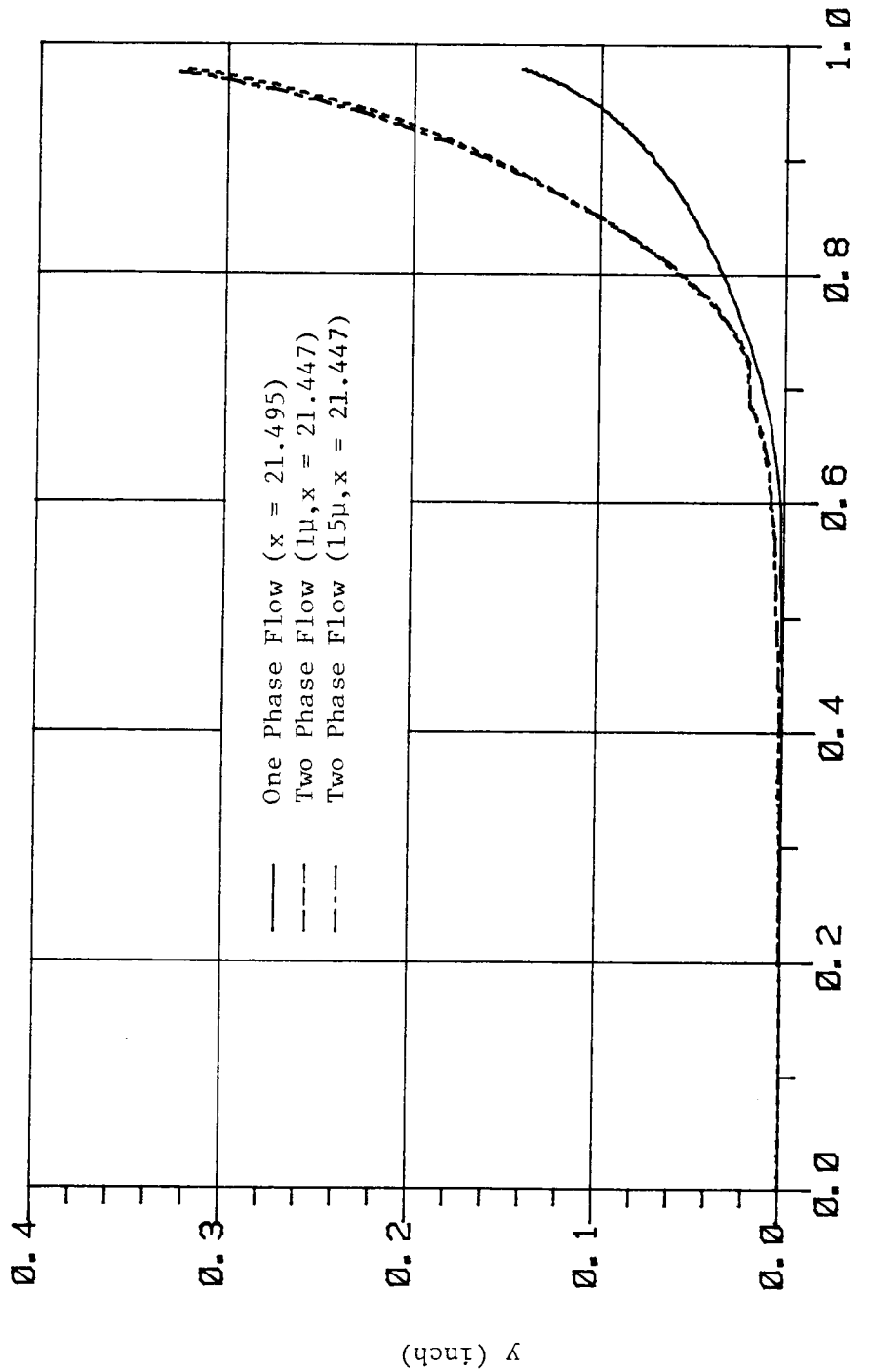


Figure 44. Gas Velocity Profile for One Phase Flow and Two Phase Flows with ϕ = 1.43%.

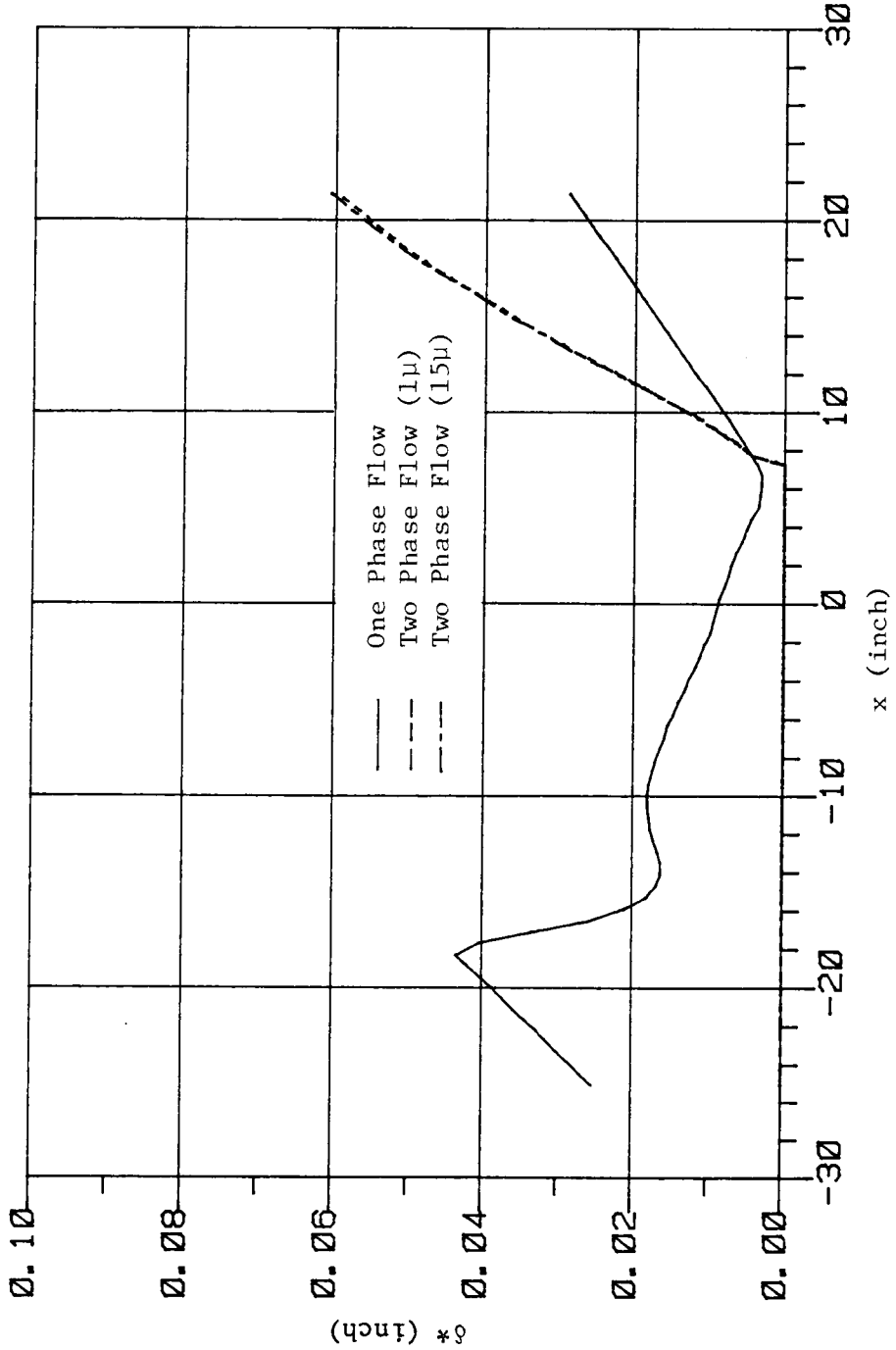


Figure 45. Displacement Thickness for One Phase Flow and Two Phase Flows with ϕ = 1.43%.

should be modified for axisymmetric internal flow when the shape factor (H) is larger than 2.9. To check this condition, the shape factor distribution along the wall were computed and the values given in Figure 46 are less than 2.5 for all three cases. Momentum thickness (θ) and friction coefficient (C_f) are plotted respectively in Figures 47 and 48. All the data show that the numerical values for two phase flows are higher than those for one phase flow. It should be mentioned again that the turbulent boundary layer analysis for the two phase flows was applied only to the wall downstream of the nozzle throat and that the numerical values for displacement thickness and shape factor at the throat are the same for both one phase and two phase flow.

Because of the different assumptions, inlet conditions and so forth between the simple effective viscosity model and the viscous-inviscid interaction model, the comparison of numerical accuracy between those two models is not practical. The present research provides a qualitative study, even though the quantitative comparison is not useful. To demonstrate the differences or similarities of behavior of particles affected by the existence of wall turbulent boundary layers, two plots are presented. From the results shown in Figures 49 and 50, for both approaches, the particle free zone and high gradient particle condensation regions appear similar. Contour lines of constant flow variable values are generally shifted downstream when the boundary layer is modeled. When the results are compared between Figures 39 and 49, the shapes of the contour lines are similar except that the high gradient regions for the simple effective viscosity model are wider than those of viscous-inviscid interaction model. For further study of the difference

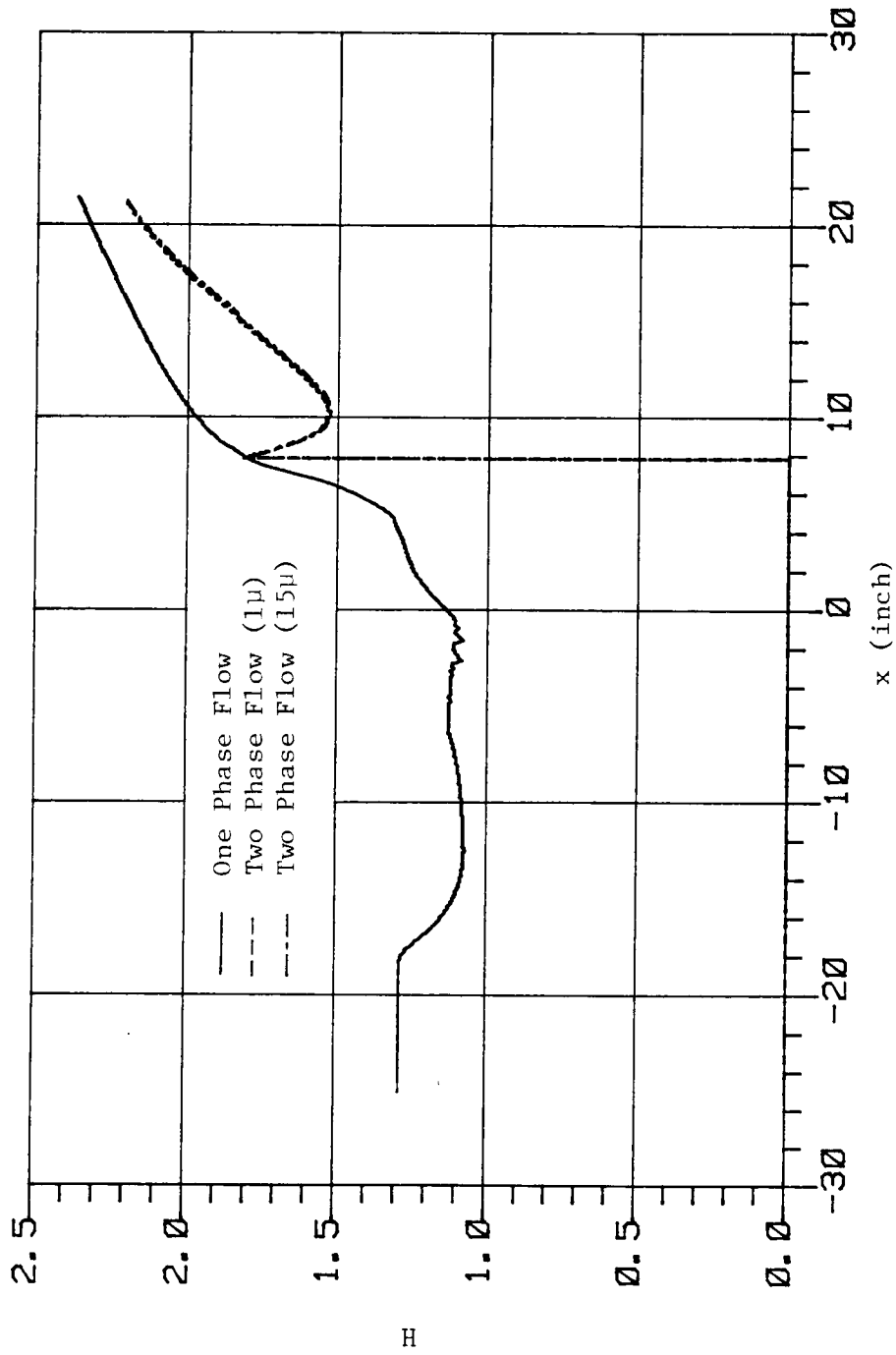


Figure 46. Shape Factor for One Phase Flow and Two Phase Flows with $\phi = 1.43\%$.

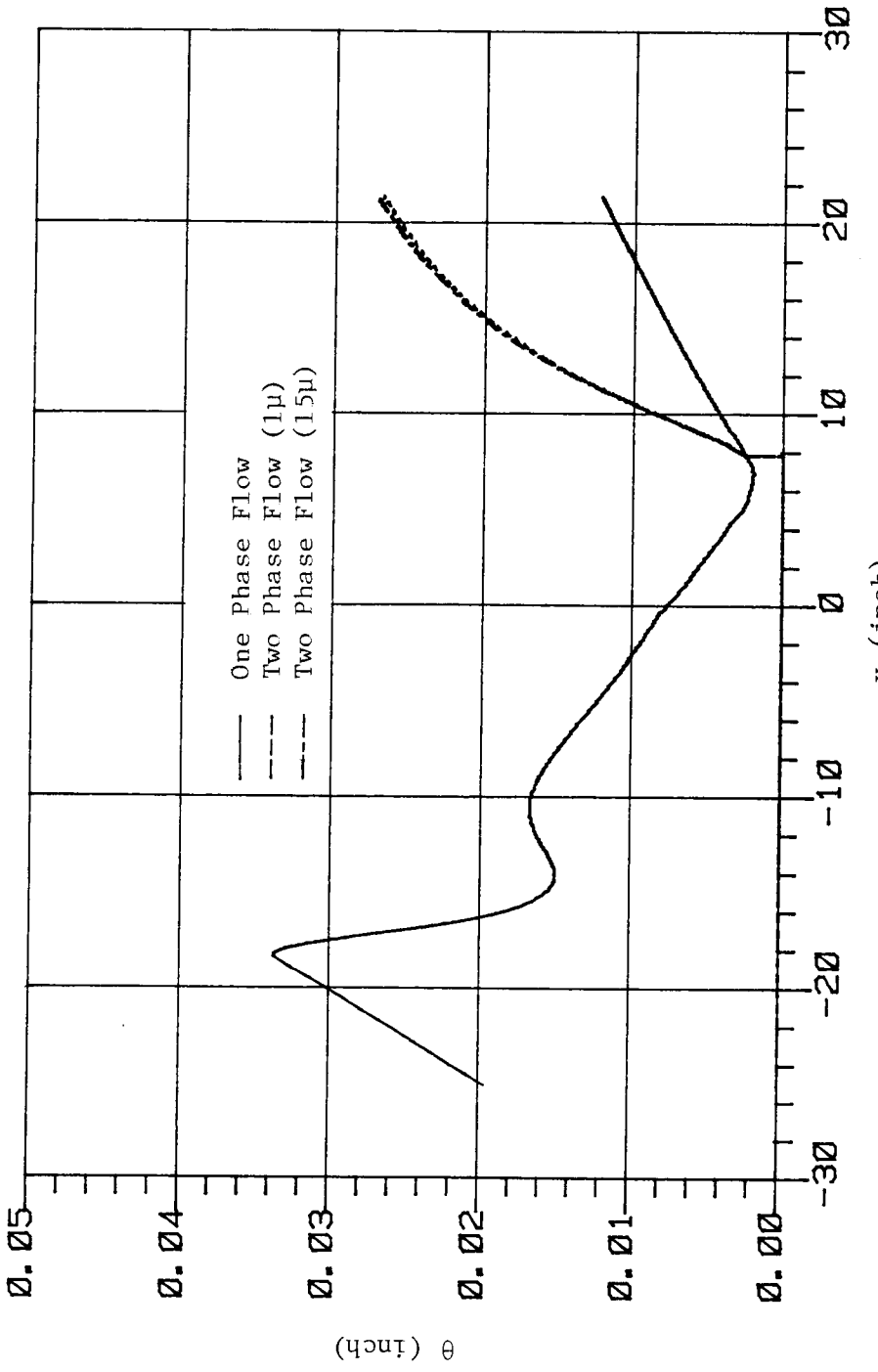


Figure 47. Momentum Thickness for One Phase Flow and Two Phase Flows with ϕ = 1.43%.

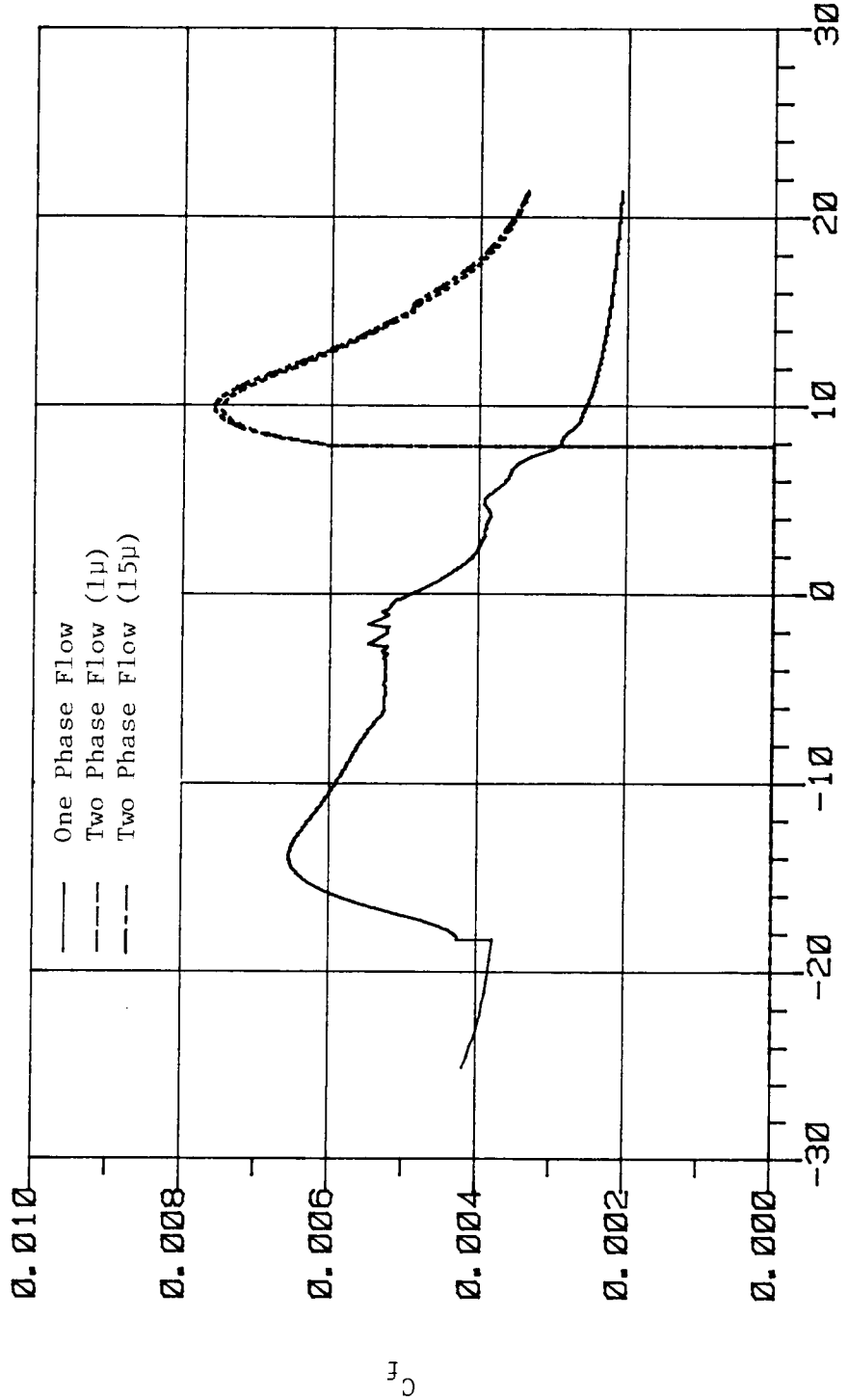


Figure 48. Friction Coefficient for One Phase Flow and Two Phase Flows with ϕ = 1.43%.

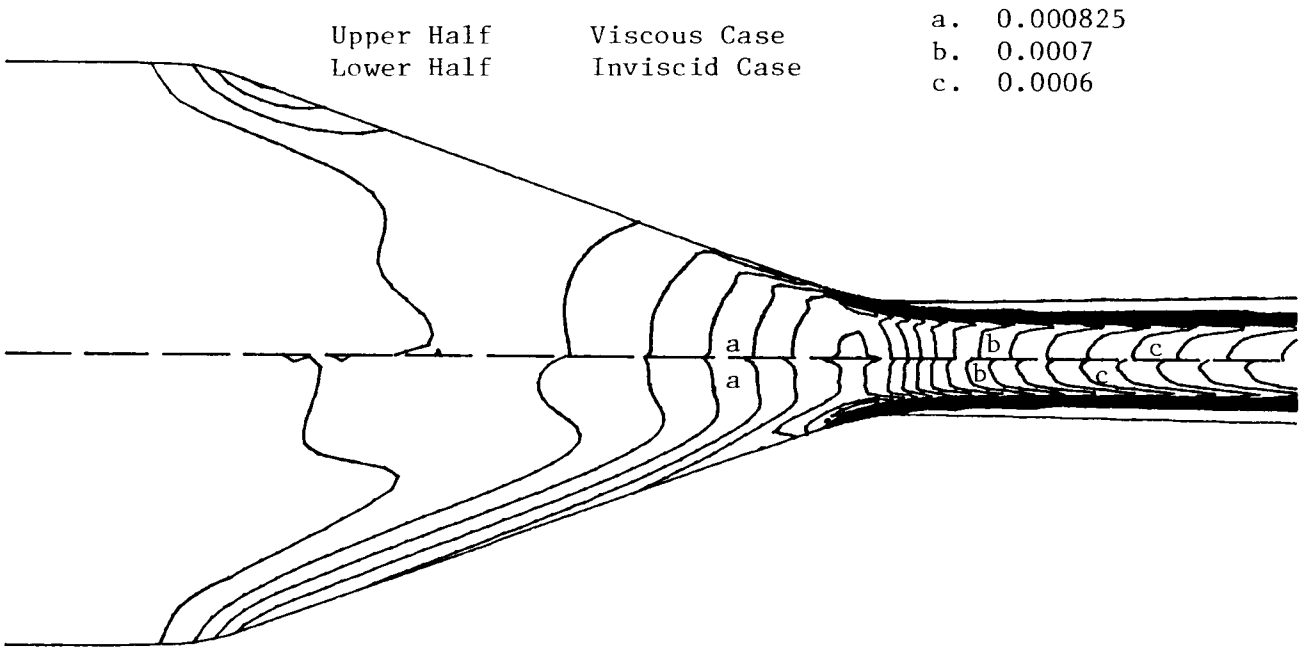


Figure 49. Particle Concentration Contour for Two Phase Flow with $r_j = 15\mu$ and $\phi = 1.43\%$.

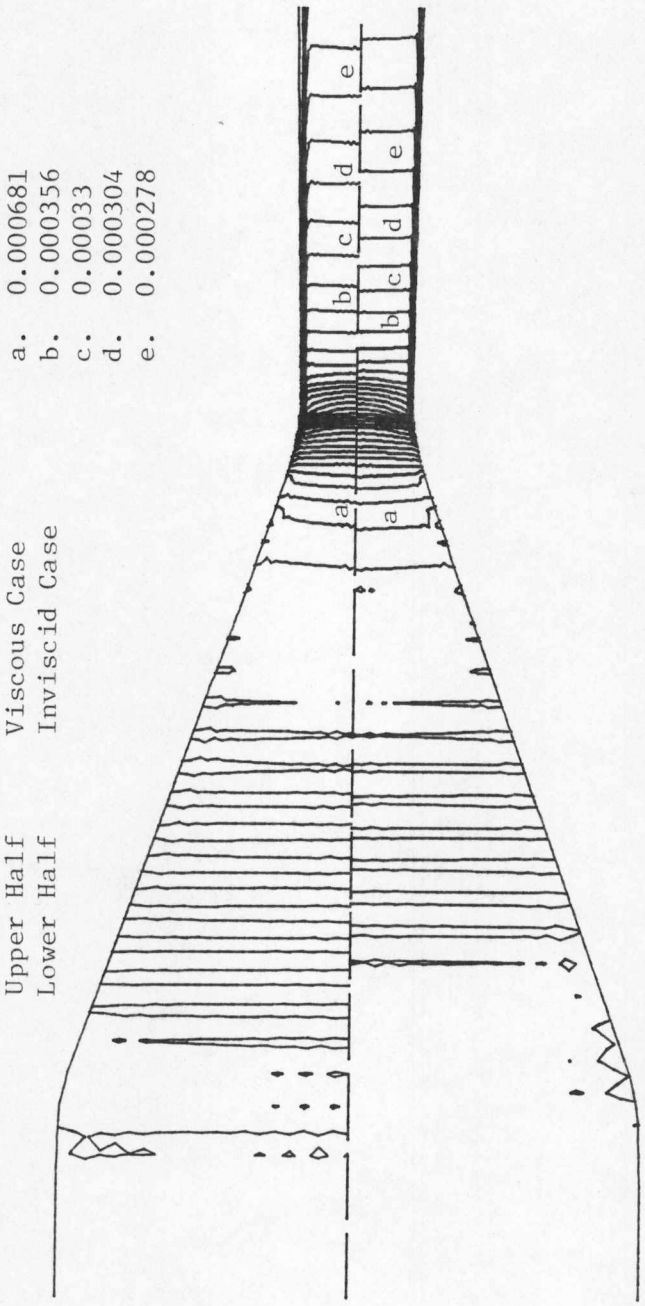
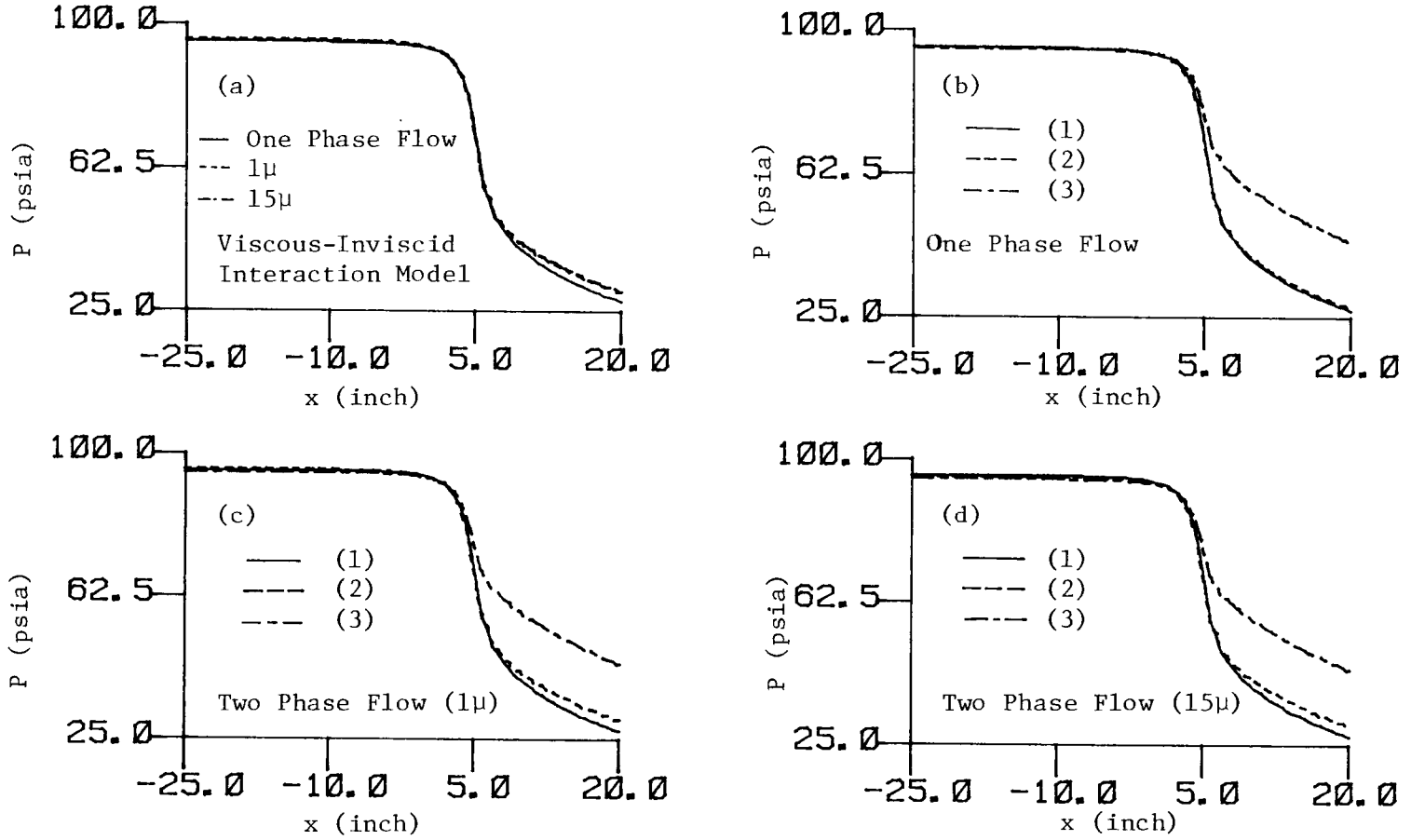


Figure 50. Particle Concentration Contour for Two Phase Flow with $r_j = 1\mu$ and $\phi = 1.43\%$.

between inviscid gas model, effective viscosity model and viscous-inviscid interaction model, the pressure along the wall for the one and two phase flow are presented in Figure 51. It is obvious that the boundary layer will increase the pressure and this effect becomes strong for the simple effective viscosity model. Of course, it should be mentioned again that the arbitrary values of effective viscosity and different inlet conditions make the comparisons difficult to evaluate precisely.



(1) Inviscid Model (2) Viscous-Inviscid Model (3) Effective Viscosity Model

Figure 51. Pressure Distribution along the Wall.

CHAPTER V

CONCLUSIONS AND RECOMMENDATIONS

Conclusions

A time-dependent, two-step, explicit MacCormack scheme was applied to a set of partial differential equations describing the motion of two phase, gas-particle flows. Both inviscid gas and viscous gas solutions were obtained. For the viscous cases, two approaches were tried. One approach was a purely viscous flow and the other was a viscous-inviscid interaction approach. An integral method and a simple effective viscosity model were introduced to treat turbulent boundary layer effects, but the particle dispersion due to turbulence was not considered in the present study. Extensive numerical investigations and their numerical results showed that the model satisfied the basic physical phenomena and the numerical method conserved global and species mass, energy and momentum to within a few percent. The numerical solutions provide the gas and particle velocity, temperature, pressure and density distributions, in a conical rocket nozzle, and in the combustor outlet, nozzle, and channel inlet of the Coal Fired Flow Facility being developed at UTSI. For viscous cases, the gas phase Mach numbers and interpretive behavior of turbulent boundary layers in two phase flow were provided. Based on a significant amount of development of the numerical scheme, the present solution procedure was shown to be stable, accurate and reliable.

The special techniques described in this study were used to solve specific numerical problems or model physical phenomenon. The idea of and treatment of the particle free zone with pseudo-wall boundary conditions reduced significant global conservation error to about 1% mass flow rate for a 15μ particle case in CFFF. A modified MacCormack finite difference scheme for the limiting particle streamline (pseudo-wall) and a fourth-order smoothing term were required to solve the flow field for large particle cases. A time smoothing idea was used to accelerate the convergence of the solution procedure for subsonic flow in inlets.

Recommendations

Even though this study has made considerable progress in establishing an understanding of the two phase flow problems, it became clear that further work is required in refining this understanding. Because techniques based on extrapolation methods for particle concentration on the wall for boundary conditions have a limited physical meaning, an intensive study of near wall physics is suggested in the future. Two approaches may be helpful. First, Turkel [42] introduced the Lagrange-Euler method to solve the moving boundary problem. Second, the Flux Corrected Transport (FCT) idea described by Book [43] might be used to solve the continuity equation for particle concentration on the wall. In this study, the particle phase is assumed to be "sufficiently" continuous. Individual particle trajectories, and particle-wall collision behavior cannot be predicted. To study these effects, it might be that a Lagrange viewpoint and trajectory model can be applied. For the efficiency of the computer code, the results given in Table 5 show that the

Table 5

Computational Time[a]

Model	Case	Total Time Steps	Total CPU Time[b] (hr)
Inviscid Gas Model	One phase	2003	2.7
	1μ, 1.43%	2647	4.5
	1μ, 14.3%	4026	6.0
	15μ, 1.43%	9223	18.0
Simple Effecive Viscosity Model	One phase	3784	5.19
	1μ,1.43%	236	0.7
	15μ, 1.43%	5003	13.6
Viscous-Inviscid Interaction Model	One phase	250	0.24
	1μ,1.43%	2150	4.0
	15μ,1.43%	4100	9.57

[a]The machine is VAX 11/780 and the grid numbers for CFFF are 81 x 21.

[b]The approximate values are calculated from the arbitrary time intervals.

computational times for some cases are large. Even though the different machines can solve this problem, it is suggested that the implicit method presented by MacCormack [44] may easily apply to modify the present code and reduce the computational time. In order to solve viscous gas problems, it is suggested that a nonuniform computational plane grid be used to replace the uniform computational grid used in the present code. This approach may lead to higher order mapping techniques. For further study of two phase turbulent flow, a two-equation turbulent model presented by Elghobashi, et al. [45] may be useful. If the viscous-inviscid interaction method developed in the study is to be further developed, an inverse integral method and empirical or theoretical study of fully two phase, turbulent boundary layer velocity profiles should be conducted in future research programs.

In this study, only one kind of particle in the flow region is considered for each case. The particle collision is neglected. To prove this assumption, the ratio of mean free path to the interparticle spacing is presented in Table 6. From these results, it is easy to see the mean free path is much larger than the interparticle spacing. The effect of particle collision is very small. If different kinds of particles exist in the same flow field, the particle collision shall be considered due to the different magnitude of particle velocity. The agglomeration and/or decomposition of the particles are not neglected. For the turbulent flow, the particle dispersion exists and the particle collision shall be considered also.

Table 6

The Ratio of Mean Free Path of Particle-to-Particle Collision to the Interparticle Spacing[a]

Conical Nozzle (1μ, 30%)	CFFF (1μ, 1.43%)	CFFF (1μ, 14.3%)	CFFF (15μ, 1.43%)
6.7383301E+01	4.6351013E+02	8.9346512E+01	2.8625876E+02
6.7315216E+01	4.6362399E+02	8.9581779E+01	2.8751016E+02
6.7412994E+01	4.6319510E+02	8.9092957E+01	2.8787411E+02
6.7632393E+01	4.6364899E+02	8.9472107E+01	2.8765182E+02
6.7726883E+01	4.6340915E+02	8.9270409E+01	2.8714355E+02
6.7851395E+01	4.6352298E+02	8.9363007E+01	2.8659598E+02
6.7908722E+01	4.6344714E+02	8.9318314E+01	2.8597156E+02
6.7906967E+01	4.6347211E+02	8.9318741E+01	2.8470660E+02
6.7840393E+01	4.6342175E+02	8.9313377E+01	2.8183575E+02
6.7749397E+01	4.6340915E+02	8.9287277E+01	2.7687460E+02
6.7638680E+01	4.6335876E+02	8.9285019E+01	2.7116370E+02
6.7480408E+01	4.6330841E+02	8.9249092E+01	2.6831052E+02
6.7277061E+01	4.6323260E+02	8.9241478E+01	2.7374472E+02
6.7094330E+01	4.6314429E+02	8.9205399E+01	2.9539923E+02
6.7116089E+01	4.6299323E+02	8.9182426E+01	3.5080078E+02
6.8191254E+01	4.6294312E+02	8.9187531E+01	5.1467468E+02
7.4694252E+01	4.6260355E+02	8.9054138E+01	b
1.1153696E+02	4.6288000E+02	8.9271652E+01	b
5.5010394E+02	4.6207684E+02	8.8393433E+01	b
2.0376475E+04	4.8278140E+02	9.1342926E+01	b
1.7662459E+04	5.0598920E+02	9.4551422E+01	b

[a]The numerical values are calculated at the exit plane from the following relation which was shown in reference [46].

$$\frac{\lambda}{n^{-1/3}} = \left(\frac{\rho_j}{m_j}\right)^{-2/3} (36\pi)^{-1/3}$$

[b]Particle free zone.

The radiation model applied in this study is only a simple approximate approach. In order to find out the effect of the radiative energy, the ratio of radiative heat transfer to convection heat transfer is calculated and presented in Table 7. The data show that the radiative heat transfer is negligible in the conical nozzle and CFFF with small particle case. For the large particle, the radiative energy becomes large. For the more reliable and accurate research on this topic, the radiation models mentioned in the references 47 and 48 are suggested. However, it is important that the wall is assumed adiabatic in this case, so that the net radiative heat transfer between two phase flow and wall is neglected.

Besides additional theoretical study of the particle concentration boundary conditions, and work on speeding up the numerical solution with recent improvements to the family of MacCormack schemes, the program must be adapted to MHD type flows. For application to MHD flows, the gas specific heats cannot be treated as constant, so that the energy equation and the thermodynamic properties will require modification. Also, the flow in an MHD nozzle occurs with highly cooled walls, so the adiabiatic wall condition will need modification to model heat transfer from the nozzles. The radiation heat source term must be approximated for a high emissivity gas with a significant number of scattering centers (particulates). Also, the particle drag law and Nusselt number correlations may require improvement.

Finally, for very high temperature coal combustion, a major uncertainty is the lack of knowledge of the production of coal or ash particles in the combustion process in terms of number densities and mass

Table 7

The Ratio of Radiative Heat Transfer to Convective Heat Transfer[a]

Conical Nozzle (1μ, 30%)	CFFF (1μ, 1.43%)	CFFF (1μ, 14.3%)	CFFF (15μ, 1.43%)
7.9788522E-05	1.8956594E-02	2.0995997E-02	3.1268844E-01
8.0170248E-05	1.8956449E-02	2.0990362E-02	3.1267598E-01
8.0807607E-05	1.8956484E-02	2.1001359E-02	3.1266427E-01
8.2011509E-05	1.8956628E-02	2.0992629E-02	3.1265706E-01
8.3896783E-05	1.8956276E-02	2.0997297E-02	3.1265402E-01
8.6343105E-05	1.8956246E-02	2.0995127E-02	3.1264880E-01
8.9139110E-05	1.8956069E-02	2.0996574E-02	3.1264475E-01
9.1926369E-05	1.8956291E-02	2.0996090E-02	3.1263539E-01
9.4512448E-05	1.8956289E-02	2.0997081E-02	3.1263342E-01
9.6889060E-05	1.8955898E-02	2.0998193E-02	3.1263900E-01
9.9066980E-05	1.8956106E-02	2.0997666E-02	3.1266430E-01
1.0096618E-04	1.8956123E-02	2.0998582E-02	3.1269038E-01
1.0252272E-04	1.8955449E-02	2.0998405E-02	3.1267935E-01
1.0373395E-04	1.8955080E-02	2.0999162E-02	3.1257629E-01
1.0445918E-04	1.8955253E-02	2.1000884E-02	3.1232110E-01
1.0371178E-04	1.8955193E-02	2.1000279E-02	3.1188118E-01
9.8016317E-05	1.8955367E-02	2.1003539E-02	b
8.1778730E-05	1.8954761E-02	2.0998631E-02	b
6.1160412E-05	1.8955212E-02	2.1017607E-02	b
5.0014227E-05	1.8946452E-02	2.0974904E-02	b
4.8123977E-05	1.8938361E-02	2.0933380E-02	b

[a]The numerical values are calculated from the following relation at the exit plane.

$$\frac{\sigma(4\pi r_j^2)(\varepsilon_j T_j^4 - \varepsilon T^4)}{h_c(4\pi r_j^2)(T_j - T)}$$

[b]Particle free zone.

flux distributions at the combustor exit (or nozzle inlet). Therefore, parametric sensitivity studies must be performed to investigate the effects of assumed particle distributions and fluxes to see if this lack of physical information is critical. In such sensitivity studies, the effects of, or necessity for, treating the gas as viscous or inviscid will also require elucidation.

LIST OF REFERENCES

LIST OF REFERENCES

1. Nickerson, G. R., D. E. Coats and R. W. Hermsen, "A Computer Program for the Prediction of Solid Propellant Rocket Motor Performance," AFRPL-TR-80-34, Volume I, June 1980.

2. Hoglund, R. F., "Recent Advances in Gas-Particle Nozzle Flows," ARS Journal, p. 662, May 1962.

3. Kliegel, J. R., "One Dimensional Flow of a Gas Particle System," TR-59-0000-00746, Space Technology Laboratory, July 1959.

4. Kliegel, J. R. and G. R. Nickerson, "Flow of Gas-Particle Mixtures in Axially Symmetric Nozzles," Progress in Astronautics and Rocketry, Volume 6, Academic Press, New York, pp. 173-194, 1962.

5. Rudinger, G., "Gas-Solid Suspensions," Von Karman Institute for Fluid Dynamics, Lecture Series 90, May 1976.

6. Zucrow, M. J. and J. D. Hoffman, Gas Dynamics, Volume II, John Wiley and Sons, Inc., New York, 1977.

7. Peters, C. E., "Internal Aerodynamics of Rocket Engines," Von Karman Institute for Fluid Dynamics, Course Note 58, Chapter 3, April 1966.

8. Regan, J. F., H. D. Thompson and R. F. Hoglund, "Two-Dimensional Analysis of Transonic Gas-particle Flows in Axisymmetric Nozzles," Journal Spacecraft, 8(4), p. 346, April 1971.

9. Jacques, L. J. and J. A. M. Seguin, "Two Dimensional Transonic Two-Phase Flow in Axisymmetric Nozzles," AIAA Paper No. 74-1088, October 1974.

10. Chang, I-Shih, "One-and Two-Phase Nozzle Flows," AIAA Paper No. 80-0272, January 1980.

11. Crowe, C. T., "Review-Numerical Models for Dilute Gas-Particle Flows," Journal of Fluids Engineering, Volume 104, pp. 297-303 September 1982.

12. DiGiacinto, M., F. Sabetta and R. Piva, "Two-Way Coupling Effects in Dilute Gas-Particle Flows," Journal of Fluids Engineering, Volume 104, pp. 304-312, September 1982.

13. Hoffman, J. D., "An Analysis of the Effects of Gas-Particle Mixtures on the Performance of Rocket Nozzles," Report No. TM-63-1, Purdue University, January 1963.

14. Torobin, L. E., and W. H. Gauvin, "Fundamental Aspects of Solid-Gas Flow," Canadian Journal of Chemical Engineering, 37, pp. 129-141, August 1959.

15. Drake, R. M., Jr., "Discussion on G. C. Vliet and G. Leppert: Forced Convection Heat Transfer from An Isothermal Sphere to Water," Journal of Heat Transfer, 83, pp. 170-172, 1961.

16. Carlson, D. J. and R. F. Hoglund, "Particle Drag and Heat Transfer in Rocket Nozzles," AIAA Journal, 2, p. 1980, 1964.

17. Crowe, C. T., "Drag Coefficient of Particles in a Rocket Nozzle," AIAA Journal, 5, pp. 1021-1022, 1967.

18. Crowe, C. T., W. R. Babcock and P. C. Willoughby, "Drag Coefficient for Particles in Rarefied Low Mach Number Flows," Progress in Heat and Mass Transfer, 6, Porgammon Press, pp. 419-431, 1972.

19. Kliegel, J. R., "Gas Particle Nozzle Flows," Ninth Symposium (International) on Combustion Academic Press, pp. 811-827, 1963.

20. Henderson, C. B., "Drag Coefficient of Spheres in Continuum and Rarefied Flows," AIAA Journal, 14, pp. 707-708, 1976.

21. Schaff, S. and P. Chambre, "Flow of Rarefied Gases," Fundamentals of Gas Dynamics, Princeton Series, Volume III, Princeton University Press, p. 725, 1958.

22. Bird, R. B., W. E. Steward and E. N. Lightfoot, Transport Phenomena, John Wiley and Sons, Inc., New York, p. 409, 1960.

23. Tracy Donegan, "Unsteady Viscous-Inviscid Interaction Procedures for Transonic Airfoil Flows," Master Degree Thesis, UTSI, December 1983.

24. Whitfield, D. L., "Integral Solution of Compressible Turbulent Boundary Layer Using Improved Velocity Profile," AEDC-TR-78-42, December 1978.

25. Cline, M. C., "VNAP: A Computer Porgram for Computation of Two-Dimensional, Time-Dependent Compressible, Viscous, Internal Flow," LA-7326, November 1978.

26. MacCormack, R. W., "The Effect of Viscosity in Hypervelocity Impact Cratering," AIAA Paper No. 69-354, AIAA Hypervelocity Conference, Cincinnati, Ohio, April 1969.

27. Roache, P. J., Computational Fluid Dynamics, Hermosa Publishers, 1976.

28. Yee, H. C., "Numerical Approximation of Boundary Conditions with Applications to Inviscid Equation of Gas Dynamics," NASA-TM-81265, 1978.

29. Gottlieb, D. and E. Turkel, "Boundary Conditions for Multistep Finite-Difference Methods for Time-Dependent Equations," Journal of Computational Physics, 26, pp. 181-196, 1978.

30. Kreiss, H. O., "Stability Theory for Difference Approximations of Mixed Initial Boundary Value Problems, I," Mathematics of Computation, 22, pp. 703-714, 1968.

31. Serra, R. A., "Determination of Internal Gas Flows by a Transient Numerical Technique," AIAA Journal, 10, p. 603, 1972.

32. Oliger, J. and Sundström, A., "Theoretical and Practical Aspects of Some Initial Boundary Value Problems in Fluid Dynamics," SIAM Journal on Applied Mathematics, 35, p. 419, 1978.

33. Cline, M. C., "VNAP 2: A Computer Program for Computation of Two Dimensional, Time-Dependent, Compressible, Turbulent Flow," LA-8872, August 1981.

34. Moretti, G. and M. Abbett, "A Time-Dependent Computational Method for Blunt Body Flows," AIAA Journal, 4, p. 2136, 1966.

35. Moretti, G. and M. Pandolfi, "On the Calculation of Subsonic Flows in Ducts," Polytechnic Institute of New York, Report M/AE 80-18, June 1980.

36. Richtmyer, R. and K. W. Morton, Difference Methods for Initial Value Problems, John Wiley and Sons, Inc., New York, 1967.

37. MacCormack, R. W., "Numerical Solution of the Interaction of a Shock Wave with a Laminar Boundary Layer," Lecture Notes in Physics, M. Holt, editor, Volume 8, Springer-Verlag, New York, pp. 151-163, 1971.

38. Kutler, P., L. Sakell and G. Aiello, "On the Shock-on-Shock Interaction Problem," AIAA Paper No. 74-524, June 1974.

39. Nash, J. F., "A Practical Calculation Method for Compressible Turbulent Boundary Layer in Two-Dimensional and Axisymmetric Flows," Lockheed-Georgia Company, Research Memorandum - ER-9428, August 1967.

40. Schlichting, H., Boundary-Layer Theory, Sixth Edition, McGraw-Hill, New York, p. 599, 1968.

41. Whitfield, D. L., "Analytical Description of the Complete Two-Dimensional Turbulent Boundary-Layer Velocity Profile," AEDC-TR-77-79, September 1977.

42. Turkel, E., "Order of Accuracy and Boundary Conditions for Large Scale Time Dependent Patial Differential Equations, Von Karman Institute for Fluid Dynamics, Lecture Series 1979-6, March 1979.

43. Book, David L., Finite-Difference Techniques for Vectorized Fluid Dynamics Calculations, Springer-Verlag, New York, pp. 29-55, 1981.

44. MacCormack, R. W., "A Numerical Method for Solving the Equations of Compressible Viscous Flow," AIAA Paper 81-0110, St. Louis, Missouri, January 12-15, 1981.

45. Elghobashi, S. E. and T. W. Abou-Arab, "A Two-Equation Turbulence Model for Two-Phase Flows," Physics of Fluids, 26 (4), April 1983.

46. Hetsroni, Gad, Handbook of Multiphase Systems, Hemisphere Publishing Corporation, pp. 7-6, 1982.

47. Hunter, S. C., S. S. Cherry, J. R. Kliegel and C. H. Waldman, "Gas Particle Nozzle Flows with Reaction and Particle Size Change," AIAA Reports 81-0037, January 1981.

48. Ozisik, M. N., Radiative Transfer, Wiley-Interscience Publication, Chapter 9, 1973.

APPENDICES

APPENDIX A

DERIVATION OF COMPRESSIBLE, TWO PHASE, GAS-PARTICLE FLOW EQUATIONS

The continuum equations are derived on the basis of a control volume and closed system approaches. It is also assumed that the particles are uniformly distributed locally, so that number densities and particle loading mass densities can be treated as continuum variables.

Conservation of Gas Phase Mass

The control volume approach is illustrated below. If $\vec{V}$ is the gas velocity, $\vec{n}$ is an outward unit normal, and ds and dv are surface and volume elements, respectively, then the expression of gas mass conservation is

$$-\frac{\partial}{\partial t}\int_v \rho dv = \int_s \rho\vec{V}\cdot\vec{n}ds.$$

Using the divergence theorem, the above equation can be written as

$$\int_v [\frac{\partial \rho}{\partial t} + \nabla\cdot(\rho\vec{V})]dv = 0.$$

For arbitrary, fixed volumes

$$\frac{\partial \rho}{\partial t} + \nabla\cdot(\rho\vec{V}) = 0$$

or

$$\frac{\partial \rho}{\partial t} + \rho\nabla\cdot\vec{V} + (\vec{V}\cdot\nabla)\rho = 0.$$

In component, the scalar forms are

$$\frac{\partial \rho}{\partial t} + \rho\frac{\partial u}{\partial x} + \rho\frac{\partial v}{\partial r} + u\frac{\partial \rho}{\partial x} + v\frac{\partial \rho}{\partial r} + \delta\frac{\rho v}{r} = 0 \qquad \text{(A1)}$$

where $\delta = 0$ for planar flow, $\delta = 1$ for axisymmetric flow.

Gas Phase Momentum Equations

For the assumption of an inviscid gas, with particle interaction due to drag of the particles, the governing equations can be obtained by a control volume approach and written as:

$$\frac{\partial u}{\partial t} + u\frac{\partial u}{\partial x} + v\frac{\partial u}{\partial r} + \frac{1}{\rho}\frac{\partial P}{\partial x} = f_x$$

$$\frac{\partial v}{\partial t} + u\frac{\partial v}{\partial x} + v\frac{\partial v}{\partial r} + \frac{1}{\rho}\frac{\partial P}{\partial r} = f_y$$

the f_x and f_y are effective drag forces per unit mass. They arise from gas-particle interaction through particle drag. Therefore, they must be derived for a particle cloud acting on the gas.

Drag Force

Consider a unit volume of gas which contains N_j particles, the total drag force exerted on a volume V of gas is then

$$\vec{D} = N_j V \vec{D}_j .$$

The mass of gas in the volume V is

$$M = \rho V .$$

Therefore the drag force per unit mass of gas is

$$\vec{f} = -\frac{\vec{D}}{M} = -\frac{N_j \vec{D}_j}{\rho}$$

where the particle drag formula $\vec{D}_j = C_D(\pi r_j^2)\frac{1}{2}\rho \left| \vec{V}-\vec{V}_j \right| (\vec{V}-\vec{V}_j)$.

Let $C_D = (\frac{24}{Re_j})\, f_j = \dfrac{24 f_j \mu_g}{\rho \left| \vec{V}-\vec{V}_j \right| (2r_j)}$, $N_j = \dfrac{\rho_j}{(\frac{4}{3}\pi r_j^3)m_j}$

and $A = \dfrac{9}{2}\dfrac{\mu_g f_j}{m_j r_j^2}$

then

$$\vec{f} = -(\frac{\rho_j}{\rho})\ A\ (\vec{V} - \vec{V}_j)$$

where m_j and r_j are the mass density and radius of particle, respectively. Hence, the momentum equations for the gas phase are

$$\frac{\partial u}{\partial t} + u\frac{\partial u}{\partial x} + v\frac{\partial u}{\partial r} + \frac{1}{\rho}\frac{\partial P}{\partial x} = -A\ (\frac{\rho_j}{\rho})\ (u - u_j) \qquad (A2)$$

$$\frac{\partial v}{\partial t} + u\frac{\partial v}{\partial x} + v\frac{\partial v}{\partial r} + \frac{1}{\rho}\frac{\partial P}{\partial r} = -A(\frac{\rho_j}{\rho})(v - v_j). \qquad (A3)$$

Conservation of Gas Phase Energy

The governing equation in enthalpy form is, from the first law of thermodynamic and open system fixed control volume analysis

$$\rho C_p \frac{DT}{Dt} = \frac{DP}{Dt} + q''' + w'''$$ (note q''' and w''' are positive into gas by assumption)

written for an ideal, perfect gas with constant C_p. The term q''' reflects the energy exchange with the particles, and w''' represents the work done by the drag forces acting on the gas. Expanding the equation out, it becomes

$$\rho C_p\ (\frac{\partial T}{\partial t} + u\frac{\partial T}{\partial x} + v\frac{\partial T}{\partial r}) = \frac{\partial P}{\partial t} + u\frac{\partial P}{\partial x} + v\frac{\partial P}{\partial r} + q''' + w''' .$$

Using the ideal gas equation of state, the derivatives of T with respect to t, x and r, and the relations $a^2 = \frac{\gamma P}{\rho}$ the equation can be rewritten as:

$$\frac{\partial P}{\partial t} + u\frac{\partial P}{\partial x} + v\frac{\partial P}{\partial r} - a^2(\frac{\partial \rho}{\partial t} + u\frac{\partial \rho}{\partial x} + v\frac{\partial \rho}{\partial r}) = \frac{R}{C_v} q''' + \frac{R}{C_v} w''' .$$

Heat Source Per Unit Volume

A volume V of gas containing N_j particles per unit volume is considered here. Each particle will contribute a heat source at the rate

$$\dot{q}_j = h_c(4\pi r_j^2)(T_j - T) + \sigma(4\pi r_j^2)(\varepsilon_j T_j^4 - \varepsilon T^4).$$

The heat transfer rate due to all particles in V is

$$\dot{Q} = N_j V \dot{q}_j$$

and the heating rate per unit volume is

$$q''' = \frac{\dot{Q}}{V} = N_j \dot{q}_j .$$

By using the following relations,

$$Pr = \frac{C_p \mu_g}{K} \quad , \quad N_j = \frac{\rho_j}{\frac{4}{3}\pi r_j^3 m_j} \quad , \quad Nu_j = \frac{h_c(2r_j)}{K} \quad , \quad A = \frac{9}{2}\frac{\mu_g f_j}{m_j r_j^2}$$

and

$$C = \frac{Nu_j C_p}{2 f_j Pr}$$

the $\frac{R}{C_v} q'''$ can be written as

$$\frac{R}{C_v} q''' = (\gamma - 1)q''' = (\gamma - 1)\,\rho_j A[\frac{2}{3} C(T_j - T)$$

$$+ \frac{3\sigma}{A m_j r_j}(\varepsilon_j T_j^4 - \varepsilon T^4)].$$

Work Source Due to Drag Force

The work that the particles do on the gas with respect to the closed system of gas is derived as follows:

$$W''' = \rho \vec{f} \cdot (\vec{V}_j - \vec{V}) = \rho[-(\frac{\rho_j}{\rho})A(\vec{V} - \vec{V}_j)] \cdot (\vec{V}_j - \vec{V})$$

$$= \rho_j A[(u - u_j)^2 + (v - v_j)^2].$$

Therefore

$$\frac{R}{C_v} W''' = (\gamma - 1)\rho_j A[(u - u_j)^2 + (v - v_j)^2].$$

Substituting the relations $\frac{R}{C_v} q'''$ and $\frac{R}{C_v} w'''$ into the energy equation, the energy equation can be written as:

$$\frac{\partial P}{\partial t} + u \frac{\partial P}{\partial x} + v \frac{\partial P}{\partial r} - a^2\left(\frac{\partial \rho}{\partial t} + u \frac{\partial \rho}{\partial x} + v \frac{\partial \rho}{\partial r}\right) = AB\rho_j \tag{A4}$$

where

$$B = (\gamma - 1)[(u - u_j)^2 + (v - v_j)^2 + \frac{2}{3} C(T_j - T)$$

$$+ \frac{3\sigma}{Am_j r_j} (\varepsilon_j T_j^4 - \varepsilon T^4)].$$

Conservation of Particle Mass

Since the particles do not lose or gain mass by any mechanism, it follows immediately that

$$\frac{\partial \rho_j}{\partial t} + u_j \frac{\partial \rho_j}{\partial x} + v_j \frac{\partial \rho_j}{\partial r} + \rho_j \frac{\partial u_j}{\partial x} + \rho_j \frac{\partial v_j}{\partial r} + \delta \frac{\rho_j v_j}{r} = 0 \tag{A5}$$

from a control volume approach similar to that used for the gas phase.

Particle Momentum Equation

Since there are no pressure or shear forces acting on the particle, the momentum equation due to the drag force can be written as:

$$\rho_j\left[\frac{\partial \vec{V}_j}{\partial t} + (\vec{V}_j \cdot \nabla)\vec{V}_j\right] = -\rho \vec{f}$$

where $\rho\vec{f}$ is the drag force of the particles acting on the gas. By substituting the relation $\vec{f} = -(\frac{\rho_j}{\rho})\, A\,(\vec{V} - \vec{V}_j)$ into the above equation, the momentum equation for the particles can be expressed in component forms:

$$\frac{\partial u_j}{\partial t} + u_j \frac{\partial u_j}{\partial x} + v_j \frac{\partial u_j}{\partial r} = A(u - u_j) \tag{A6}$$

$$\frac{\partial v_j}{\partial t} + u_j \frac{\partial v_j}{\partial x} + v_j \frac{\partial v_j}{\partial r} = A(v - v_j). \tag{A7}$$

Conservation of Particle Energy

For a unit volume of two phase flow, the particles have the total energy per unit volume

$$\rho_j e_j = \rho_j (C_j T_j + \frac{u_j^2}{2} + \frac{v_j^2}{2}).$$

A control volume analysis gives the following

$$-\frac{\partial}{\partial t}\int_v \rho_j e_j dv = \int_s \rho_j e_j \vec{V}_j \cdot \vec{n}\, ds - \int_v q'''dv - \int_v W'''dv$$

where q''' and w''' are positive if the energy transfer into the particle phases. Using the Gauss's divergence theorem, the energy equation becomes

$$\frac{\partial}{\partial t}(\rho_j e_j) + \nabla \cdot (\rho_j e_j \vec{V}_j) - q''' - W''' = 0.$$

Applying the conservation of particle into the above equation, the energy equation is rewritten as:

$$\rho_j (\frac{\partial e_j}{\partial t} + u_j \frac{\partial e_j}{\partial x} + v_j \frac{\partial e_j}{\partial r}) - q''' - W''' = 0.$$

By substituting the derives of e_j into the above equation and applying the particle momemtum equation, the particle energy equation becomes

$$\rho_j C_j [\frac{\partial T_j}{\partial t} + u_j \frac{\partial T_j}{\partial x} + v_j \frac{\partial T_j}{\partial r}] \rho_j u_j A(u - u_j)$$

$$+ \rho_j v_j A(v - v_j) - q''' - W''' = 0.$$

The work done on the particles at the particle velocity is

$$W''' = N_j W_j''' = N_j \vec{D}_j \cdot \vec{V}_j = N_j(-\frac{\rho \vec{f}}{N_j}) \cdot \vec{V}_j = -\rho \vec{f} \cdot \vec{V}_j$$

$$= \rho_j A(\vec{V} - \vec{V}_j) \cdot \vec{V}_j = \rho_j A u_j (u - u_j) + \rho_j A v_j (v - v_j).$$

From the aforementioned results, the heat transfer into the particle phase is

$$q''' = -\rho_j A[\frac{2}{3} C(T_j - T) + \frac{3\sigma}{A m_j r_j} (\varepsilon_j T_j^4 - \varepsilon T^4)].$$

Therefore, the energy equation for the particle becomes

$$\frac{\partial T_j}{\partial t} + u_j \frac{\partial T_j}{\partial x} + v_j \frac{\partial T_j}{\partial r} = D \qquad \text{(A8)}$$

where

$$D = -\frac{A}{C_j} [\frac{2}{3} C(T_j - T) + \frac{3\sigma}{A m_j r_j} (\varepsilon_j T_j^4 - \varepsilon T^4)$$

$$= -\frac{2AC}{3C_j} (T_j - T) - \frac{3\sigma}{m_j r_j C_j} (\varepsilon_j T_j^4 - \varepsilon T^4).$$

APPENDIX B

TURBULENT BOUNDARY LAYER RELATIONS

The direct integral method is incorporated into the present work to consider the effect of turbulent boundary layer. In order to understand the relations applied in this study, the equation and relations of parameters, which are presented by Whitfield [24], are shown in this appendix.

Integral Equation

$$\frac{1}{r_w^{\delta}\rho_e u_e^2}\frac{d}{dx}\left(r_w^{\delta}\rho_e u_e^2\theta\right) + H_{\delta *}\frac{\theta}{u_e}\frac{du_e}{dx} = \frac{C_f}{2} \tag{B1}$$

$$\frac{1}{2r_w^{\delta}\rho_e u_e^3}\frac{d}{dx}\left(r_w^{\delta}\rho_e u_e^3\theta H_{\theta *}\right) + H_{\delta **}\frac{\theta}{u_e}\frac{du_e}{dx} = \frac{C_f}{2}D. \tag{B2}$$

Shape Factor Correlations

$$\frac{\delta^*}{\theta} = H_{\delta *} = \bar{H}(1 + 0.113\ M_e^2) + 0.290\ M_e^2$$

$$\frac{\theta^*}{\theta} = H_{\theta *} = \frac{2 - 0.54\ \tanh[1.1(\bar{H} - 1)] + 0.028\ M_e^2}{1 + 0.014\ M_e^2}$$

$$\frac{\delta^{**}}{\theta} = H_{\delta **} = \left(\frac{0.064}{\bar{H} - 0.8} + 0.251\right) M_e^2$$

and $$\frac{\theta}{\bar{\theta}} = 1 - \frac{0.92\ M_e^2}{7.09 + M_e^2}\tanh[1.49(\bar{H} - 0.9)]$$

where

$$\bar{H} = \frac{\bar{\delta}^*}{\bar{\theta}}\ . \tag{B3}$$

Skin Friction Coefficient

$$C_f = \frac{1}{F_c} \frac{0.3e^{-1.33\bar{H}}}{[\log_{10}(\frac{R_{e\theta}}{F_c})]\ 1.74 + 0.31\bar{H}} \tag{B4}$$

where

$$F_c = (1 + \frac{\gamma - 1}{2} M_e^2)^{1/2} \quad , \quad R_{e_\theta} = \frac{\rho_e u_e \theta}{\mu_e} \ . \tag{B5}$$

Shear-Work Integral

$$D = \int_o^\infty \frac{\tau}{\tau_w} \frac{\partial(\frac{u}{u_e})}{\partial(\frac{y}{\bar{\theta}})} \, d(\frac{y}{\bar{\theta}}) \tag{B6}$$

where

$$\frac{\tau}{\tau_w} = 1 \qquad \text{for } 0 \leq y+ \leq 100$$

$$\frac{\tau}{\tau_w} = \frac{\rho(0.41y)^2 \left|\frac{\partial u}{\partial y}\right| \frac{\partial u}{\partial y}}{\tau_w} = \frac{2}{C_f} \frac{\rho}{\rho_e} (0.41 \frac{y}{\bar{\theta}})^2 \left| \frac{\partial(\frac{u}{u_e})}{\partial(\frac{y}{\bar{\theta}})_\theta} \right| \frac{\partial(\frac{u}{u_e})}{\partial(\frac{y}{\bar{\theta}})_\theta}$$

for middle region.

$$\frac{\tau}{\tau_w} = \frac{0.0168\rho u_e \bar{\delta}^* \frac{\partial u}{\partial y}}{\tau_w} = 0.0168 \frac{2}{C_f} \frac{\rho}{\rho_e} \bar{H} \frac{\partial(\frac{u}{u_e})}{\partial(\frac{y}{\bar{\theta}})} \tag{B7}$$

for outer region

The point in the boundary layer separating the middle region from the outer region at a particular location is that point where

$$(0.41y)^2 \left|\frac{\partial u}{\partial y}\right| = 0.0168 \ u_e \bar{\delta}^* . \tag{B8}$$

Velocity-Temperature Relation

The density ratio in the expression for the shear-stress distribution is specified by the modified Crocco relation for an adiabatic wall

$$\frac{\rho_e}{\rho} = \frac{T}{T_e} = 1 + r_{co}(\gamma - 1)M_e^2 \left(1 - \frac{u^2}{u_e^2}\right)/2 \tag{B9}$$

where recovery factor $r_{co} = Pr^{0.333}$.

Definition of Basic Parameters

$$\frac{C_f}{2} = \frac{\tau_w}{\rho_e u_e^2}$$

$$\bar{\delta}^* = \int_0^\infty \left(1 - \frac{u}{u_e}\right)dy$$

$$\bar{\theta}^* = \int_0^\infty \frac{u}{u_e}\left(1 - \frac{u}{u_e}\right)\,dy$$

$$\theta = \int_0^\infty \frac{\rho u}{\rho_e u_e}\left(1 - \frac{u}{u_e}\right)dy \tag{B10}$$

$$\delta^* = \int_0^\infty \left(1 - \frac{\rho u}{\rho_e u_e}\right)dy$$

$$\theta^* = \int_0^\infty \frac{\rho u}{\rho_e u_e}\left(1 - \frac{u^2}{u_e^2}\right)dy$$

$$\delta^{**} = \int_0^\infty \frac{u}{u_e}\left(1 - \frac{\rho}{\rho_e}\right)dy\,.$$

APPENDIX C

DERIVATION OF CHARACTERISTIC EQUATIONS OF TWO PHASE FLOW FOR WALL BOUNDARY CONDITION

Governing Equations

$$\rho_\tau + \bar{V}\rho_\eta + \rho\alpha u_\eta + \rho\beta v_\eta = -u\rho_\zeta - \rho u_\zeta - \frac{\delta\rho v}{\bar{\eta}} = \psi_1 \tag{C1}$$

$$u_\tau + \bar{V}u_\eta + \frac{\alpha}{\rho} P_\eta = -uu_\zeta - \frac{1}{\rho} P_\zeta - A\frac{\rho_j}{\rho}(u - u_j) = \psi_2 \tag{C2}$$

$$v_\tau + \bar{V}v_\eta + \frac{\beta}{\rho} P_\eta = -uv_\zeta - A\frac{\rho_j}{\rho}(v - v_j) = \psi_3 \tag{C3}$$

$$P_\tau + \bar{V}P_\eta - a^2(\rho_\tau + \bar{V}\rho_\eta) = -uP_\zeta + a^2u\rho_\zeta + AB\rho_j = \psi_4 \tag{C4}$$

$$\rho_{j_\tau} + \bar{V}_j\rho_{j_\eta} + \rho_j\alpha u_{j_\eta} + \rho_j\beta v_{j_\eta} = -u_j\rho_{j_\zeta} - \rho_j u_{j_\zeta} - \frac{\delta\rho_j v_j}{\bar{\eta}} = \psi_5 \tag{C5}$$

$$u_{j_\tau} + \bar{V}_j u_{j_\eta} = -u_j u_{j_\zeta} + A(u - u_j) = \psi_6 \tag{C6}$$

$$V_{j_\tau} + \bar{V}_j v_{j_\eta} = -u_j v_{j_\zeta} + A(v - v_j) = \psi_7 \tag{C7}$$

$$T_{j_\tau} + \bar{V}_j T_{j_\eta} = -u_j T_{j_\zeta} + D = \psi_8 \tag{C8}$$

where the ζ and η subscripts denote partial derivatives with respect to those variables.

Characteristic Curves

A linear combination of the equations (C1) - (C8) can be found by multiplying those equations by ℓ_i, i = 1-8, respectively, and summing them. After the rearrangement, this linear combination can be written as:

$$d_{w_1}\rho + d_{w_2}u + d_{w_3}v + d_{w_4}P + d_{w_5}\rho_j + d_{w_6}u_j + d_{w_7}v_j + d_{w_8}T_j = \ell_1\psi_1 + \ell_2\psi_2 + \ell_3\psi_3 + \ell_4\psi_4 + \ell_5\psi_5 + \ell_6\psi_6 + \ell_7\psi_7 + \ell_8\psi_8 \tag{C9}$$

where

$$\vec{w}_1 = (\bar{V}\ell_1 - a^2\bar{V}\ell_4,\ \ell_1 - a^2\ell_4)\ ,\quad \vec{w}_2 = (\rho\alpha\ell_1 + \bar{V}\ell_2\ ,\ \ell_2)$$

$$\vec{w}_3 = (\rho\beta\ell_1 + \bar{V}\ell_3\ ,\ \ell_3)\ ,\quad \vec{w}_4 = (\frac{\alpha}{\rho}\ell_2 + \frac{\beta}{\rho}\ell_3 + \bar{V}\ell_4\ ,\ \ell_4)$$

$$\vec{w}_5 = (\bar{V}_j\ell_5\ ,\ \ell_5)\ ,\quad \vec{w}_6 = (\rho_j\alpha\ell_5 + \bar{V}_j\ell_6\ ,\ \ell_6)$$

$$\vec{w}_7 = (\rho_j\beta\ell_5 + \bar{V}_j\ell_7\ ,\ \ell_7)\ ,\quad \vec{w}_8 = (\bar{V}_j\ell_8\ ,\ \ell_8)$$

and

$$d_{w_1}\rho = \nabla\rho \cdot \vec{w}_1 = (\bar{V}\ell_1 - a^2\ \bar{V}\ell_4)\ \rho_\eta + (\ell_1 - a^2\ell_4)\rho_\tau$$

is defined as the derivative of ρ in the direction of the vector $\vec{w}_1$.

Let ℓ_i be chosen so that $\vec{w}_i$ are linearly dependent, or, in other words, lie in one direction. If ℓ_i exist, the curve that contains the vector $\vec{w}_i$ is called the characteristic curve, its normal $\vec{N}$ is called the characteristic normal, and equation (C9) is called the compatibility equation. Let $\vec{N} = (N_\eta, N_\tau)$ is the characteristic normal in the $\eta - \tau$ plane, $\vec{N}\cdot\vec{w}_i = 0$ for $i = 1 - 8$.

In matrix form, the equations become

$$\begin{bmatrix} A & B \\ B & C \end{bmatrix} \begin{bmatrix} L_1 \\ L_2 \end{bmatrix} = 0$$

where

$$A = \begin{bmatrix} \bar{V}N_\eta + N_\tau & 0 & 0 & -a^2(\bar{V}N_\eta + N_\tau) \\ \rho\alpha N_\eta & \bar{V}N_\eta + N_\tau & 0 & 0 \\ \rho\beta N_\eta & 0 & \bar{V}N_\eta + N_\tau & 0 \\ 0 & \dfrac{\alpha N_\eta}{\rho} & \dfrac{\beta N_\eta}{\rho} & \bar{V}N_\eta + N_\tau \end{bmatrix}$$

$$B = \begin{bmatrix} 0 & 0 & 0 & 0 \\ 0 & 0 & 0 & 0 \\ 0 & 0 & 0 & 0 \\ 0 & 0 & 0 & 0 \end{bmatrix}$$

$$C = \begin{bmatrix} \bar{V}_j N_\eta + N_\tau & 0 & 0 & 0 \\ \rho_j \alpha N_\eta & \bar{V}_j N_\eta + N_\tau & 0 & 0 \\ \rho_j \beta N_\eta & 0 & \bar{V}_j N_\eta + N_\tau & 0 \\ 0 & 0 & 0 & \bar{V}_j N_\eta + N_\tau \end{bmatrix}$$

$$L_1 = \begin{bmatrix} \ell_1 \\ \ell_2 \\ \ell_3 \\ \ell_4 \end{bmatrix}$$

and

$$L_2 = \begin{bmatrix} \ell_5 \\ \ell_6 \\ \ell_7 \\ \ell_8 \end{bmatrix}. \qquad \text{(C10)}$$

In order to get nontrivial solution ℓ_i, the coefficient matrix must be singular, in other words, its determinant must be equal to zero. Setting the determinant equal to zero yields

$$[(\bar{V}N_\eta + N_\tau)^2 - a^2\alpha^{*2}N_\eta^2]\ (\bar{V}N_\eta + N_\tau)^2\ (\bar{V}_j N_\eta + V_\tau)^4 = 0$$

where

$$\alpha^{*2} = \alpha^2 + \beta^2 .$$

Noting that $\frac{d\eta}{d\tau} = -\frac{N_\tau}{N_\eta}$, one can obtain the following characteristic curves by setting the factors of the above equation to be zero.

$$\frac{d\eta}{d\tau} = \bar{V} \mp a\alpha^* \tag{C11}$$

$$\frac{d\eta}{d\tau} = \bar{V} \tag{C12}$$

$$\frac{d\eta}{d\tau} = \bar{V}_j . \tag{C13}$$

Solution for the ℓ_i

To evaluate the parameter ℓ_i, one applies the mathematical theory of matrix to find out the possible solutions of matrix equation (C10) on the different characteristic curves. Substituting equations (C11), (C12) and (C13), respectively, into the equation (C10), and using the matrix operation yield the following results:

$$\ell_4 = 1,\ \ell_1 = \ell_2 = \ell_3 = \ell_5 = \ell_6 = \ell_7 = \ell_8 = 0 \tag{C14}$$

$$\ell_2 = 1,\ \ell_3 = -\frac{\alpha}{\beta},\ \ell_1 = \ell_4 = \ell_5 = \ell_6 = \ell_7 = \ell_8 = 0 \tag{C15}$$

$\Big\}$ for $\frac{d\eta}{d\tau} = \bar{V}$

$$\ell_1 = 1,\ \ell_2 = \mp \frac{\rho\alpha}{a\alpha^*},\ \ell_3 = \mp \frac{\rho\beta}{a\alpha^*}$$

$$\ell_4 = \frac{1}{a^2},\ \ell_5 = \ell_6 = \ell_7 = \ell_8 = 0 \tag{C16}$$

$\Big\}$ for $\frac{d\eta}{d\tau} = \bar{V} \mp a\alpha^*$

$$\left.\begin{aligned} &\ell_1 = \ell_2 = \ell_3 = \ell_4 = \ell_5 = \ell_6 = \ell_7 = 0,\ \ell_8 = 1 && \text{(C17)}\\ &\ell_1 = \ell_2 = \ell_3 = \ell_4 = \ell_5 = \ell_6 = \ell_8 = 0,\ \ell_7 = 1 && \text{(C18)}\\ &\ell_1 = \ell_2 = \ell_3 = \ell_4 = \ell_5 = \ell_7 = \ell_8 = 0,\ \ell_6 = 1 && \text{(C19)} \end{aligned}\right\} \text{for } \frac{d\eta}{d\tau} = \bar{V}_j.$$

Compatibility Equations

Substituting the equations (C14) - (C19) into the equation (C9), one can express the compatibility equation in the following forms:

$$\left.\begin{aligned} &dP - a^2 d\rho = \psi_4 d\tau && \text{(C20)}\\ &\beta du - \alpha dv = (\beta\psi_2 - \alpha\psi_3)d\tau && \text{(C21)} \end{aligned}\right\} \text{for } d\eta = \bar{V}d\tau$$

$$dP \pm \frac{\rho\alpha a}{\alpha^*} du \pm \frac{\rho\beta a}{\alpha^*} dv = (\psi_4 + a^2\psi_1 \pm \frac{\rho\alpha a\psi_2}{\alpha^*} \pm \frac{\rho\beta a\psi_3}{\alpha^*})d\tau \quad \text{(C22)}$$

$$\text{for } d\eta = (\bar{V} \pm a\alpha^*)d\tau$$

$$\left.\begin{aligned} &du_j = \psi_6 d\tau && \text{(C23)}\\ &dv_j = \psi_7 d\tau && \text{(C24)}\\ &dT_j = \psi_8 d\tau && \text{(C25)} \end{aligned}\right\} \text{for } d\eta = \bar{V}_j d\tau.$$

Discussions

(1) From the theory of numerical characteristic scheme, the slope of characteristic curve cannot be negative on the wall. The characteristic curve $\frac{d\eta}{d\tau} = \bar{V} - a\alpha^*$ is incorrect to apply on the wall.

(2) Because no compatibility equation is available to solve the particle concentration, the continuity equation and extrapolation scheme are introduced in this study.

(3) Due to the assumption of slip condition for the particle phase, only equations (C23) and (C25) are applied to solve the variables u_j and T_j. The variable v_j can be found out from the slope of wall and u_j.

(4) Comparing the equations (C20)-(C22) with those shown in in reference 25, one can understand the expressions for the two phase flow are same as those of one phase flow except the ψ_i terms.

(5) To investigate further the equations (C23) and (C25), it is easy to see that the numerical treatment is the same as the one-sided difference scheme under the assumption of slip condition.

APPENDIX D

DERIVATION OF CHARACTERISTIC EQUATIONS OF TWO PHASE FLOW FOR INLET AND EXIT BOUNDARY CONDITIONS

Governing Equations

$$\rho_\tau + u\rho_\zeta + \rho u_\zeta = -\bar{V}\rho_\eta - \rho\alpha u_\eta - \rho\beta v_\eta - \frac{\delta\rho v}{\bar{\eta}} = \psi_1 \tag{D1}$$

$$u_\tau + uu_\zeta + \frac{1}{\rho} P_\zeta = - \bar{V}u_\eta - \frac{\alpha}{\rho} P_\eta - A\frac{\rho_j}{\rho}(u - u_j) = \psi_2 \tag{D2}$$

$$v_\tau + uv_\zeta = -\bar{V}v_\eta - \frac{\beta}{\rho} P_\eta - A\frac{\rho_j}{\rho}(v - v_j) = \psi_3 \tag{D3}$$

$$P_\tau + uP_\zeta - a^2(\rho_\tau + u\rho_\zeta) = - \bar{V}P_\eta + a^2\bar{V}\rho_\eta + AB\rho_j = \psi_4 \tag{D4}$$

$$\rho_{j_\tau} + u_j\rho_{j_\zeta} + \rho_j u_{j_\zeta} = - \bar{V}_j\rho_{j_\eta} - \rho_j\alpha u_{j_\eta} - \rho_j\beta v_{j_\eta} - \frac{\delta\rho_j v_j}{\bar{\eta}} = \psi_5 \tag{D5}$$

$$u_{j_\tau} + u_j u_{j_\zeta} = - \bar{V}_j u_{j_\eta} + A(u - u_j) = \psi_6 \tag{D6}$$

$$v_{j_\tau} + u_j v_{j_\zeta} = - \bar{V}_j v_{j_\eta} + A(v - v_j) = \psi_7 \tag{D7}$$

$$T_{j_\tau} + u_j T_{j_\zeta} = - \bar{V}_j T_{j_\eta} + D = \psi_8 . \tag{D8}$$

Characteristic Curves

Following the procedure of Appendix C, one can show the characteristic curves to be

$$\frac{d\zeta}{d\tau} = u \tag{D9}$$

$$\frac{d\zeta}{d\tau} = u \mp a \tag{D10}$$

$$\frac{d\zeta}{d\tau} = u_j \cdot \tag{D11}$$

Compatibility Equations

Again, following the development procedure of Appendix C, one can show the compatibility equations to be

$$dP - a^2 d\rho = \psi_4 d\tau \tag{D12}$$

$$dv = \psi_3 d\tau \tag{D13}$$

for $\frac{d\zeta}{d\tau} = u$

$$dP - \rho a du = (a^2\psi_1 - \rho a\psi_2 + \psi_4)d\tau \quad \text{for } \frac{d\zeta}{d\tau} = u - a \tag{D14}$$

$$dP + \rho a du = (a^2\psi_1 + \rho a\psi_2 + \psi_4)d\tau \quad \text{for } \frac{d\zeta}{d\tau} = u + a \tag{D15}$$

$$du_j = \psi_6 d\tau \tag{D16}$$

$$dv_j = \psi_7 d\tau \tag{D17}$$

$$dT_j = \psi_8 d\tau \tag{D18}$$

for $\frac{d\zeta}{d\tau} = u_j$.

Discussions

(1) From the theory of numerical characteristic scheme, the slope of characteristic curves must be negative for the inlet plane. Because the values of u and u_j are positive in this study, only the equation (D14) under the subsonic inlet condition satisfies this requirement.

(2) Because there are eight unknowns in the governing equations and only the equation (D14) is applied to the inlet condition, it is necessary to give the seven prescribed inlet conditions.

(3) Because the supersonic exit condition is assumed in this study, the extrapolation method is applied to all the variables.

(4) Even though the present results are restricted to the cases with subsonic inlet and supersonic exit conditions, the computer code has been set up for supersonic inlet or subsonic exit cases. For the supersonic inlet condition, all the eight unknowns must be prescribed. The equations (D12), (D13) and (D15) and extrapolation of particle variables are applied to the cases with subsonic exit. It may be useful to apply the equations (D16)-(D18) to the exit plane for solving the particle variables.

APPENDIX E

DESCRIPTION OF COMPUTER PROGRAM

By using the structure of VNAP Code [25], the computer program, GPF, developed in this dissertation consists of one main program, one function, and nineteen subroutines. In order to understand the function of the computer program, a description of main program, subroutines, inputs and outputs is given in the following.

Main Program

As shown in Figure 52, the flow diagram is helpful for familiarity with this code. Program GPF initiates a run by reading in the input data. Next, the program title and input data descriptions are printed. The subroutine GEOM is called to calculate the wall coordinates and slope. If the integral method for treating the turbulent boundary layer is considered, the another kind of wall coordinates for this approach is computed. The input data are converted to the internal units in which the program operates. If requested, GPF called subroutine ONEDIM to calculate the one-dimensional one phase, initial value surface. The final part of this program is the time-step loop, which calculate the next step. In this loop, the predictor-corrector procedure is applied to each time step. The subroutines INTER, WALL, INLET and EXITT are used to calculate all the grid points in the flow field. If necessary, the subroutine VISCOS and viscous-inviscid interaction technique are introduced. The mass flow, energy flux and momentum thrust are calculated and printed by the action of subroutine MASFLO. The solution are printed and punched for restart or plotting.

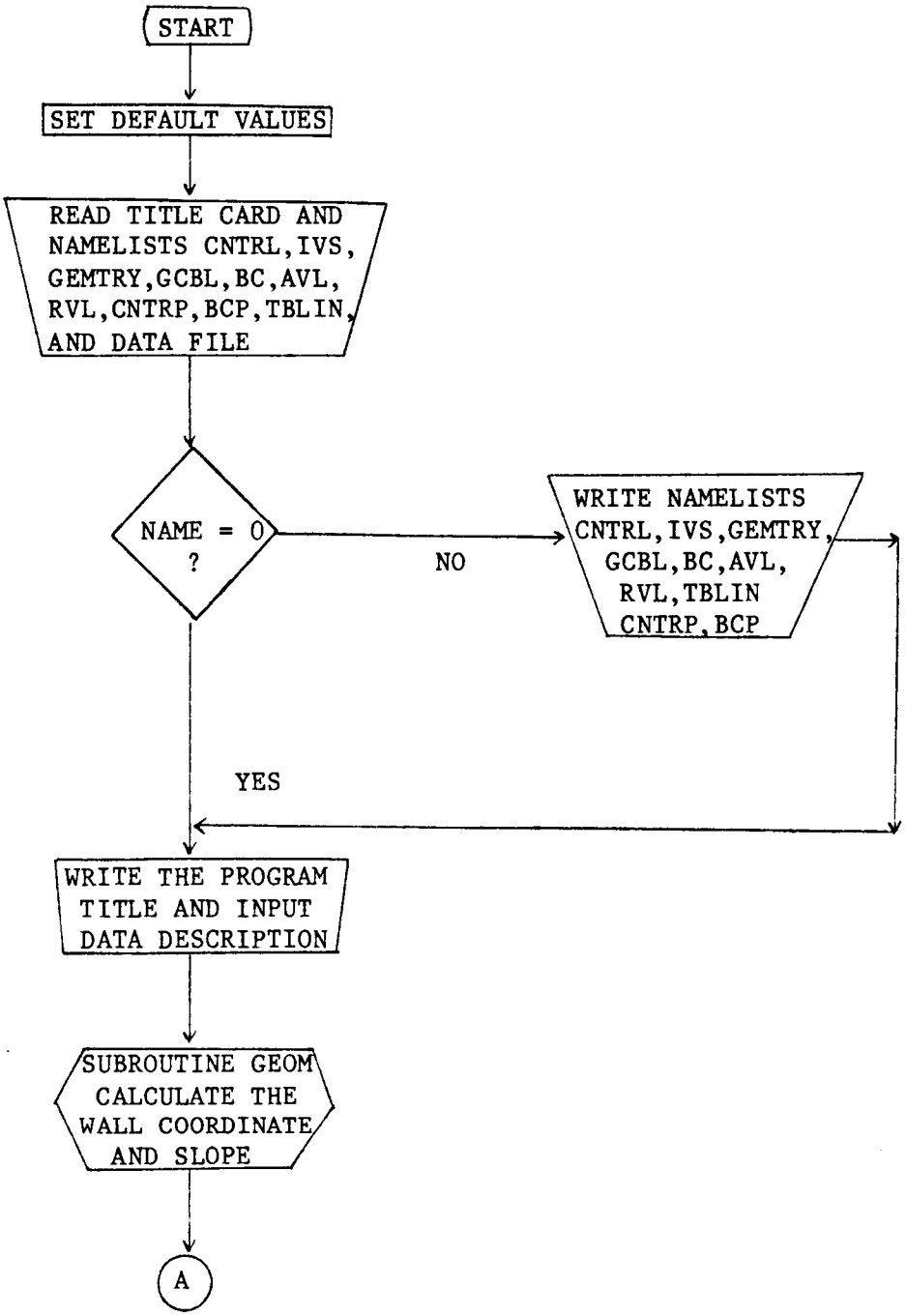


Figure 52. Computer Program Flow Diagram.

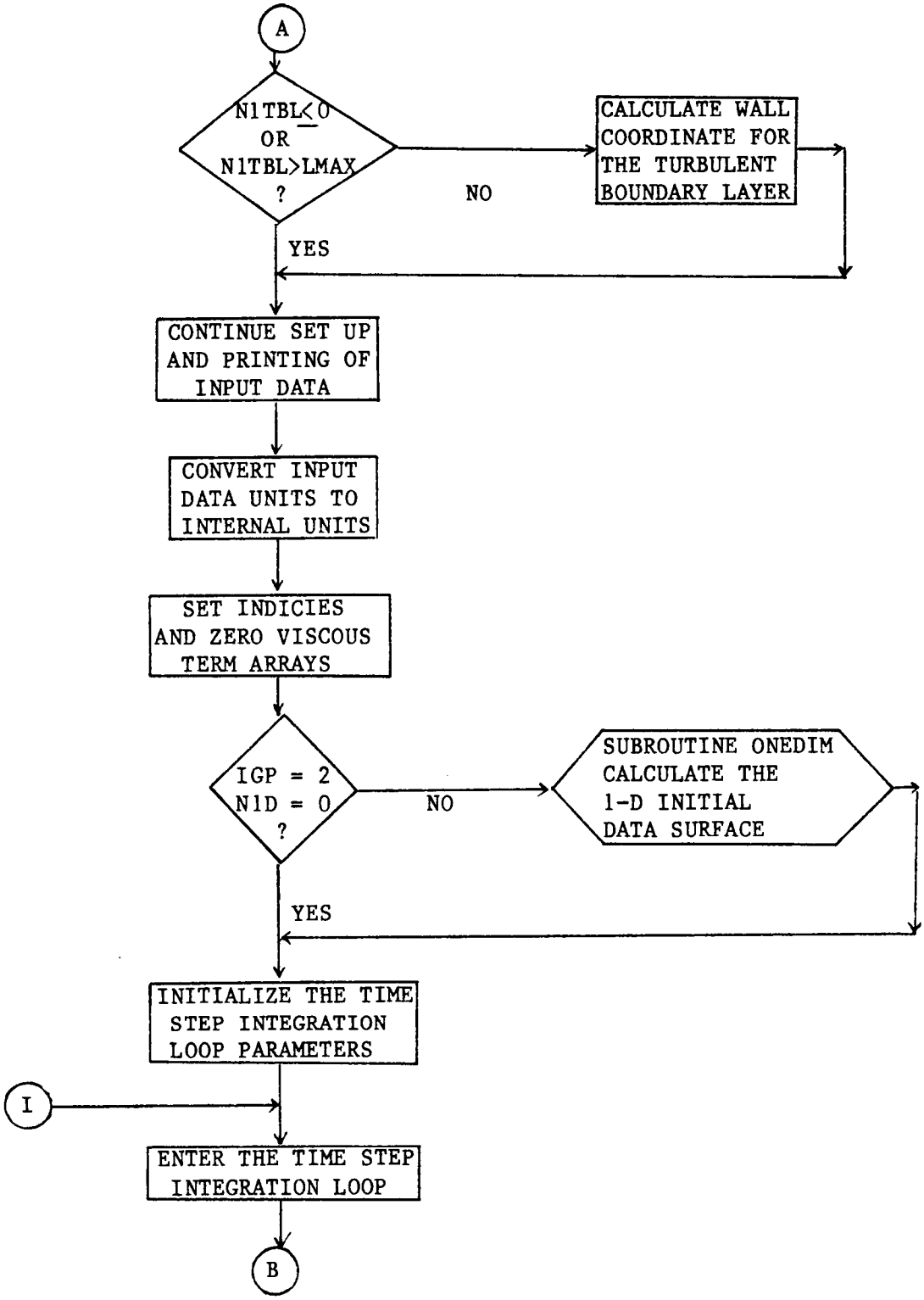


Figure 52 (continued)

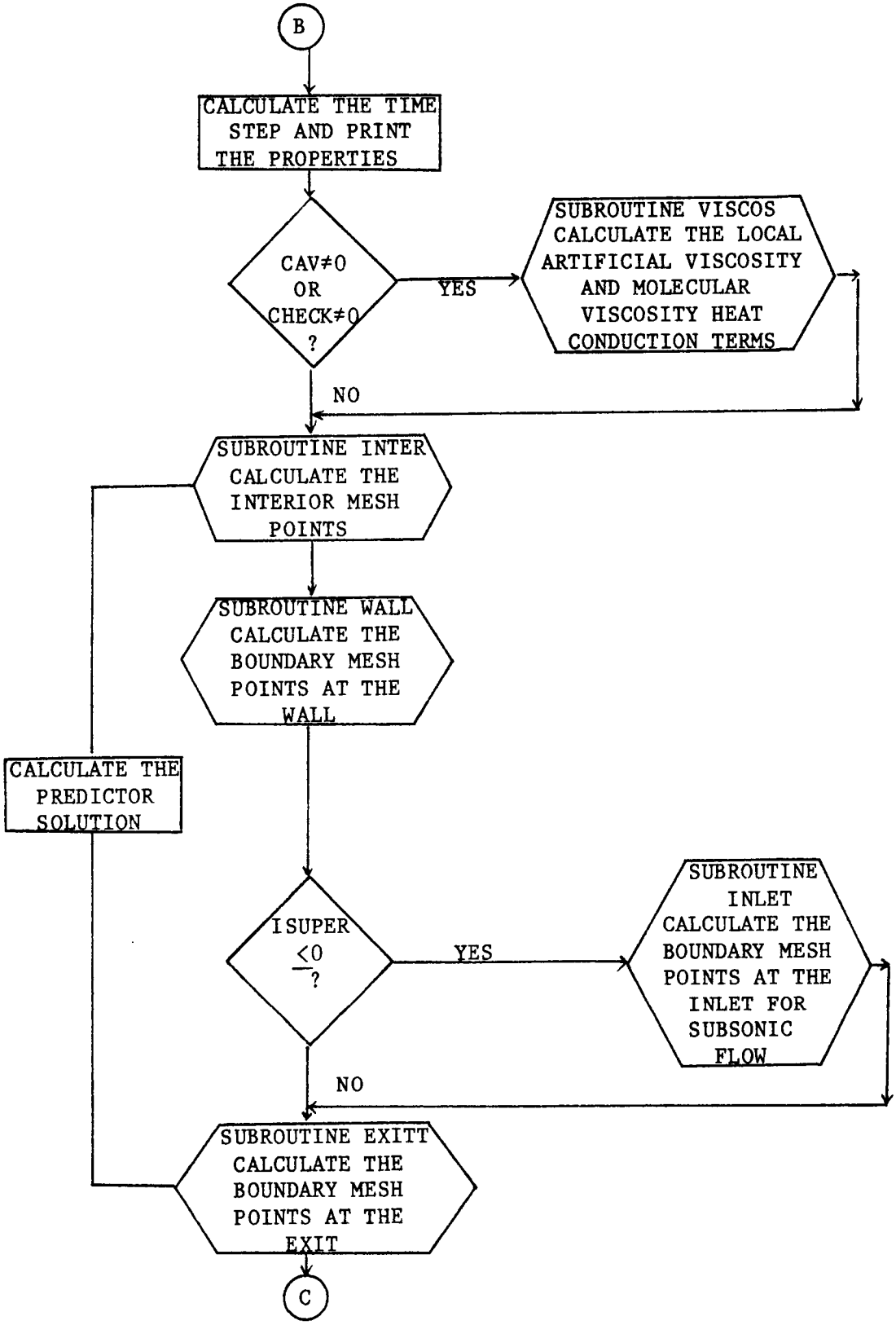


Figure 52 (continued)

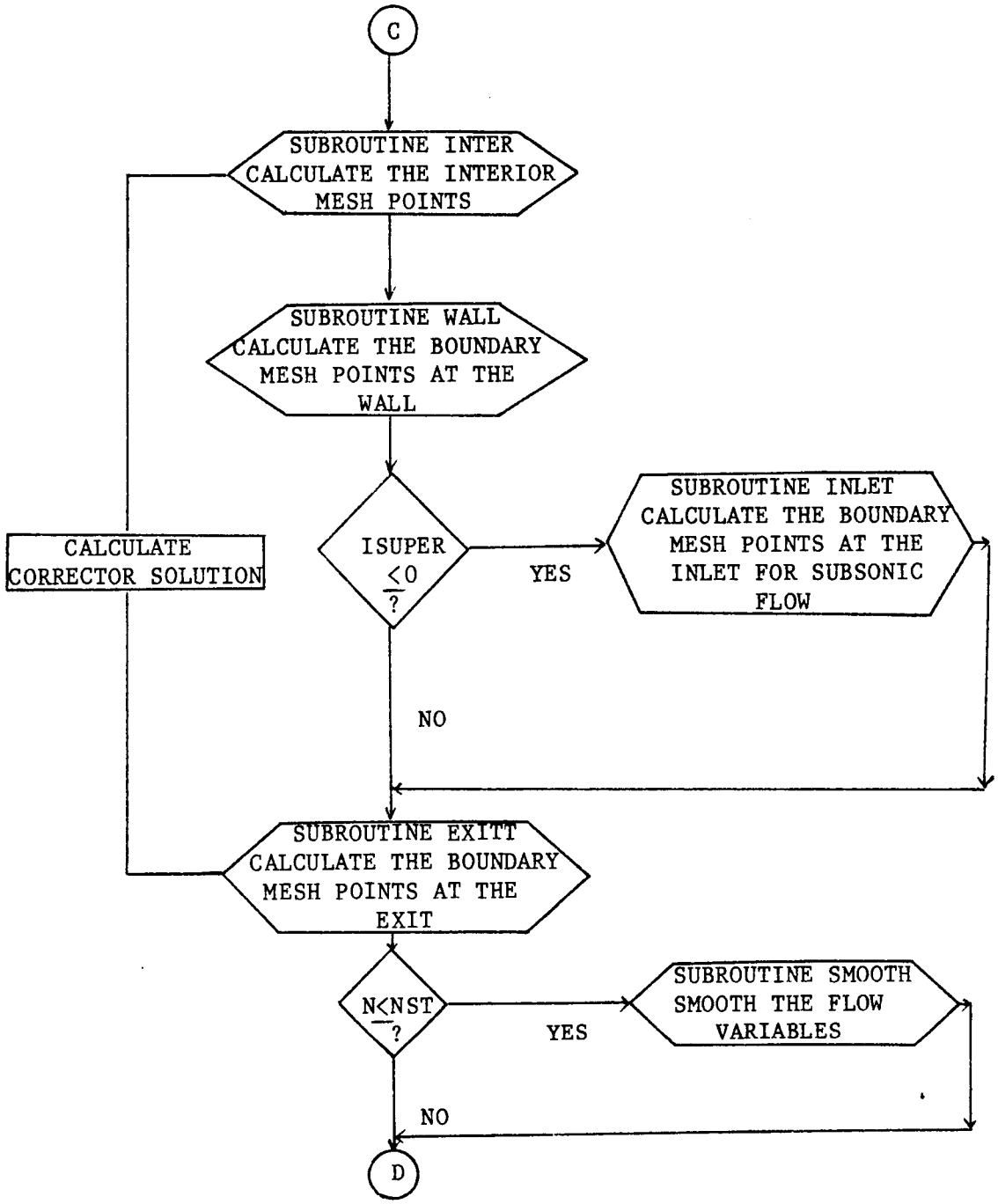


Figure 52 (continued)

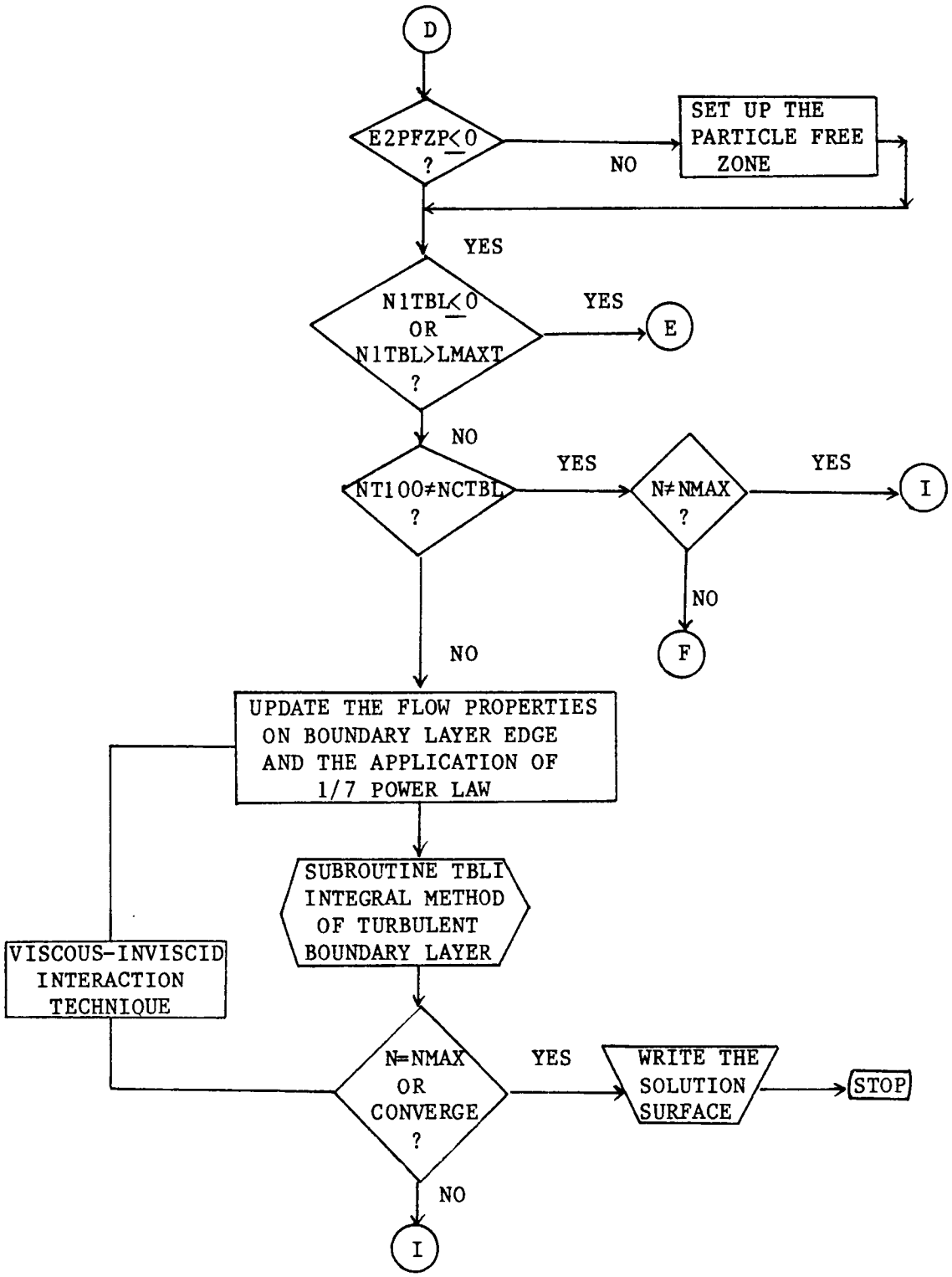


Figure 52 (continued)

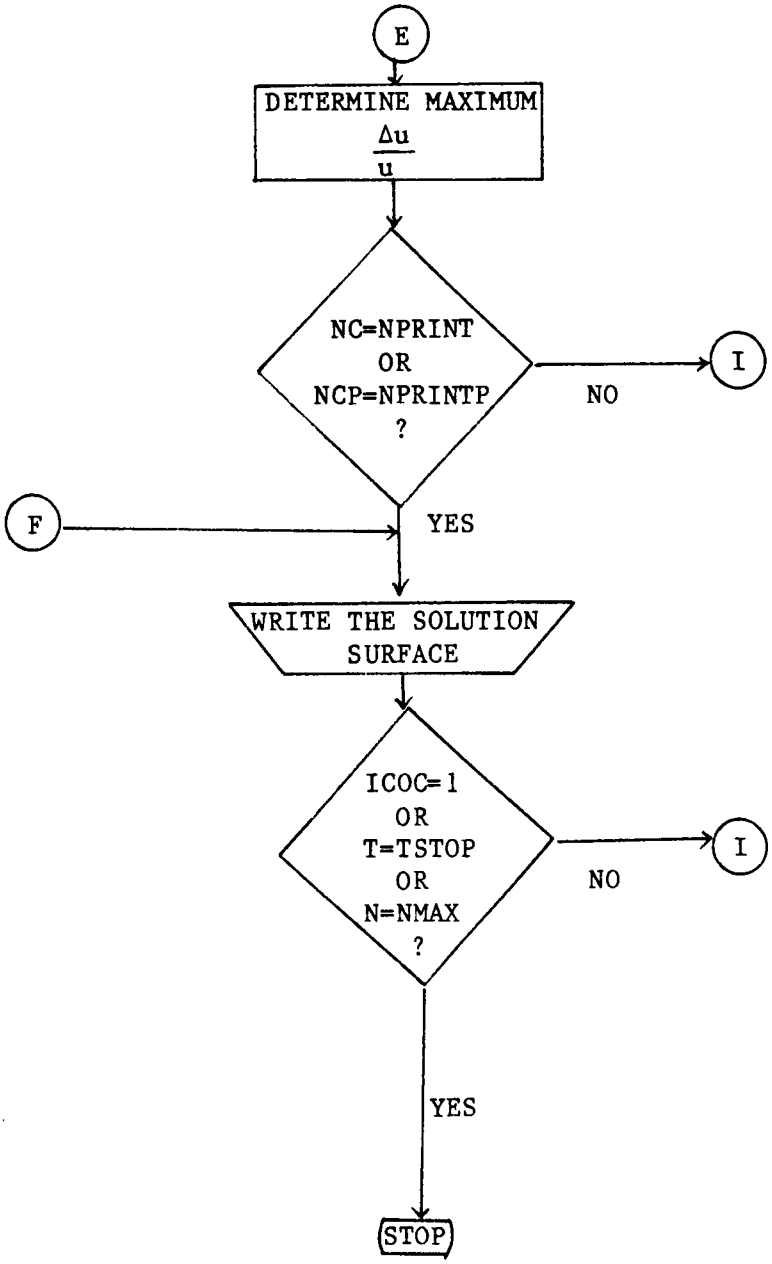


Figure 52 (continued)

Subroutines and Function

1. Subroutine GEOM: calculates the wall coordinates and slopes
2. Subroutine MTLUP: is called by GEOM to interpolate the wall for equally spaced coordinates.
3. Function DIF: is called by GEOM to calculate the slope of the wall.
4. Subroutine ONEDIM: calculates the 1-D initial data surface.
5. Subroutine EOS: calculates the equation of state quantities
6. Subroutine MAP: calculates the mapping functions that map the physical plane to a rectangular computational plane.
7. Subroutine MASFLO: calculates the mass flow, thrust, momentum flux, and energy flux at inlet, throat and exit planes.
8. Subroutine SMOOTH: smoothes the flow variables if requested
9. Subroutine VISCOS: calculates the local artificial viscosity and molecular viscosity-heat conduction terms.
10. Subroutine INTER: calculates the interior mesh points
11. Subroutine WALL: calculates the boundary mesh points at the wall.
12. Subroutine WALLP: is called by wall to calculate the particle properties at the wall mesh points.
13. Subroutine INLET: calculates the boundary mesh points at the inlet for subsonic flow.
14. Subroutine EXITT: calculates the boundary mesh points at the exit.

15. Subroutine COFGP: calculates the coefficients A, B, C and D in the governing equations.
16. Subroutine TBLI: solves the turbulent boundary layer problems by the integral method.
17. Subroutine SIMP: is called by TURB to integrate the shear-work integral D by Simpson rules.
18. Subroutine TURB: is called by TBLI to calculate the shear-work integral D.
19. Subroutine LININT: is called by TBLI to linearly interpolate the Mach number, wall radius, temperature and density on the boundary layer edge.
20. Subroutine SPLN: is called by TBLI to splinely interpolate the Mach number, wall radius, temperature and density on the boundary layer edge.

Inputs and Outputs

In this code, twelve data files are created to interact with the main program. The five data files with unit numbers 11, 12, 13, 14 and 15 are set up to store the calculations of turbulent boundary layer problems. For coordinates of the particle limiting streamline and wall, the files with unit numbers 4, 8 and 9 are used to store those data. The data file, unit 3, is created to store the solution for the final time step at any computer run. This result can be used to restart the computer run at the next time. In order to find out the time history of pressure at a fixed grid point, the values at any fixed time step are stored in unit 10. Finally, the input data files, units 1 and 2, are

important to begin the calculation in this code. In order to restart the computer run, the data stored in unit 3 are transformed into the unit 1. The important parameters which control the function of this code are given in unit 2. The contents of data file with unit 2 are described as follows.

The input data in unit 2 consist of a case title followed by nine namelists. The case title may be up to 80 characters long. Following the title card, the namelist inputs proceed in the following order:

1. Namelist CNTRL: inputs the parameter that control the overall logic of the program.
2. Namelist IVS: specifies the flow variables for the initial data surface.
3. Namelist GEMTRY: specifies the parameter that define the wall contour.
4. Namelist BC: specifies the flow variables of gas phase at the inlet and exit boundaries.
5. Namelist AVL: specifies the parameters that determine the artificial viscosity, damping strength, smoothing region and time smoothing.
6. Namelist RVL: specifies the molecular viscosity and thermal conductivity parameters.
7. Namelist CNTRP: inputs the parameters that relate with the particle phase.
8. Namelist BCP: specifies the flow variables of particle phase at the inlet and exit boundaries.

9. Namelist TBLIN: inputs the parameters that relate with the turbulent boundary layer.

Finally, the program output consists of printed output and purchases data for restart and plotting. If requested, the values of terms in the governing equations can be printed to check the order at any time step and any grid point. For the calculations of inviscid gas-particle flow or turbulent boundary layer by integral method, the namelist RVL is left blank and the value of viscosity is controlled by the parameters given in Namelists CNTRP or TBLIN.

VITA

Chii-Jong Hwang was born in the Republic of China on July 9, 1952. He received his primary school and high school education in the Republic of China and obtained his degree of Bachelor of Science in Engineering Science at National Cheng Kung University, Tainan, Tiawan, the Republic of China, in June 1975.

After graduation, he served two years in the army as a platoon leader. In 1977-1978, he became a teaching assistant at National Cheng Kung University and Kun Sung Technological Institute.

He came to the United States in September 1978, and joined The Tennessee Technological University as a full-time graduate student. He was granted the Master of Science degree in June 1980. In September 1980, he entered The University of Tennessee Space Institute, Tullahoma where he majored in Mechanical Engineering.

Mr. Hwang is a member of the Honor Societies of Tau Beta Pi and Phi Kappa Phi, and a student member of American Society of Mechanical Engineers.